ASSESSMENT OF GENERATED METEOROLOGICAL DATA FOR USE IN SOLAR ENERGY SIMULATIONS

by
Robert Adam Gansler

A thesis submitted in partial fulfillment
of the requirements for the degree of

Master of Science
(Mechanical Engineering)

at the
UNIVERSITY OF WISCONSIN-MADISON
1993

Abstract

Meteorological data are needed to design and size solar energy applications. The necessary data are not available in sufficient quantity so it is often necessary to synthesize these data with statistical models. This study investigates existing meteorological models with various solar applications. The models investigated are the SOLMET long term radiation data, the typical meteorological year, the TRNSYS Type 54 weather generator, an average day model, and the TRNSYS Type 75 compressed weather generator.

Data for solar energy simulations have generally been available for hourly intervals. Consequently, a research area that has not received until recently has been that of minute radiation. The variation of radiation within an hour has been assumed to have a negligible effect on a system's performance. The differences in performance estimates resulting from the use of hourly and minute-by-minute data are determined for a photovoltaic system.

Acknowledgements

It was definitely an uphill struggle to complete my work here. I would have never been able to accomplish half of the things that I did without the help of my fellow graduate students. Special thanks to Jeff and Doug, for because of them, I know a great deal more about computer systems than I ever wanted to know. Though it sometimes reached the point that they would try to run away if I tried to talk to them, they were always more than helpful in solving the multitude of problems that I brought their way.

I would also like to thank my advisors, Professor Klein and Professor Beckman. They were always willing to put forth the difficult questions that made me strive to figure out the answers. Thanks also to Professor Mitchell for the time that he helped advise me. He helped bring things back down to earth when it was so easy to get lost in all of the numbers and figures. I am also indebted to Professor Duffie who was willing to answer some of my questions that nobody seemed able to answer.

Finally, I would like to express my heartfelt appreciation to my parents for all the support that they have given me over the years. They always showed that they believed in me, especially in the times that I did not believe in myself.

Table of Contents

List of Figures

Chapter 4

Appendix A

Appendix B

List of Tables

Chapter 1

Chapter 4

Chapter 5

Nomenclature

a	Curve fitting parameter
a_0	Material constant
a_{ref}	Curve fitting parameter at reference conditions
A_c	Collector area
b_0	Incidence angle modifier
c_t	Minute clearness index
CFD	Cumulative Frequency Distribution
COM	Type 75 compressed weather generator
d	Minute diffuse fraction
D	Hourly diffuse fraction
E_{GO}	Band gap at 0 Kelvin
F	Solar fraction
F_R	Collector heat removal factor
G	Minute horizontal solar radiation
G_d	Minute diffuse radiation
G_0	Minute extraterrestrial horizontal radiation
G_T	Minute tilted radiation
$G_{T,NOCT}$	Solar flux at NOCT
GEN	Type 54 weather generator
H	Daily horizontal radiation
$\overline{H}$	Monthly average horizontal radiation
H_d	Daily diffuse radiation
$\overline{H}_d$	Monthly average diffuse radiation
H_0	Daily extraterrestrial horizontal radiation
H_T	Daily radiation on a tilted surface
I	Hourly horizontal radiation

I	Current
I_0	Hourly extraterrestrial horizontal radiation
I_d	Hourly diffuse radiation
I_L	Light current
$I_{L,\ ref}$	Light current at reference conditions
$I_{mp,\ ref}$	Maximum power point current at reference conditions
I_O	Diode reverse saturation current
$I_{O,\ ref}$	Diode reverse saturation current at reference conditions
$I_{sc,\ ref}$	Short circuit current at reference conditions
I_T	Hourly radiation on a tilted surface
I_{TC}	Critical level of radiation
k	Boltzman constant
k	Minute clearness index (Suehrcke)
k_0	Minimum minute clearness index (Suehrcke)
k_1	Intermediate minute clearness index (Suehrcke)
k_2	Intermediate minute clearness index (Suehrcke)
k_3	Maximum minute clearness index (Suehrcke)
$\bar{k}$	Hourly clearness index (Suehrcke)
k_{dev}	Device constant
k_t	Hourly clearness index
k_{tm}	Mean hourly clearness index
K_t	Daily clearness index
$\bar{K}_t$	Monthly average daily clearness index
LTD	Long Term Data
m	Airmass $(1/\cos\theta_z)$
$\dot{m}$	Collector mass flow rate per unit area
$\dot{m}_L$	Load flow rate
NOCT	Nominal Operating Cell Temperature

P	Power
PV	Photovoltaic
r_d	Ratio of hourly to daily total diffuse radiation
r_t	Ratio of hourly to daily total horizontal radiation
R	Load resistance
R_s	Series resistance
S	Solar irradiation on PV cell
S_{ref}	Solar irradiation at reference conditions
T	Daily ambient temperature
T_a	Ambient temperature
T_c	PV cell temperature
$T_{c,\,NOCT}$	Nominal operating cell temperature
$T_{c,ref}$	PV cell temperature at reference conditions
T_h	Hourly ambient temperature
$\overline{T}$	Monthly average daily ambient temperature
$\overline{T}_h$	Monthly average hourly ambient temperature
T_{set}	Water temperature required by load
T_{main}	Makeup water temperature from mains
TMY	Typical Meteorological Year
U_L	Loss coefficient
V	Voltage
$V_{mp,\,ref}$	Maximum power point voltage at reference conditions
$V_{oc,\,ref}$	Open circuit voltage at reference conditions

α	solar altitude angle
Δ	Difference between hourly and minute modeled I_d
Δ_d	Difference between data and modeled G_d
Δ_T	Difference between data and modeled G_T

η_c	PV cell efficiency
μ_{isc}	Temperature coefficient of short circuit current
$\varnothing$	Utilizability
$\varnothing_1$	Lag-one autocorrelation coefficient
$\tau\alpha$	Product of transmittance and absorptance
$(\tau\alpha)$	Transmittance-absorptance product
$(\tau\alpha)_n$	Transmittance-absorptance product at normal incidence
θ_1,θ_2	Parameters in c_t CFD model
θ_z	Solar zenith angle
ω	Hour angle
ω_s	Sunset hour angle

CHAPTER 1. Introduction

Solar energy simulations are weather-driven and thus require meteorological data to perform simulations. Simulations using a single year of meteorological data only reflect the performance of the system for that particular year. It would be statistically more correct to employ many years of data to determine system performance. Long term weather data (e.g., 20 or more years) are available in some locations. Even with today's technology, however, the computing time required for such a large set of data is significant. If the simulations are to be used repetitively for design purposes, the computing time becomes prohibitive. As a consequence, a single year of "typical" data has often been employed for simulation needs. Typical meteorological year (TMY) data have been derived from the long term data (LTD) [Menicucci and Fernandez, 1979]. However, there has been no systematic study on the accuracy of this smaller set of data as it is used in simulations. Menicucci and Fernandez did an exhaustive study of TMY data as compared to LTD. However, they did not provide any conclusions on the justification of using TMY data in simulations.

Even with the typical meteorological year data, there are only a limited number of locations for which simulations can be performed. The lack of data has prompted the development of meteorological data synthesizers. One method for generating weather data is to use monthly-average values of meteorological quantities and statistical distributions to produce daily values of these same quantities. The daily values are selected by applying the long term, location-independent statistical patterns inherent in the meteorological records. Hourly values can then, in turn, be determined from the

daily values using statistical correlations [Duffie and Beckman, 1991; Knight, 1988].

Hourly meteorological data have traditionally been used as the input for solar energy simulations. However, their use may not be justified in some systems. Large variations in meteorological variables can occur within the space of an hour. This variation could result in different predicted system performance than if hourly average values were used. The solar radiation data available on a minute-by-minute basis is quite limited, but sufficient data are available to indicate the importance of using short-term data in modeling studies.

1.1 Cumulative Frequency Distribution of Clearness Indices

In this study, cumulative frequency distributions of clearness indices are employed extensively. A clearness index is the ratio of terrestrial to extraterrestrial radiation on a horizontal surface. The extraterrestrial radiation in W/m^2 can be expressed as:

$$G_0 = G_{sc} \, [1+0.033 \cos (360n/365)] \cos \theta_z \qquad (1.1)$$

where G_{sc} is the solar constant of 1367 W/m^2, n is the day of the year, and θ_z the solar zenith angle. The zenith angle is given by:

$$\cos \theta_z = \cos \varnothing \cos\delta \cos\omega + \sin\varnothing \sin\delta \qquad (1.2)$$

where $\varnothing$ is the latitude, δ is the declination angle, and ω is hour angle. The declination and hour angles are given by:

$$\delta = 23.45 \sin\left(\frac{360(284+n)}{365}\right) \qquad (1.3)$$

$$\omega = 15(\text{time}-12) \qquad (1.4)$$

where time is the solar time in hours.

For the purposes of this study, G_{sc} is taken be a constant over the period of a minute. Thus, a minute clearness index is expressed as

$$c_t = G/G_0 \qquad (1.5)$$

where G is the measured average radiation over a one minute interval. To calculate an hourly clearness index, Equation 1.1 must be integrated from ω_1 to ω_2, the initial and final hour angles for the hour to produce I_0, the hourly extraterrestrial radiation. The hourly clearness index is then:

$$k_t = I/I_0 \qquad (1.6)$$

To calculate a daily clearness index, Equation 1.1 must be integrated from sunrise to sunset, $-\omega_s$ to ω_s where

$$\cos \omega_s = -\tan\varnothing \tan\delta \qquad (1.7)$$

The result of the integration will be the value of H_0, the daily extraterrestrial radiation. The daily clearness index is then:

$$K_t = H/H_0 \qquad (1.8)$$

A cumulative frequency distribution of clearness indices has an x-axis of fractional time ranging from 0 to 1. The y-axis represents the clearness index ranging from 0 to 1. A point on the curve represents

the fractional amount of time that the actual clearness index is less than or equal to the corresponding value on the x-axis. Cumulative frequency distributions are obtained by integrating probability distributions. Figure 1.1 shows a probability distribution while Figure 1.2 shows its associated cumulative frequency distribution.

Liu and Jordan developed cumulative frequency distributions of daily clearness indices, K_t. They found that the distributions were very nearly identical for different locations having the same average daily clearness index, $\overline{K}_t$. They developed a set of generalized curves that reflected this location-independent behavior.

The Bendt [1981] distribution was developed to analytically represent the distribution of daily clearness indices. This analytical model was arrived at in a different manner than the original Liu and Jordan curves. While Liu and Jordan defined the distribution such that the mean is the long term average for a particular calendar month at a location, the Bendt distribution is defined so that all months with a mean of a specified value are part of the same distribution [Duffie and Beckman, 1991]. Nevertheless, the distributions are very similar. In addition, Whillier [1965] determined that the distribution of daily and hourly clearness indices are nearly the same. Thus, the Bendt distribution can be used to represent the distribution of hourly clearness indices as well.

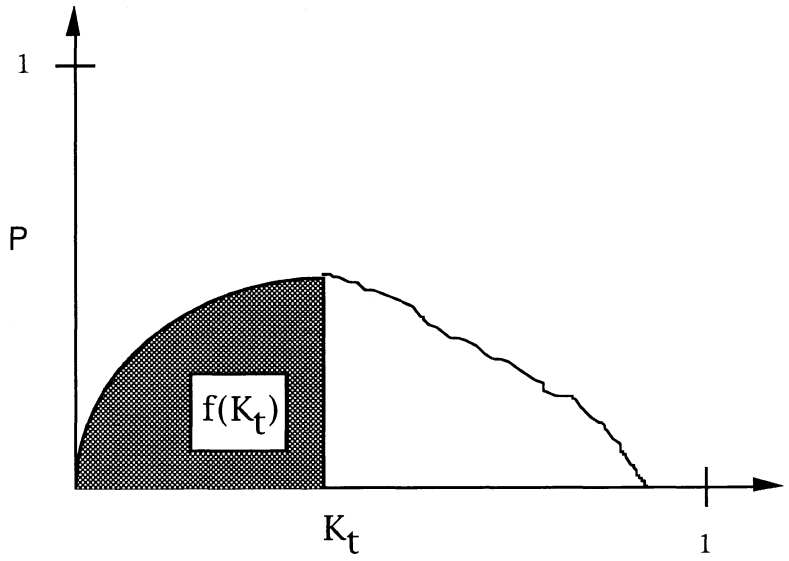

Figure 1.1 Probability Distribution of K_t

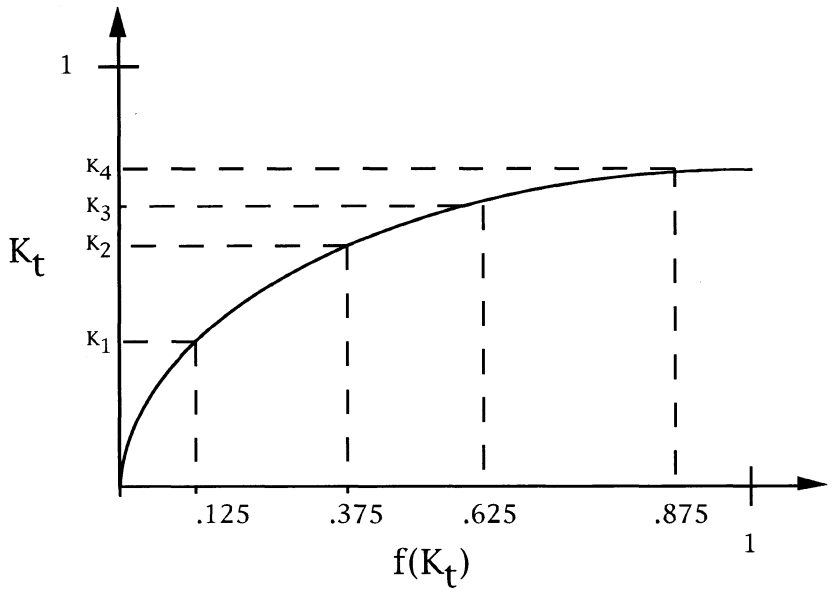

Figure 1.2 Cumulative Frequency Distribution of K_t

The Bendt distribution is defined by

$$f(K_t) = \frac{\exp(\gamma K_{t,\,min}) - \exp(\gamma K_t)}{\exp(\gamma K_{t,\,min}) - \exp(\gamma K_{t,\,max})} \qquad (1.9)$$

where $K_{t,\,min}$ is assumed to be 0.05 and $K_{t,\,max}$ is given by

$$K_{t,\,max} = 0.6313 + 0.267\,\bar{K}_t - 11.9\,(\bar{K}_t - 0.75)^8 \qquad (1.10)$$

γ was expressed implicitly by Bendt in a manner not easily solved. Herzog [1985] developed an explicit formulation for γ.

$$\gamma = -1.498 + \frac{1.184\,\xi - 27.182\,\exp(-1.5\,\xi)}{K_{t,\,max} - K_{t,\,min}} \qquad (1.11)$$

in which

$$\xi = \frac{K_{t,\,max} - K_{t,\,min}}{K_{t,\,max} - K_t} \qquad (1.12)$$

1.2 Autocorrelation

Most meteorological phenomena have some degree of autocorrelation. That is, the value of a meteorological quantity at some period in time is somewhat dependent on what it was in previous time periods. The autocorrelation of daily solar radiation has been widely investigated, e.g., Knight, [1988]; Graham, [1985]; Klein and Beckman, [1987]. An autoregressive model represents how the current value of a weather quantity depends on previous values

$$X_t = \varnothing_1 X_{t-1} + \varnothing_2 X_{t-2} + \ldots \varnothing_N X_{t-N} + \varepsilon_t \qquad (1.13)$$

where $\varnothing_i$ the lag-i autocorrelation coefficient. Many researchers [Knight, 1988]; Graham, [1985]; Klein and Beckman, [1987] say that daily solar radiation can be described by a first order autoregressive model.

$$X_t = \varnothing_1 X_{t-1} \qquad (1.14)$$

Only the lag-one coefficients have been investigated in this study. There are different methods for calculating autocorrelation coefficients. The method employed for estimating the lag-one autocorrelation coefficients is:

$$\varnothing_1 = \frac{\frac{1}{N}\sum_{i=1}^{N-1} (y_i - \overline{y})(y_{i+1} - y)}{\frac{1}{N}\sum_{i=1}^{N} (y_i - \overline{y})^2} \qquad (1.15)$$

1.3 Utilizability

Most solar-driven systems do not respond linearly to average solar radiation. As a result, the distribution of radiation around the average, as well as the average itself, are important. This effect can be quantified by a utilizability analysis. Utilizability is defined as the fraction of energy above a given critical level. Thus, at a very high critical level, such as 5000 kJ/m^2-hr (a value greater than the extraterrestrial for an hour), none of the energy is utilizable.

Klein [1978] defined daily utilizability as

$$\overline{\varnothing} = \frac{\int (I_T - I_{TC})^+ \, dt}{\int I_T \, dt} \qquad (1.16)$$

where I_T is an hourly value of tilted radiation, I_{TC} is the critical level of radiation.

Figure 1.3 shows how two hourly sequences can have the same average radiation, but different utilizability. More non-uniformity leads to higher utilizability. The first sequence has more variation in its hourly radiation values. With a critical level as shown, the first sequence shows utilizable energy while the second sequence indicates that there would be none.

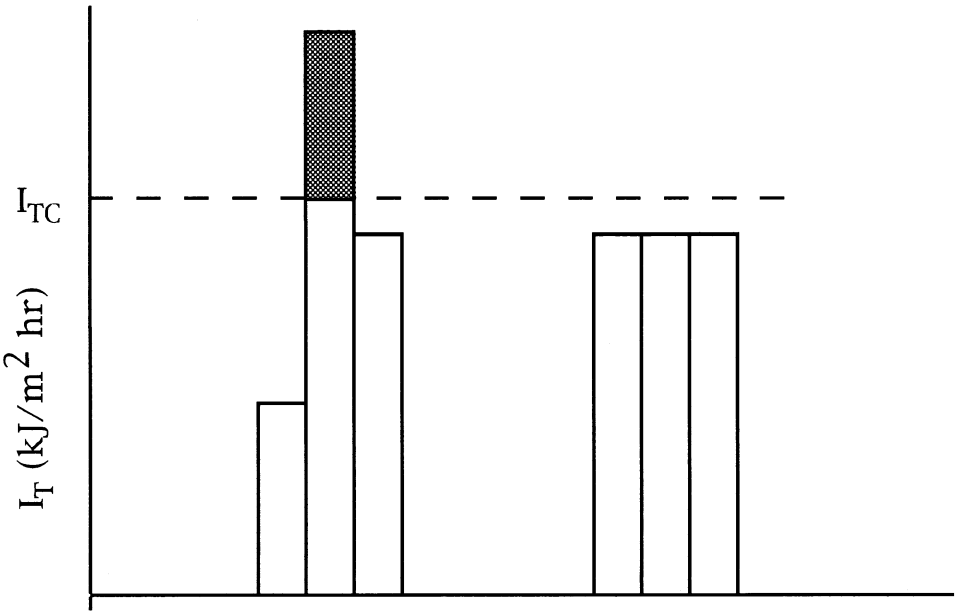

Figure 1.3 Utilizability of Solar Radiation

1.4 Solar Domestic Hot Water Systems

A solar domestic hot water system is a application in which solar radiation is transformed into heat. Water is pumped through a solar collector and the collector transfers the incident solar energy to the water thereby heating the water up. Other components that can be included in the system are heat exchangers, storage tanks, and auxiliary heaters.

The system used in the simulation studies here included all of these components. A typical system is shown in Figure 1.4. The water is pumped from the bottom of the tank to the collector. As it flows through the collector, the water is heated. This heated water

then flows back into the tank. If there is a need for hot water, some is drawn from the tank. Sometimes this water will not have been heated to the desired temperature. In this case, the auxiliary heater is employed to raise the water temperature to the desired temperature.

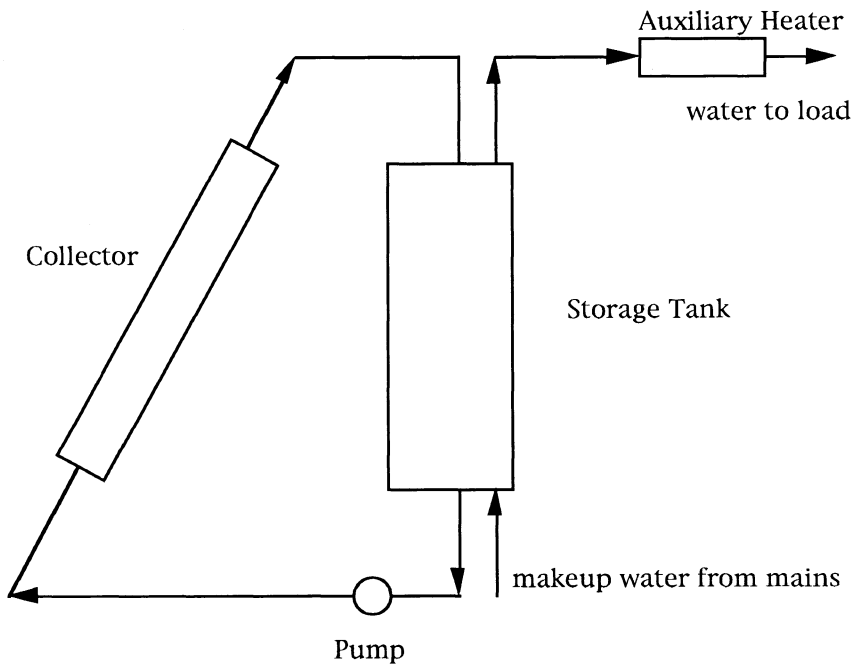

Figure 1.4 Schematic of a SDHW System

There are a number of important characteristics for a SDHW system. Of prime importance is the collector size, A_c. This term dictates how much solar energy can be collected. In addition to the area, there are other terms that affect collector performance. F_R, the collector heat removal factor, is defined as the ratio of how much useful energy the collector could obtain to the amount of useful

energy it could obtain if the entire collector surface were at the fluid inlet temperature [Duffie and Beckman, 1991]. An optical property that is integral to the collector performance is $(\tau\alpha)_n$, the transmittance-absorptance product at normal incidence. It is not the product of the transmittance and the absorptance of the collector components. Rather, it takes these terms into account along with the multiple reflections that occur within the collector itself. The incidence angle modifier, b_0, relates how the actual transmittance-absorptance product, $(\tau\alpha)$, relates to $(\tau\alpha)_n$ as the incidence angle is varied. The value of $(\tau\alpha)$ is obtained from:

$$(\tau\alpha)=(\tau\alpha)_n\left[1 + b_0\left(\frac{1}{\cos\theta} - 1\right)\right] \qquad (1.17)$$

Collector characteristics are usually given in the form of F_RU_L and $F_R(\tau\alpha)_n$.

The storage tank has two major characteristics; the volume, V, and the loss coefficient U_L. The water flow rates are also very important to the SDHW system. The two flows rates in this system are to the collector, $\dot{m}$, and to the load, $\dot{m}_L$. The important temperatures are the set temperature of water going to the load, T_{set}, and the water temperature from the mains, T_{main}, that went into to the tank to replace the drawn water. The values of these quantities are given in Table 1.1.

In this study, the quantity of interest in evaluating the performance of the SDHW system is solar fraction. The solar fraction, F, is the ratio of the energy supplied by the solar energy components to the energy required by a conventional system to meet all of the load. Since the auxiliary heater was taken to be 100% efficienct, the solar fraction is simply the ratio of the energy delivered by the solar

energy components to the total energy requirements of the load.

Parameter	Value
b_0	0.1
F	%
$F_R U_L$	15 $\frac{kJ}{m^2\ hr\ K}$
$F_R(\tau\alpha)_n$	0.7
$\dot{m}$	50 $\frac{kg}{hr\ m^2}$
$\dot{m}_L$	21.43 $\frac{kg}{hr}$ from 7:00 to 21:00
	0 from 21:00 to 7:00
T_{main}	15C
T_{set}	60C
U_L	1.44 $\frac{kJ}{m^2\ hr\ K}$
V	0.39 m^3

Table 1.1 Parameters in SDHW Model

Location	Collector Area A [m^2]	Collector Area B [m^2]
Albuquerque	2.6	4.0
Fort Worth	3.6	6.5
Madison	5.4	10.5
Miami	3.3	6.0
New York City	5.5	11.5
Seattle	6.3	15.0

Table 1.2 Collector Areas Sets A and B Solar Fraction Simulations

1.5 Photovoltaic Systems

While SDHW systems transform solar energy into heat, photovoltaic devices (PV) transform the solar energy into electrical energy. The incident solar energy provides photons which are absorbed causing electrons to flow from one side of a barrier to another. This flow produces an excess of electrons on one side and a deficiency of electrons on the other. If an external circuit is used to connect the two sides, the electrons will flow from one side to the other thus producing a current.

There are many important parameters in the operation of a PV cell. The most important and the most basic are the current (I), voltage (V), and power (P). The power is simply the product of the voltage and the current.

$$P=VI \tag{1.18}$$

The power can also be expressed in terms of the voltage and resistance

$$P=V^2/R \tag{1.19}$$

since

$$V=IR \tag{1.20}$$

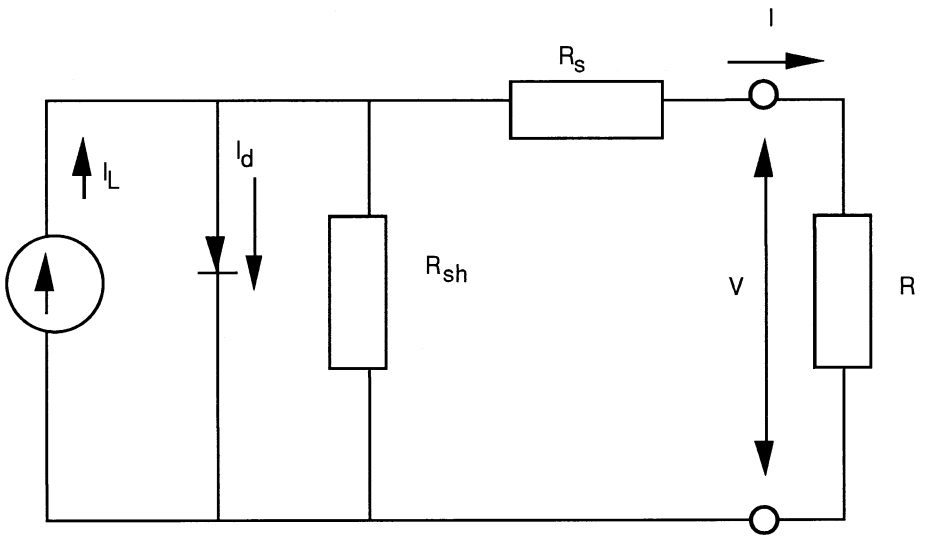

Figure 1.5 The Equivalent Circuit of a PV cell

Figure 1.5 shows the equivalent circuit of a PV cell. The modified SEL model [Al-Ibrahim, 1992] was used as the governing equations for the cell. The equations are implicit and cannot be solved directly. Table 1.2 gives the values of the parameters used in the study. The SEL model is as follows:

$$I = I_L - I_O \left[\left(\frac{V + I R_s}{a}\right) - 1\right] \qquad (1.21)$$

$$I_L = \left(\frac{S}{S_{ref}}\right)\left[I_{L,\,ref} + \mu_{isc}(T_c - T_{c,ref})\right] \qquad (1.22)$$

$$I_O = A_c\, k_{dev}\, a_0\, T_c^3\, \exp\left(\frac{E_{GO}}{kT_c}\right) \qquad (1.23)$$

$$R_s = \left[a_{ref} \ln\left(1 - \frac{I_{mp,\ ref}}{I_{L,\ ref}}\right) - V_{mp,\ ref} + V_{oc,\ ref} \right] \frac{1}{I_{mp,\ ref}} \quad (1.24)$$

$$T_c = T_a + \left(\frac{S\tau\alpha}{U_L}\right)\left(1 - \frac{\eta_c}{\tau\alpha}\right) \quad (1.25)$$

$$\eta_c = P/SA_c \quad (1.26)$$

$$\frac{\tau\alpha}{U_L} = \frac{T_{c,\ NOCT} - T_a}{G_{T,\ NOCT}} \quad (1.27)$$

NOCT is the Nominal Operating Cell Temperature, the temperature the cell reaches with no load operation [Duffie and Beckman, 1991].

$$a = a_{ref} \frac{T_c}{T_{c,\ ref}} \quad (1.28)$$

$$a_{ref} = \frac{V_{oc,\ ref}}{\ln(I_{sc,\ ref}/I_{O,\ ref})} \quad (1.29)$$

$$I_{O,\ ref} = A_c\ k_{dev}\ a_0\ T_{c,\ ref}^3\ \exp\left(\frac{E_{GO}}{kT_{c,\ ref}}\right) \quad (1.30)$$

As these equations show, the performance of the PV cell is dependent on the incident radiation and the ambient temperature. These equations are non-linear and implicit. There exist other equations for maximum power point tracking systems. However, they were not used. Instead, the preceding equations were used in an optimization process to maximize power.

Parameter	Value
a	volts
a_0	$1.54 \times 10^{45} \frac{\text{carrier}^2}{\text{m}^6\ \text{K}^3}$
a_{ref}	1.310 volts
A_c	0.5 m^2
E_{GO}	1.155 J/molecule
$G_{T,\,NOCT}$	800 W/m^2
S	W/m^2
S_{ref}	1000 W/m^2
T_a	Kelvin
T_c	Kelvin
$T_{c,\,NOCT}$	46C
$T_{c,\,ref}$	25C
I	amperes
$I_{L,\,ref}$	2.353 amperes
I_O	2.22×10^{-6} amperes
$I_{O,\,ref}$	9.38×10^{-7} amperes
$I_{mp,\,ref}$	1.985 amperes
$I_{sc,\,ref}$	2.353 amperes
k	8.62×10^{-5} J/K-molecule
k_{dev}	1.55×10^{-39} amps $m^4/carrier^2$
P	watts
R	ohms
R_s	1.547 ohms
V	volts
$V_{mp,\,ref}$	13.8 volts
$V_{oc,\,ref}$	19.3 volts
η_c	%
$\tau\alpha$	0.9
μ_{isc}	1.968×10^{-3} amps/K

Table 1.3 Parameters in PV Model

CHAPTER 2. Meteorological Models

2.1 Long Term Data (LTD)

A meteorological model used for the design of solar devices should represent the average conditions of a location as well as the statistical variations. It should do this on annual, monthly, daily, and even hourly bases. There are only a limited number of years of data from which the average conditions can be ascertained. These records are represented in the SOLMET long term data files. [SOLMET, 1978] The files are composed of hourly readings of meteorological phenomena, such as global horizontal and direct normal radiation, temperature, wind speed, wind direction, and other measurements for the period between 1952 and 1975. These records provide the best available estimates of the long term average conditions and a statistical description of the weather. It is against these records that any model which proposes to represent an annual set of meteorological data must be compared. The main disadvantage of these data is that there are only twenty-six cities for which this data has been collected. (The National Renewable Energy Laboratory (NREL) recently released a new set of long term data. The National Solar Radiation Data Base (NSRDB) will be a collection of data from 1961-1990 for 239 cities. However, there were only twenty-six primary stations. The secondary stations had their data generated by METSTAT. In all, only ten percent of the data in the NSRDB is real; the remaining ninety percent was generated by METSTAT) [NREL, 1992]).

2.2 Typical Meteorological Year (TMY)

To reduce the computational effort in simulation studies of solar

energy applications, a reduced data set termed typical meteorological year (TMY) files were developed [Menicucci and Fernandez, 1988]. The TMY files were derived directly from the LTD. The months that comprise the typical meteorological year are not averages but rather actual data. From the LTD, averages, cross-correlations and distributions were determined for a number of different weather indices. These statistical variables were determined for each month. A hierarchy of criteria was established to select from the twenty-three years of data the month which most accurately represented the LTD. The specified criteria cannot be completely met since no actual month will perfectly match the LTD conditions.

This process was performed for the twenty-six locations in the United States for which data were available. Data for many other locations, called ERSATZ data [Menicucci and Fernandez, 1988], were generated. These locations had some meteorological measurements such as cloud cover, sunshine hours, and daily integrated horizontal radiation. Correlations were developed to generate other meteorological quantities, including radiation, from the measured quantities.

2.3 Type 54 Weather Generator (GEN)

The Solar Energy Laboratory (SEL) has developed a meteorological data synthesizer called the Type 54 weather generator (GEN) [Knight, 1988]. It is a FORTRAN routine designed for use with TRNSYS [Klein, et al, 1990], the transient simulation program also developed at the SEL. GEN requires as input the monthly average daily global horizontal radiation, $\overline{H}$, ambient temperature, $\overline{T}$, and humidity ratio, ω, to produce a year of hourly meteorological data. With this model, simulations could be run for any location in which the monthly-average values of these quantities are known.

2.3.1 GEN Radiation Generation

From the monthly daily average radiation value, $\overline{H}$, the monthly average daily clearness index, $\overline{K}_t$, is computed.

$$\overline{K}_t = \overline{H}/\overline{H}_0 \qquad (2.1)$$

where $\overline{H}_0$, the monthly average daily extraterrestrial radiation, is evaluated at the mean day of the month.

The average daily clearness index is used to develop a cumulative frequency distribution of daily clearness indices, K_t, about a Bendt distribution of $\overline{K}_t$ (see Figure 1.2). By dividing the fractional time axis into equally sized segments whose number corresponds to the number of days in the month, the K_t values are determined. Figure 1.2 shows how the values of K_t would be determined if there were only four days in the month. These clearness indices are then ordered so that their lag-one autocorrelation is approximately 0.30. For an annual series of daily total radiation, the lag-one autocorrelation is in the range of 0.15 to 0.30 [Knight, 1988]. An annual series of daily radiation is used to determine the lag-one autocorrelation coefficient because monthly series of daily radiation can have values of $\varnothing_1$ ranging from -0.16 to 0.55 [Knight, 1988] that show seasonal and location dependence.

Once the daily clearness indices are known, the mean hourly clearness index can be determined from

$$k_{tm} = K_t (a + b \cos\omega) \qquad (2.2)$$

where

$$a = 0.409 + 0.5016 \sin(\omega_s - 60) \qquad (2.3)$$

$$b = 0.6609 + 0.4767 \sin(\omega_s - 60) \qquad (2.4)$$

However, a given hour will not have the mean hourly clearness index. The hourly clearness indices, k_t, are determined from the mean by a stochastic model developed by Graham [1985]. Knight [1988] used this model to find k_t from k_{tm}. The Graham model is as follows:

$$F_{kt} = \frac{1}{1 + \exp(-1.585\ h_{kt})} \qquad (2.5)$$

where

$$h_{kt} = \frac{k_t - k_{tm}}{\sigma} \qquad (2.6)$$

and

$$\sigma = 0.1557 \sin\frac{\pi K_t}{0.933} \qquad (2.7)$$

The distribution of k_t about k_{tm} is dependent on both the hour and the value of K_t. Thus, the k_t sequence will not be stationary. The Graham model transforms the k_t into a normally distributed variable, χ, with a mean of 0 and a variance of 1. The transformed variable is represented by

$$\chi_t = \varnothing\chi_{t-1} + \varepsilon_t \qquad (2.8)$$

At each hour, a value of χ is generated by selecting a random value of ε_t from a Gaussian distribution and applying Equation 2.8 with ε_t having a mean of zero and a variance of $1-\varnothing^2$.

The cumulative frequency distribution for a Gaussian distribution

with a mean of 0 and a variance of 1 is

$$F_{Gaussian} = \frac{1}{2}\left[1+\text{erf}\left(\frac{\chi}{\sqrt{2}}\right)\right] \qquad (2.9)$$

where

$$\text{erf}(y) = \frac{2}{\sqrt{\pi}}\int_0^y e^{-t^2}\,dt \qquad (2.10)$$

Equating the two cumulative frequency distribution functions and solving for k_t gives

$$k_t = k_{tm} - \frac{\sigma_a}{1.585}\ln\left[\frac{1}{0.5\left[1+\text{erf}\left(\frac{\chi}{\sqrt{2}}\right)\right]^{-1}}\right] \qquad (2.11)$$

To make sure that the hourly radiation values add up to the target daily value, the k_t values are corrected such that

$$\sum^{hours} k_t\, I_0 = K_t\, H_0 \qquad (2.12)$$

The diffuse fraction of radiation, D, is determined from Erbs' [1980] hourly diffuse fraction correlation. D is the percentage of the horizontal radiation, I, which is diffuse radiation, I_d. It depends on the value of k_t.

$$I_d = DI \qquad (2.13)$$

for $k_t \leq 0.22$

$$D = 1.0 - 0.09\ k_t$$

for $0.22 < k_t \leq 0.80$,

$$D = 0.9511 - 0.1604\ k_t + 4.388\ k_t^2 - 16.638\ k_t^3 + 12.336\ k_t^4$$

for $k_t > 0.80$,

$$D = 0.165$$

2.3.2 GEN Temperature Generation

Another stochastic model is used in the Type 54 weather generator to determine the ambient temperature. A distribution of daily temperatures are generated from the monthly average.

$$F_{temp} = \frac{1}{1 + \exp(-3.396\ h)} \qquad (2.14)$$

$$h = \frac{T - \bar{T}}{\sigma_m \sqrt{N_m/24}} \qquad (2.15)$$

$$\sigma_m = 1.45 - .0290\ \bar{T} + 0.664\ \sigma_{yr} \qquad (2.16)$$

where σ_{yr} is the standard deviation of the 12 monthly average temperatures, $\bar{T}$, about the yearly average temperature.

Subsequently, the hourly temperature values for a given day can be found by an employing that day's average temperature and the method described above for determining k_t. Erbs [1984] has found that σ_m is approximately the same as the standard deviation of the hourly temperatures. The resulting equation is

$$T_h = \overline{T}_h - \frac{\sigma_m \sqrt{N_m/24}}{3.396} \ln\left[\frac{1}{0.5\left[1 + \mathrm{erf}\left(\frac{\chi}{\sqrt{2}}\right)\right]^{-1}}\right] \qquad (2.17)$$

$$\frac{(\overline{T}_h - \overline{T})}{A} = 0.4632 \cos(t^* - 3.8005) + 0.0984 \cos(2t^* - 0.360) + 0.0168 \cos(3t^* - 0.822) + .0138 \cos(4t^* - 3.513) \qquad (2.18)$$

$$t^* = 2\pi (t - 1)/24 \qquad (2.19)$$

$$A = 25.8 \overline{K}_t - 5.21 \qquad (2.20)$$

t is hour of the day defined as t = 1 at 1AM and t = 24 at midnight.

Knight [1988] investigated the autocorrelation of hourly temperature. She found that a second-order autoregressive model could represent the behavior of χ.

$$\chi_t = \varnothing_1 \chi_{t-1} + \varnothing_2 \chi_{t-2} + \varepsilon_t \qquad (2.21)$$

From studying the TMY data for Albuquerque, Madison, and Miami, Knight found values of $\varnothing_1$ and $\varnothing_2$ that were geographically and seasonally independent. Knight determined $\varnothing_1$=1.178 and $\varnothing_2$=-0.202.

GEN determines a month of hourly temperatures at the beginning of the month. When performed in the manner presented above, the generated mean may not be equal to the input value. Once again a

correction factor was employed and used upon the hourly temperatures so that their monthly-average temperature matched that of the input exactly.

There are other correlations included in the model that determine wind velocity and relative humidity. However, these statistics were not investigated here.

2.4 Type 75 Compressed Weather Generator (COM)

Radiation and ambient temperature data consist of a deterministic and random components. The deterministic component is the average weather statistic for the given time interval while the random component denotes the difference between the actual and average values. GEN incorporates the random component in its calculations of hourly values for horizontal radiation and temperature. Schaefer [1991] proposed that the random component can be ignored. In this way, the deterministic component can be represented in a reduced number of days thereby reducing the time required for simulations. The Type 75 compressed weather generator (COM) employs this methodology. Four values of K_t, taken from a Bendt distribution of $\overline{K}_t$ (see Figure 1.2), are determined such that their average, over the reduced number of days in each month, matches up with $\overline{K}_t$. Thus,

$$\sum_{i=1}^{4} \frac{K_{t_i}}{4} = \overline{K}_t \qquad (2.22)$$

Then,

$$H = K_t H_0 \qquad (2.23)$$

with H_0 evaluated at the average day of the month.

COM uses a different method than that employed in GEN to evaluate the diffuse radiation. With a reduced number of days, there will not be the same sort of distribution of k_t about k_{tm} that a full month would have. Erbs found that using k_{tm} for k_t in the determination of hourly diffuse radiation was inadequate because of the difference between the assumed and actual k_t distributions. Because of compressed set of weather data would not have the distribution of an actual k_t distribution, Schaefer employed Erbs' [1980] daily correlations for diffuse radiation.

$$H_d = D_h H \qquad (2.24)$$

For $\omega_s < 81.4$,

if $K_t < 0.715$, $D_h = 1.0 - 0.2727\ K_t + 2.4495\ K_t^2 - 11.9514\ K_t^3 + 9.3879\ K_t^4$

otherwise, $D_h = 0.143$

For $\omega_s \geq 81.4$,

if $K_t < 0.722$, $D_h = 1.0 - 0.2832\ K_t - 2.5557\ K_t^2 + 0.8448\ K_t^3$

otherwise, $D_h = 0.175$

Then, for the hourly values,

$$I = r_t\ H \qquad (2.25)$$

$$I_d = r_d\ H_d \qquad (2.26)$$

$$r_t = \frac{\pi}{24}(a + b\cos\omega)\frac{\cos\omega - \cos\omega_s}{\sin\omega_s - \frac{\pi\omega_s}{180}\cos\omega_s} \qquad (2.27)$$

where a and b are given by Equations 2.3 and 2.4.

$$r_d = \frac{\pi}{24} \frac{\cos\omega - \cos\omega_s}{\sin\omega_s - \frac{\pi\omega_s}{180}\cos\omega_s} \qquad (2.28)$$

Finally, the hourly horizontal and diffuse radiation values are corrected such that their sums are exactly equal to the known monthly-average values.

$$\sum^{days}\sum^{hours} I = \bar{H}\,N \qquad (2.29)$$

and

$$\sum^{days}\sum^{hours} I_d = \bar{H}_d\,N \qquad (2.30)$$

For the temperature profiles, the compressed weather generator uses the same Erbs average normalized diurnal temperature variation model used in GEN (Equations 2.18-2.20). In order to determine the best sequence of the four days, Schaefer performed many simulations of a SDHW system using COM and compared the results to those calculated by GEN. He came to the conclusion that a sequence of four days per month, ordered by K_t 1-3-2-4 (4=clearest day), can well represent a month in a simulation.

2.5 Average Day (AVG)

The average day model (AVG) requires the same inputs as the compressed weather generator; namely, monthly average daily

horizontal radiation and ambient temperature. Equation 2.25 is used to calculate $\bar{I}$ from $\bar{H}$ at the midpoint of the hour on the average day of the month. The Erbs temperature model (Equations 2.18-2.20) is used to determine the hourly temperatures, $\bar{T}_h$, from $\bar{T}$. The meteorological data for the average day of the month are then used each day of the month. Every day is symmetrical about noon and identical to every other day in that month in terms of horizontal radiation and ambient temperature. This model was developed to determine validity of estimating system performance using a single average day to represent the month.

CHAPTER 3. Model Analysis

3.1 Introduction

The different meteorological models were compared to the LTD on the basis of a number of criteria. Monthly daily average radiation, monthly average daily radiation profiles, monthly and annual cumulative frequency distributions of daily clearness indices, and utilizability were all investigated. Simulations of a solar domestic hot water system, (SDHW), were also performed. One would expect that the TMY data would perform the best in these tests in that they were derived from the long term and consisted of real data.

The calculations were performed by TRNSYS. The Type 16 radiation model was used to calculate the extraterrestrial (and consequently clearness indices) as well as the the tilted radiation for each hour of every simulated year. The Erbs hourly correlation method (Equation 2.13) was used to determine the diffuse radiation from the horizontal, since all radiation values were based on the horizontal data. In the determination of the tilted radiation, the Perez anisotropic sky model [Perez, 1988] was used. A constant ground reflectance of 0.2 was assumed in all simulations throughout the entire year. COM determined tilted surface radiation values internally so Type 16 was not used in the analysis of COM data.

3.2 Average Radiation

For all of the models, the differences between model and long term in terms of average daily horizontal radiation were quite small. (see Figures 3.1-3.6) This result was to be expected because all of the models are based on horizontal radiation. The TMY results do not fall as close to the LTD averages as GEN and COM do. GEN and COM are

forced to have the LTD monthly averages. Still, all of the models produce results that are very close to the LTD averages.

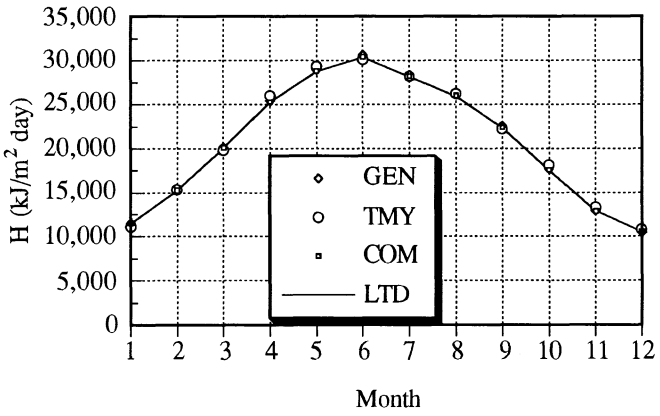

Figure 3.1 Monthly Average Daily Horizontal Radiation, Albuquerque

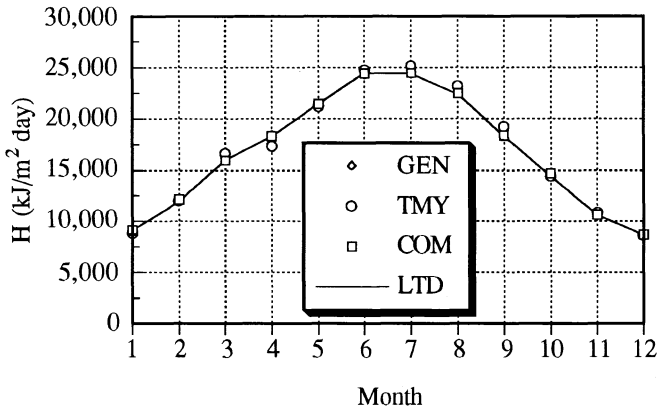

Figure 3.2 Monthly Average Daily Horizontal Radiation, Fort Worth

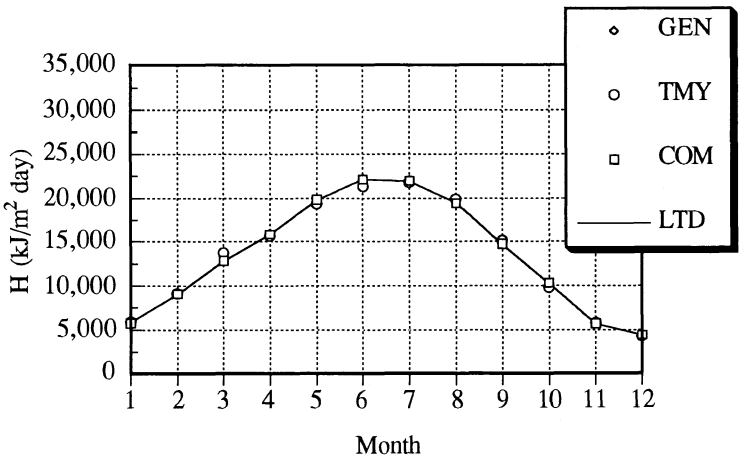

Figure 3.3 Monthly Average Daily Horizontal Radiation, Madison

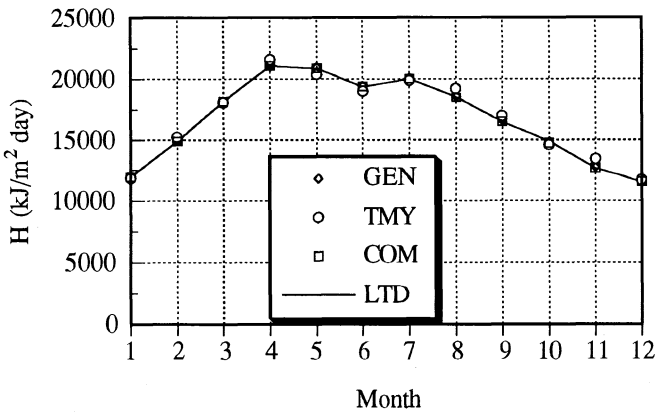

Figure 3.4 Monthly Average Daily Horizontal Radiation, Miami

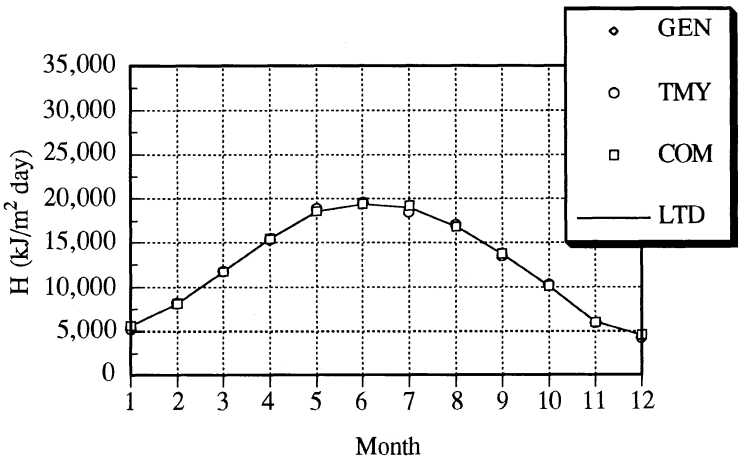

Figure 3.5 Monthly Average Daily Horizontal Radiation, New York City

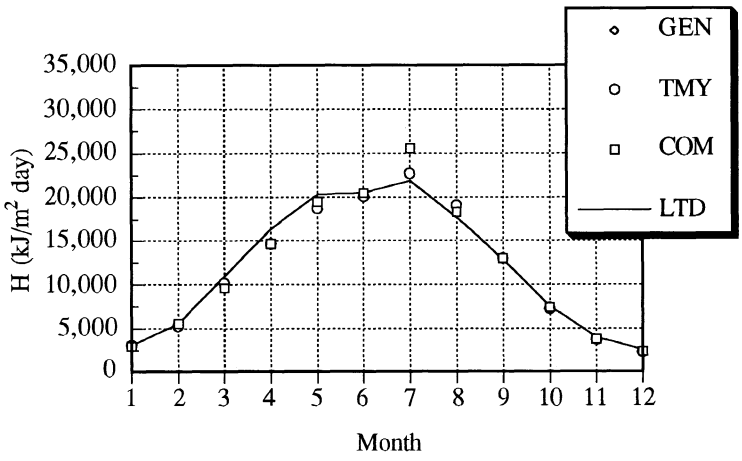

Figure 3.6 Monthly Average Daily Horizontal Radiation, Seattle

However, the differences are more pronounced for tilted radiation at a tilt equal to latitude (see Figures 3.7-3.12). GEN continues to correspond well; TMY and COM show some differences. COM in particular seems to underpredict in the winter months and then

overpredict in summer months. Nevertheless, the COM results fall close to the long term on an annual basis.

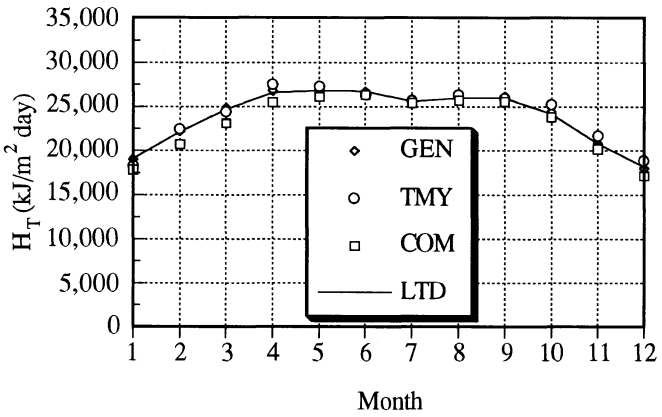

Figure 3.7 Monthly Average Daily Tilted Radiation, Albuquerque

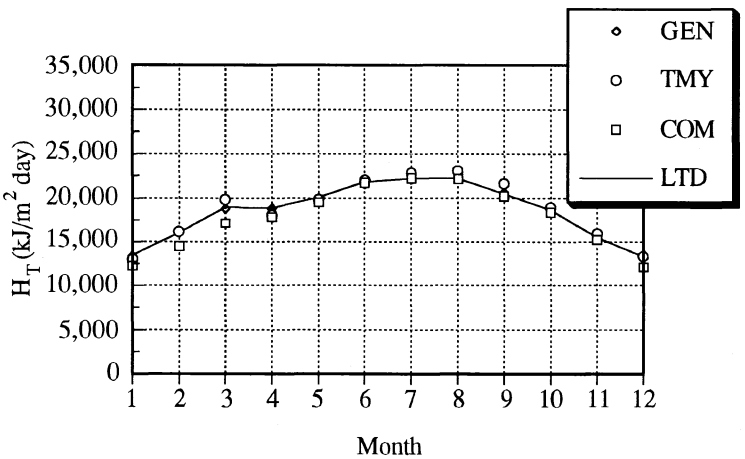

Figure 3.8 Monthly Average Daily Tilted Radiation, Fort Worth

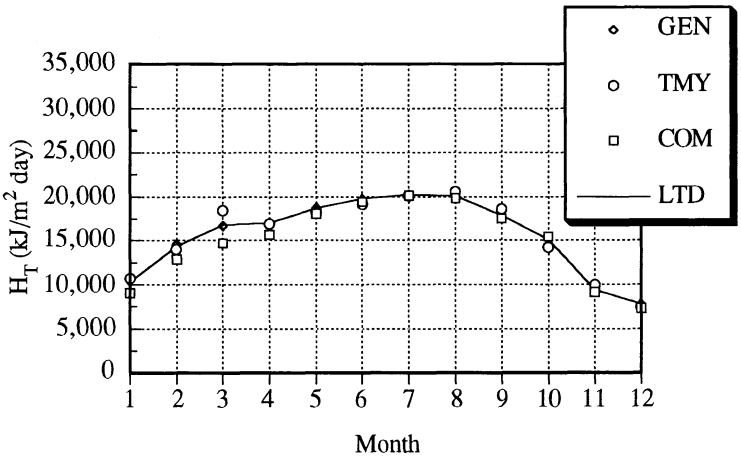

Figure 3.9 Monthly Average Daily Tilted Radiation, Madison

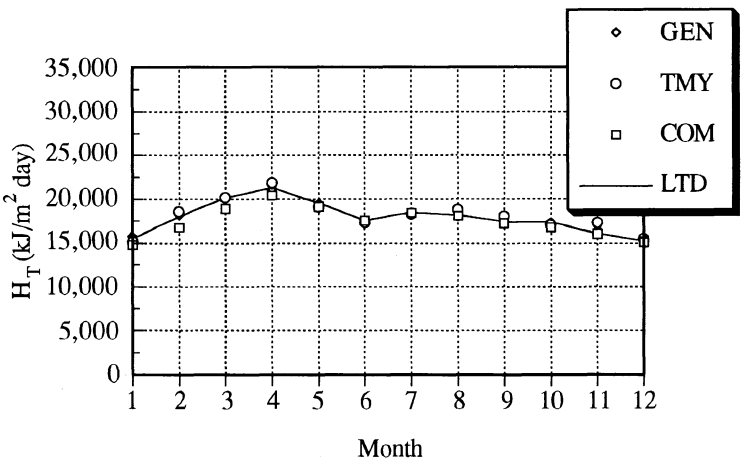

Figure 3.10 Monthly Average Daily Tilted Radiation, Miami

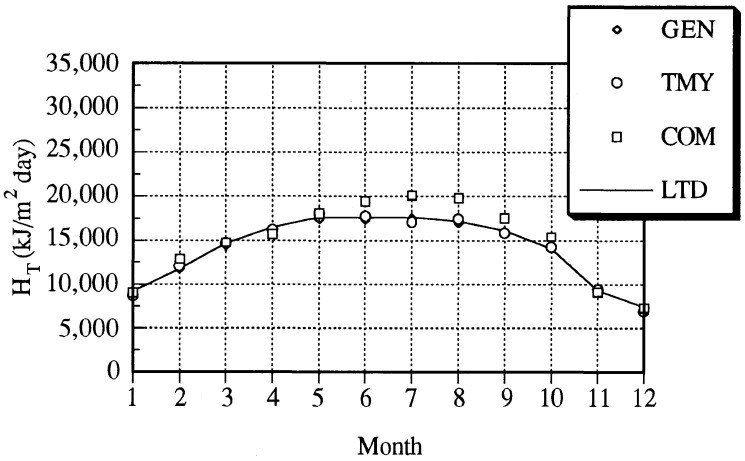

Figure 3.11 Monthly Average Daily Tilted Radiation, New York City

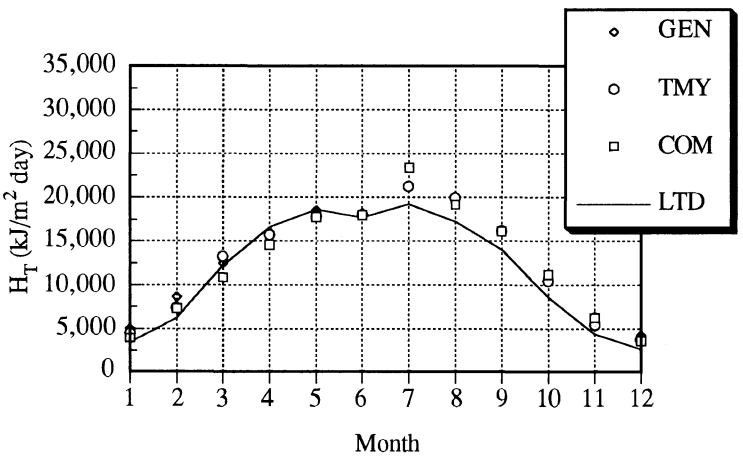

Figure 3.12 Monthly Average Daily Tilted Radiation, Seattle

3.3 Average Daily Profiles

In Appendix A, the average daily profiles of horizontal radiation for January and July are shown for the six locations. The plots show

that the models generally match the long term average diurnal patterns of horizontal radiation. They all follow a smooth cosine-like pattern centered about solar noon, as Equation 2.25 would indicate. The only exceptions are July in Seattle and Miami. Figure 3.6 shows that COM and GEN do not match the LTD value of monthly average daily horizontal radiation in Seattle either. This discrepancy leads to the conclusion that the input values used in GEN and COM are in error. With a erroneous value for $\overline{H}$, it is inevitable that the average diurnal patterns that GEN and COM produce would also be in error.

3.4 Utilizability

The utilizability analysis that was undertaken here compared hourly utilizability on an annual basis. From the way that it was defined, AVG will not be accurate in an utilizability analysis since every day is the average day, in terms of horizontal radiation. Utilizability for a tilted surface was calculated since this is the typical situation for a solar collector. Because the various solar angles change through the course of a given month, the values of hourly tilted radiation will not be the same for a given hour every day, even if the horizontal values are identical as in AVG. These geometric effects will create some non-uniformity in the AVG model's tilted radiation and thus cause the utilizability curve for AVG to deviate from a linear relationship with critical level..

In almost all cases, the AVG model predicts lower utilizability when compared to the LTD. (see Figures 3.13-3.18.) As explained earlier, it does not have much in terms of distribution; thus, its utilizability will be lower than other models. The curves for GEN, COM, and TMY fall very close to the LTD curves. TMY seems to overpredict when compared to LTD. The others seem to underpredict compared to LTD. AVG curves typically underpredict

by a considerable margin. The only exception is in Albuquerque, where every day is nearly the average day. Appendix B contains monthly bias errors in utilizability for each of the locations.

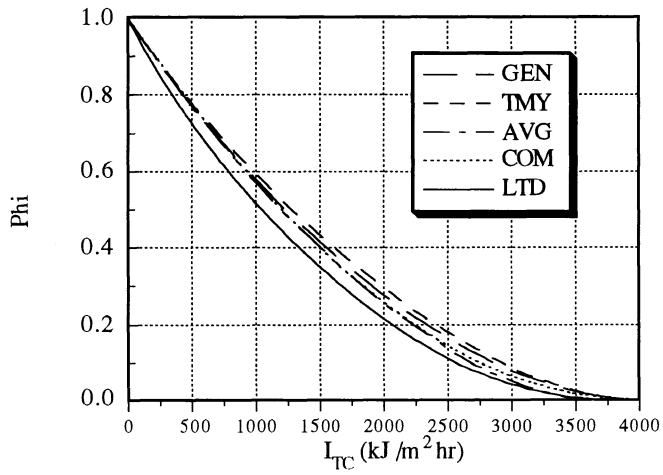

Figure 3.13 Annual Utilizability, Albuquerque

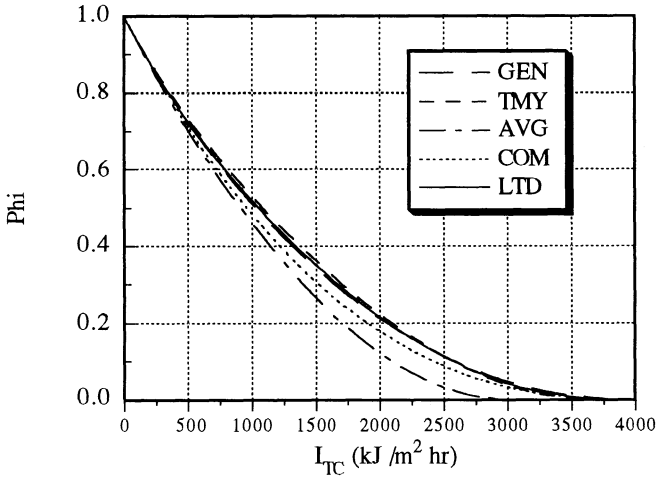

Figure 3.14 Annual Utilizability, Fort Worth

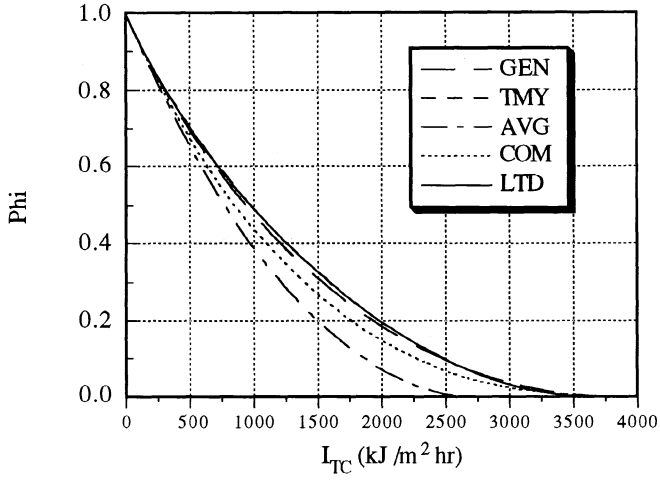

Figure 3.15 Annual Utilizability, Madison

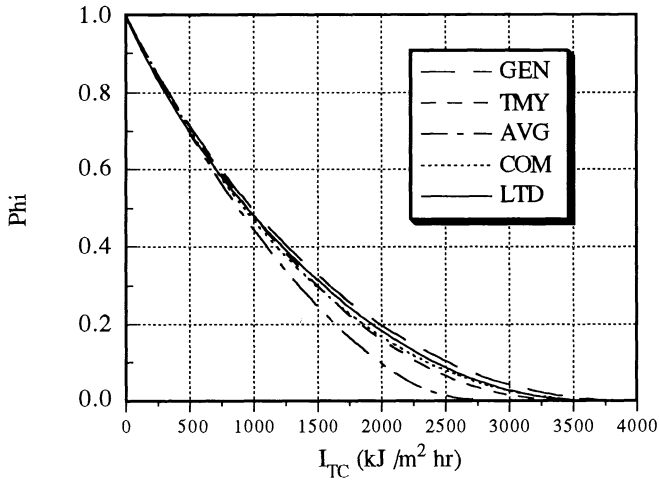

Figure 3.16 Annual Utilizability, Miami

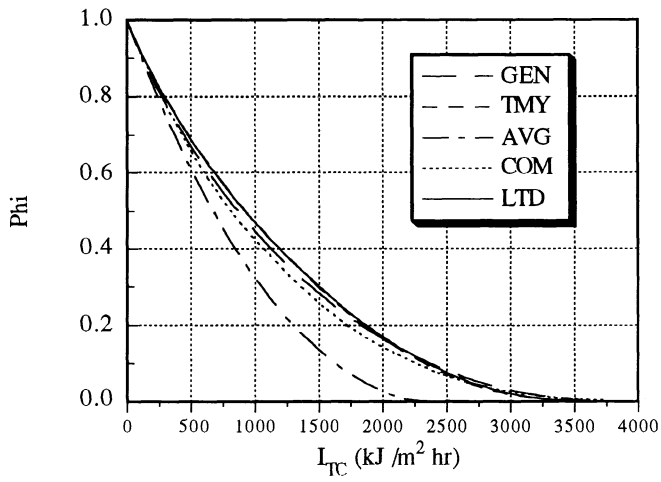

Figure 3.17 Annual Utilizability, New York City

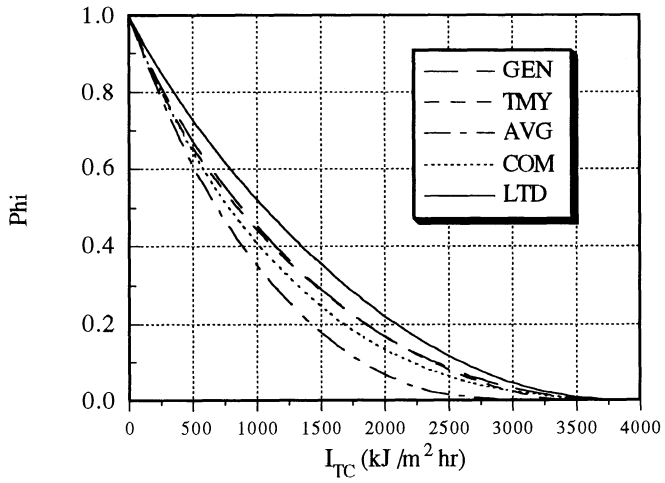

Figure 3.18 Annual Utilizability, Seattle

3.5 Cumulative Frequency Distribution

Annual cumulative frequency distributions of daily clearness indices were generated for all six locations. Both GEN and TMY fall very close to the long term in the cumulative frequency distributions (CFD) of K_t for Albuquerque. In fact, for all locations, TMY reproduces the CFD of long term almost exactly. (see Figures 3.19-3.25) GEN falls very close to the LTD curves, but not quite as close as TMY. Once again, because of the imposed uniformity, the AVG model results do not fall close to the LTD. It seems that TMY more accurately reproduces the behavior of the long term curve while GEN conforms more to a Bendt distribution, as it was designed to do. COM also does surprisingly well considering that it contains only four values of K_t per month.

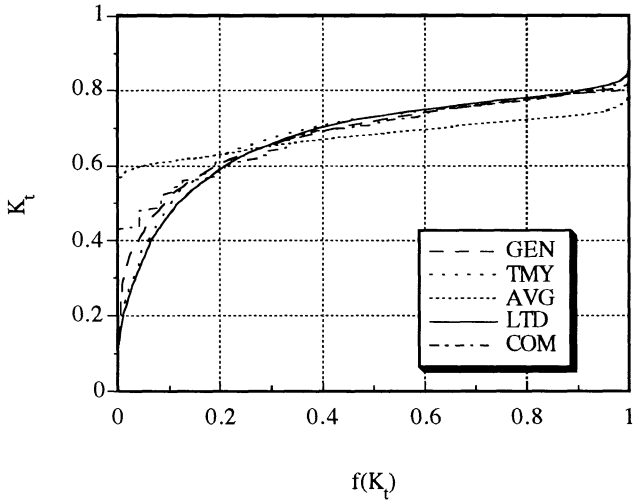

Figure 3.19 Annual Cumulative Frequency Distribution of K_t, Albuquerque

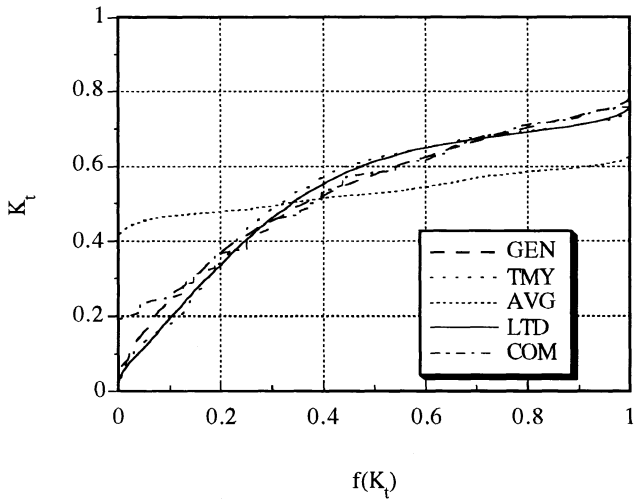

Figure 3.20 Annual Cumulative Frequency Distribution of K_t, Fort Worth

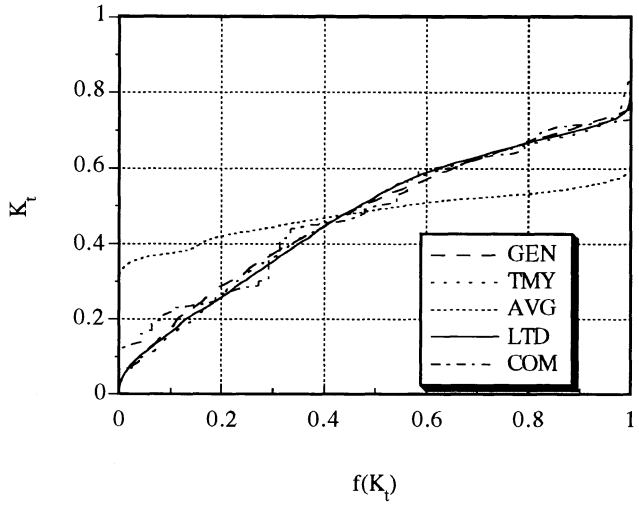

Figure 3.21 Annual Cumulative Frequency Distribution of K_t , Madison

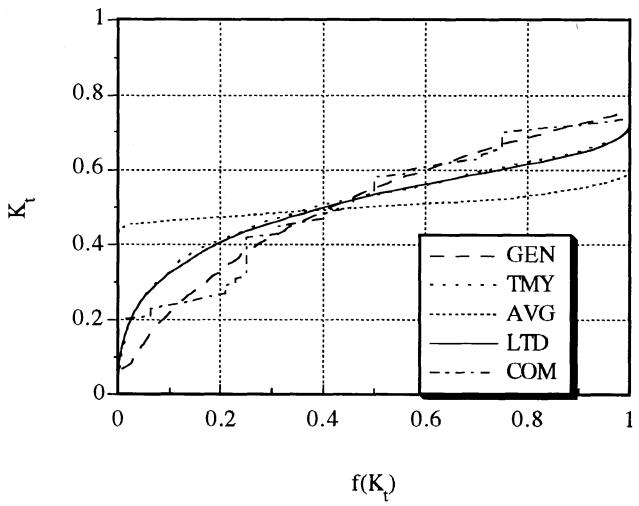

Figure 3.22 Annual Cumulative Frequency Distribution of K_t, Miami

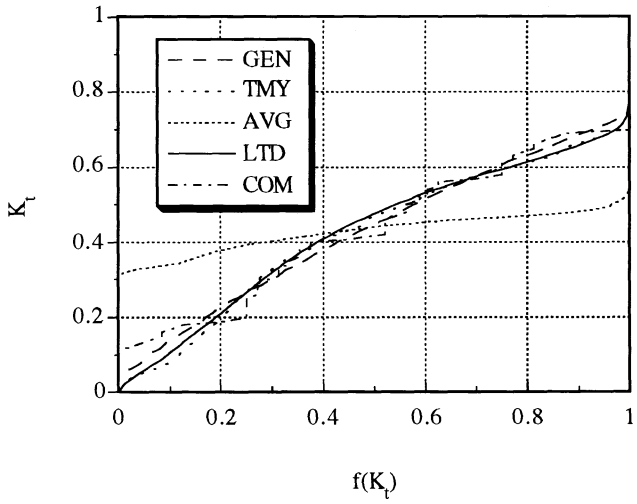

Figure 3.23 Annual Cumulative Frequency Distribution of K_t, New York City

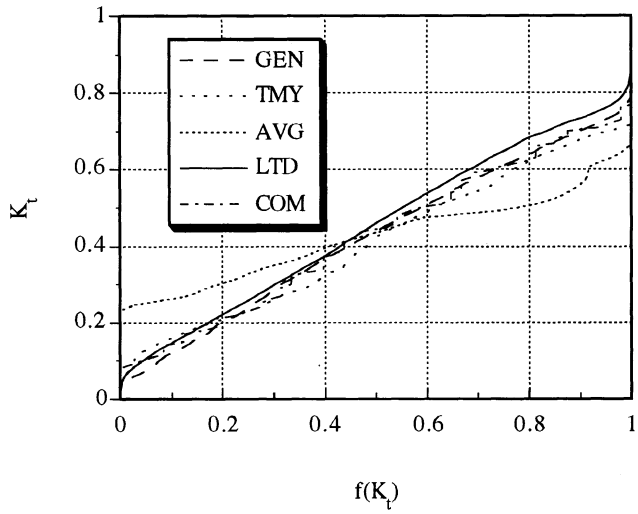

Figure 3.24 Annual Cumulative Frequency Distribution of K_t, Seattle

3.6 Criticism of Generated Weather

Both of the weather generators work on the premise of the hourly clearness indices in a month are based on the monthly daily-average clearness index, $\overline{K}_t$. Daily values of K_t are generated from $\overline{K}_t$ and the hourly clearness indices are generated from the daily values. Looking at this method statistically, the probability of a given hour clearness index, $P(k_t; K_t, \theta_z)$ can be scaled by the mean clearness index for the hour k_{tm}. By a similarity hypothesis, the scaling of $P(k_t; K_t, \theta_z) / k_{tm}$ should be similar for all θ_z.

Collares-Pereira and Aguiar [1992] claim that such similarity does not exist because it has the deficiency of mixing days and hours of differing characteristics. In its stead, they propose that the hourly clearness indices, k_t, should be grouped by its solar altitude angle, α ($\alpha = 90 - \theta_z$), and daily clearness index, K_t. They performed an analysis with data from six locations in Europe and Africa. Probability distributions were generated on the basis of days of a given K_t. For each K_t, the data were grouped by the hourly α, which they termed "h". The results for Athens, Greece, are shown in Figures 3.25 and 3.26. As Collares-Pereira and Aguiar explain, for a low K_t, the distributions are essentially the same for all solar altitude angle values. In contrast, for a high K_t, the hourly radiation does not display the same behavior. There is a marked peak at $k_t/k_{tm}=1$ and this peak becomes larger as α increases.

This discovery impacts strongly on the manner in which weather data are generated by GEN and COM. Collares-Pereira and Aguiar have stated that the manner in which the generation is accomplished was not encouraging in that the shape of the resulting synthetic distribution was not found to improve significantly with respect to pure Gaussian models. In addition, it has been reported [Fulop, 1992] that using some European averages with GEN gives markedly

erroneous results when compared to real data.

The long term data was employed to see if such zenith angle dependencies exist in U.S. data. The twenty-six years worth of data for the six locations were processed in order to find k_t, θ_z, and K_t. The data were grouped by K_t and by $\cos(\theta_z)$. Figures 3.27-3.38 show the results for the six U.S. locations. At low K_t, the curves are nearly the same, irrespective of zenith angle. At high K_t, there are noticeable differences in the curves.

At a low K_t, the probability plots are similar. There is no noticeable difference as $\cos(\theta_z)$ is varied. The distribution is very uniform. This uniformity indicates a significant variation about the value $k_t/k_{tm}=1$. At a high K_t, the distributions have a sizeable peak around $k_t/k_{tm}=1$. Furthermore, the magnitude of the peak increases at high $\cos(\theta_z)$ and at high K_t, suggesting that on clear days, hours are more likely to be at k_{tm} and the likelihood is stronger for the central hours for the day. On cloudier days, there is more of a distribution around k_{tm} and the likelihood is independent of time of day. Thus, GEN and COM may be deficient in reproducing these statistics. Collares-Pereira and Aguiar [1992] have proposed their own weather synthesis model that embodies their findings. It allows values of k_t to be determined for a day with a given K_t and it incorporates correlations developed for the standard deviation and autocorrelation in the evaluation of k_t.

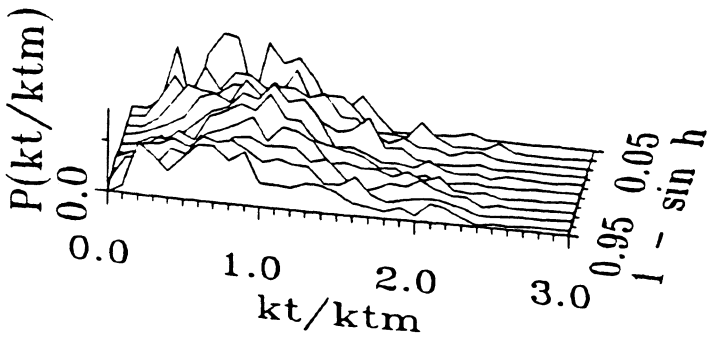

Figure 3.25 Probability Plot, $0.25 < K_t \leq 0.30$, Athens

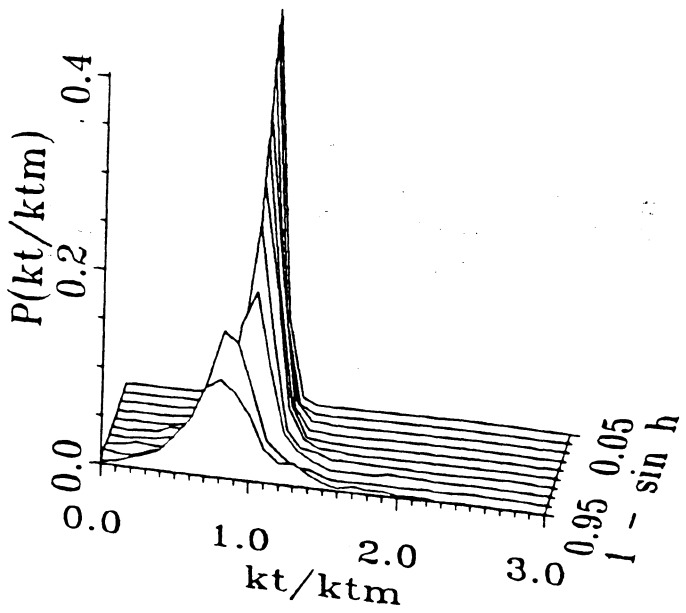

Figure 3.26 Probability Plot, $0.65 < K_t \leq 0.70$, Athens

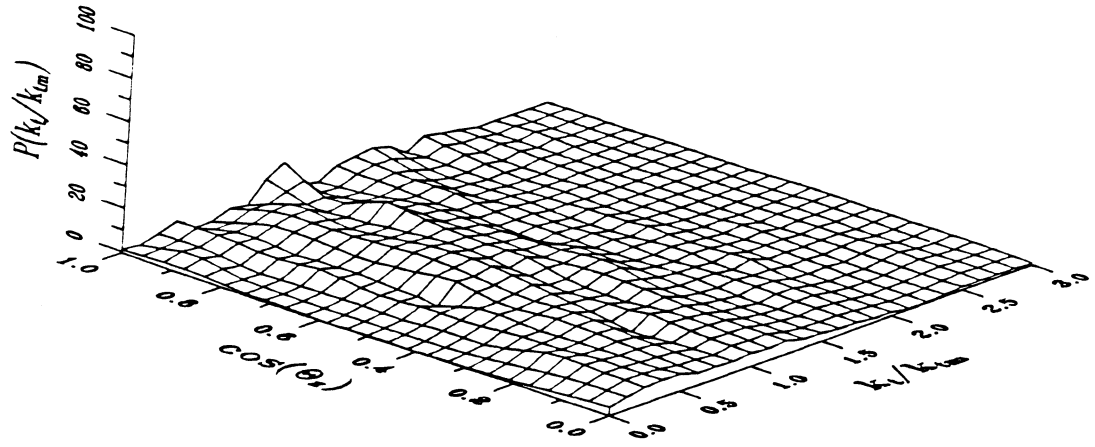

Figure 3.27 Probability Plot, $0.25 \leq K_t < 0.30$, Albuquerque

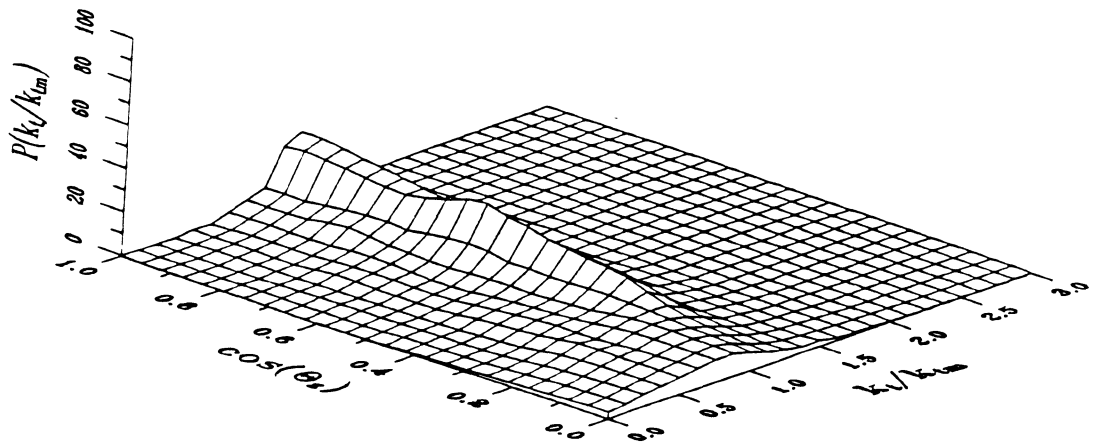

Figure 3.28 Probability Plot, $0.65 \leq K_t < 0.70$, Albuquerque

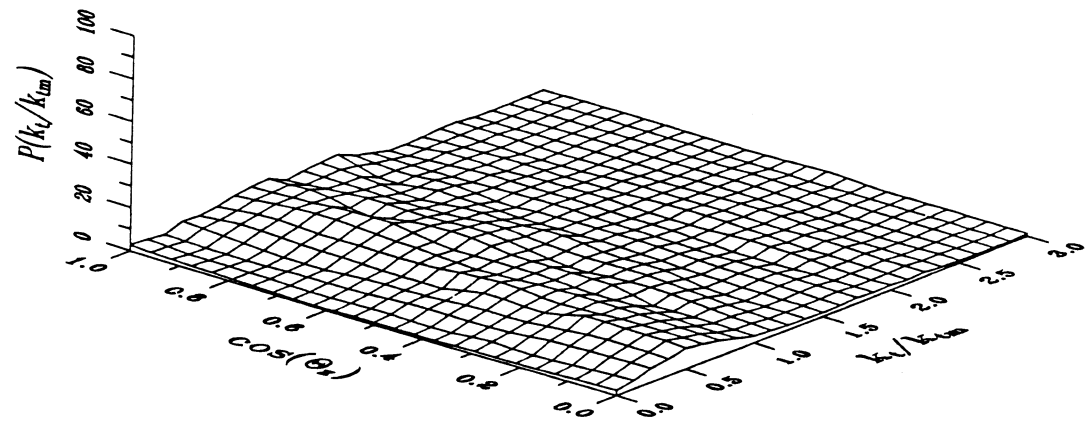

Figure 3.29 Probability Plot, $0.25 \leq K_t < 0.30$, Fort Worth

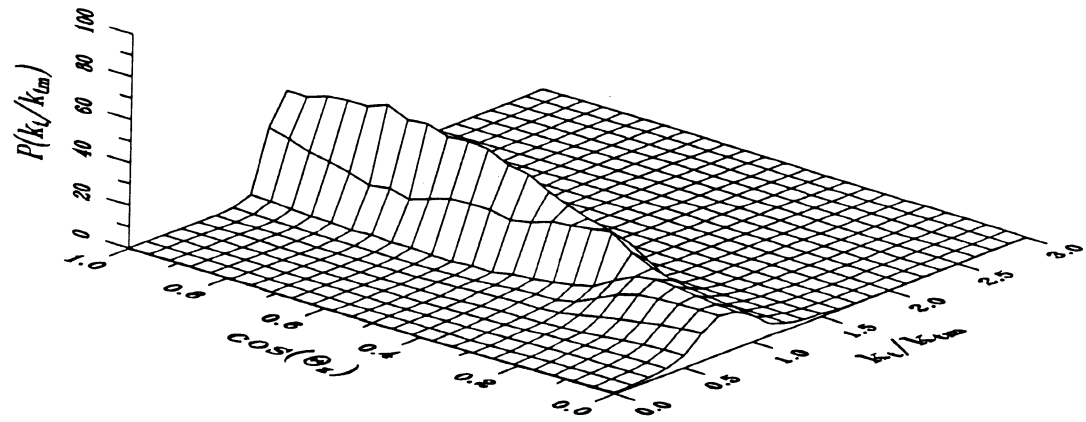

Figure 3.30 Probability Plot, $0.65 \leq K_t < 0.70$, Fort Worth

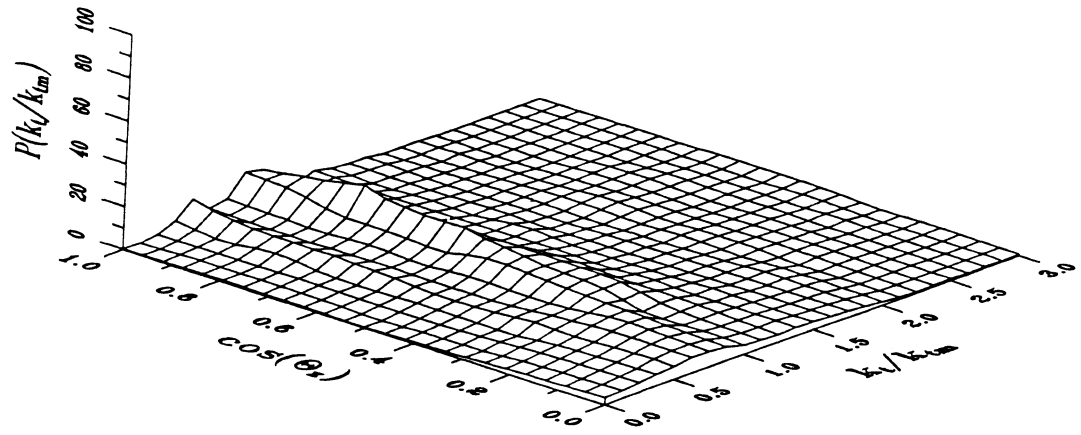

Figure 3.31 Probability Plot, $0.25 \leq K_t < 0.30$, Madison

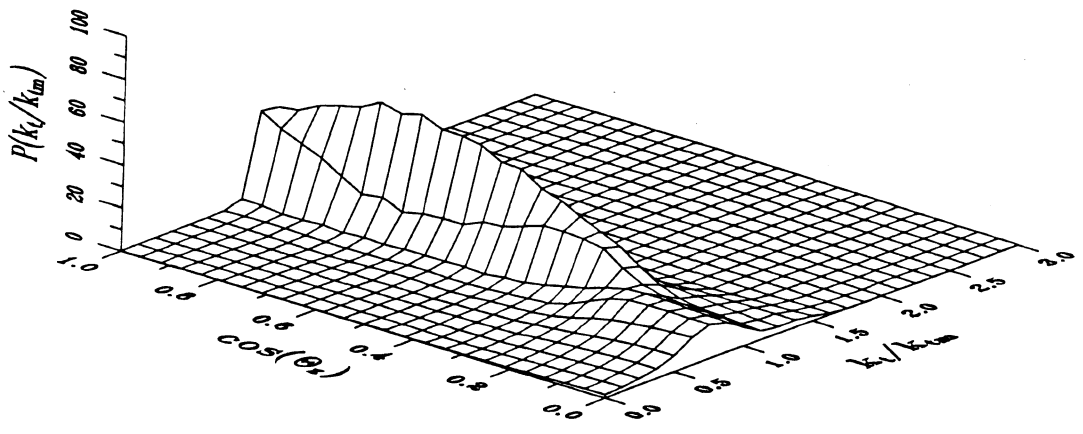

Figure 3.32 Probability Plot, $0.65 \leq K_t < 0.70$, Madison

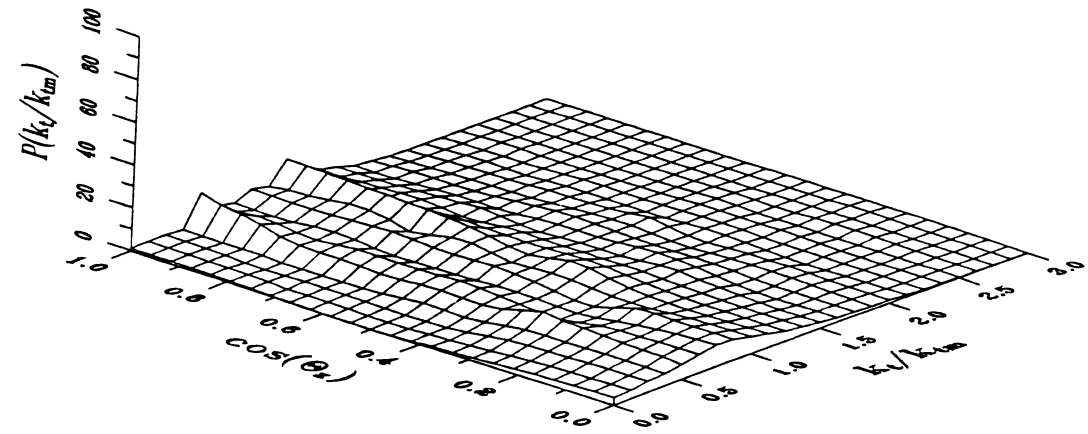

Figure 3.33 Probability Plot, $0.25 \leq K_t < 0.30$, Miami

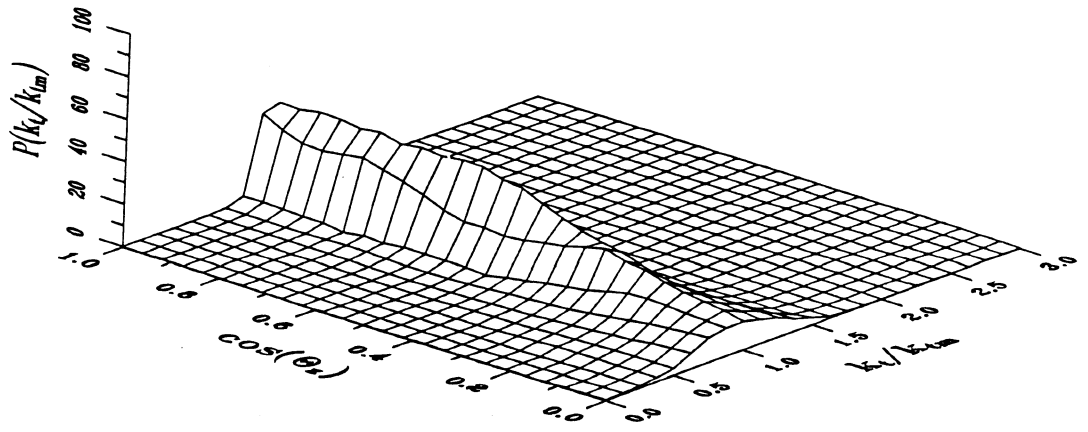

Figure 3.34 Probability Plot, $0.65 \leq K_t < 0.70$, Miami

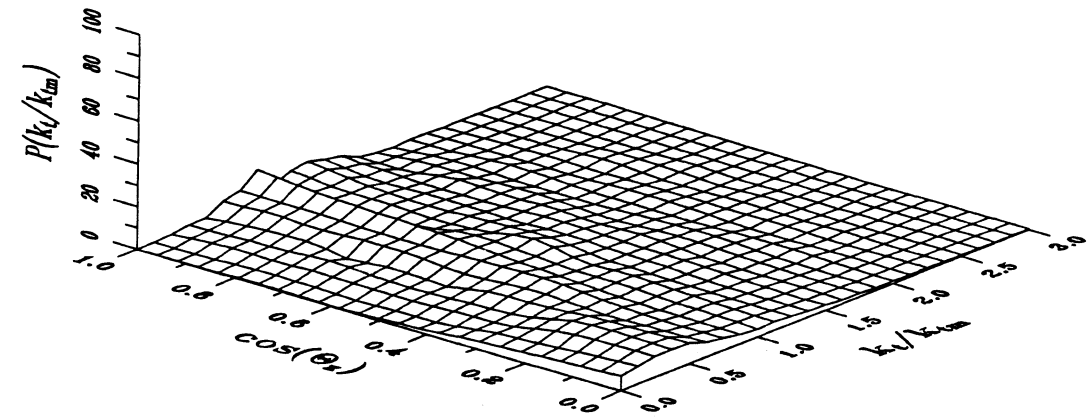

Figure 3.35 Probability Plot, $0.25 \leq K_t < 0.30$, New York City

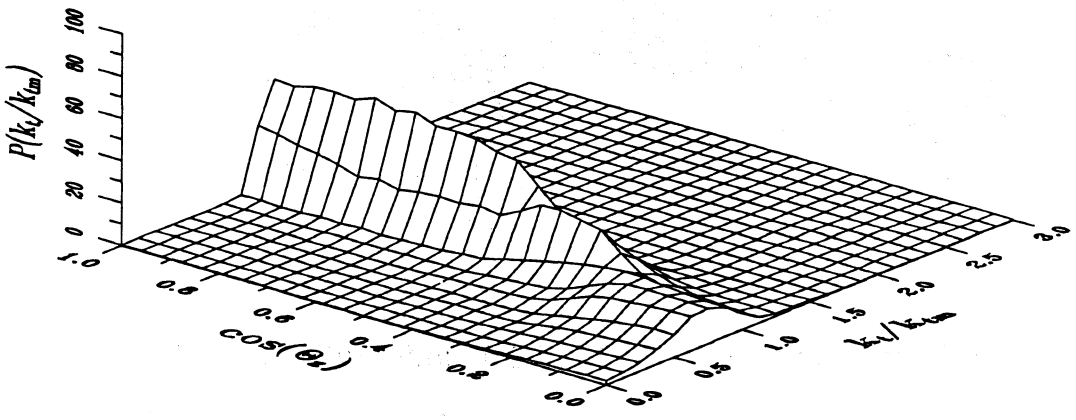

Figure 3.36 Probability Plot, $0.65 \leq K_t < 0.70$, New York City

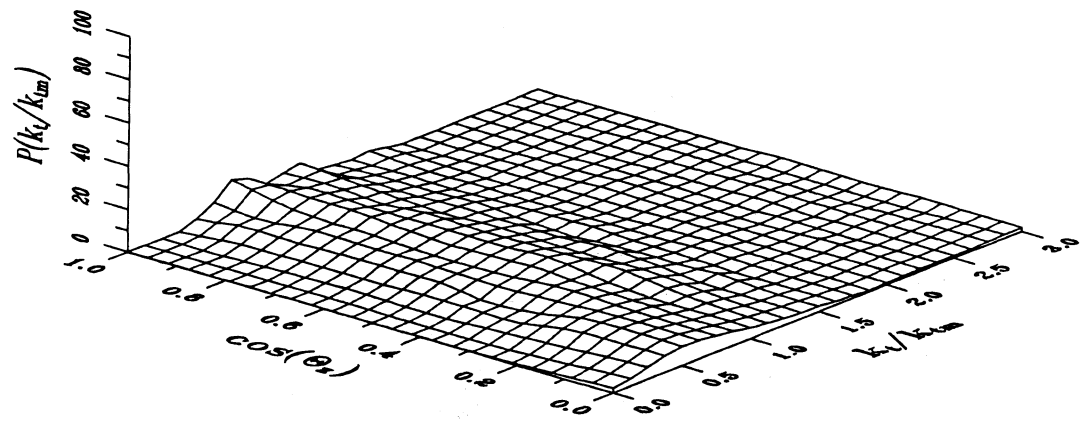

Figure 3.37 Probability Plot, $0.25 \leq K_t < 0.30$, Seattle

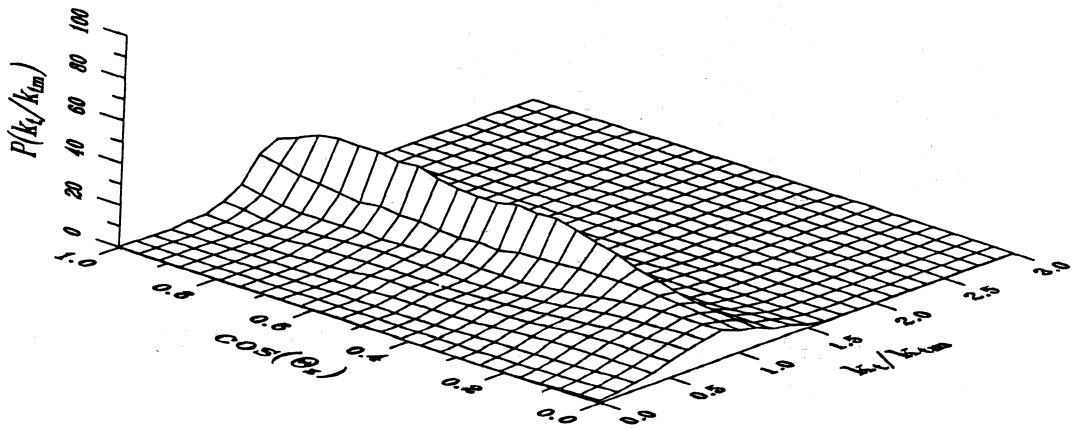

Figure 3.38 Probability Plot, $0.65 \leq K_t < 0.70$, Seattle

The two weather generators, GEN and COM, generate the k_t values from k_{tm}. However, the model for k_t was developed by binning all days together and comparing k_t to k_{tm}. While k_{tm} and σ are indeed a function of K_t, this method has proved to be insufficient. The problem is that the data are grouped by hour pair. While this may be appropriate for a monthly scale, it is not appropriate on a yearly scale. The geometry is different for a given hour in January than it is in June. Namely, the zenith angle, θ_z, changes. Figure 3.39 shows how the zenith angle of each of the hour pairs for Albuquerque changes considerably from month to month.

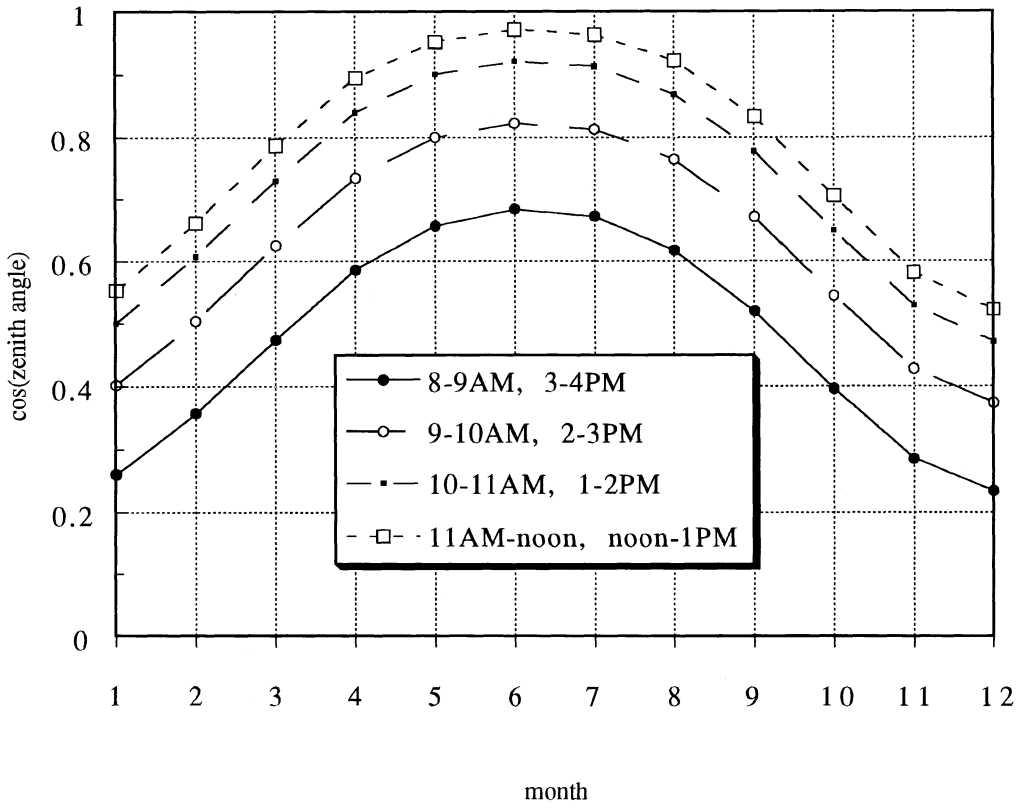

Figure 3.39 Variation of zenith angle on the Average Day of the Month, Albuquerque

As has been shown, zenith angle effects can have strong effects on clearness index distribution. While the k_t model in GEN does fit the long term data, it is because that data have been mixed as well, in terms of zenith angle. Furthermore, the equation that is used for σ, Equation 2.7 was originally derived by Graham to fit a_{kt}:

$$a_{kt}=k_t-k_{tm} \qquad (3.1)$$

The sinusoidal form of Equation 2.7 proposes that the standard deviation of a_{kt} is low for both low and high values of K_t while it peaks for intermediate values of K_t. Knight [1988] found this to be true for the long term data of Albuquerque, Madison, and New York City. This behavior implies that a probability distribution around the value of k_{tm} for a value of K_t would be be flatter and wider the farther K_t was from 0.5. However, this does not seem to be the case.

3.7 Hourly Simulation Comparisons

A solar domestic hot water system was simulated using radiation and temperature produced by different models. In Section 1.4, the important characteristics of the SDHW were described

Figure 3.40 shows how the different models worked when the annual solar fraction target was 50% with the low loss collector. Collector areas were chosen for each location so that the solar fraction would be in the vicinity of 50%. TMY seems to do the best in representing the long term performance for this setup. The AVG model consistently gives incorrect estimates. However, the other three models compare quite favorably to the long term results

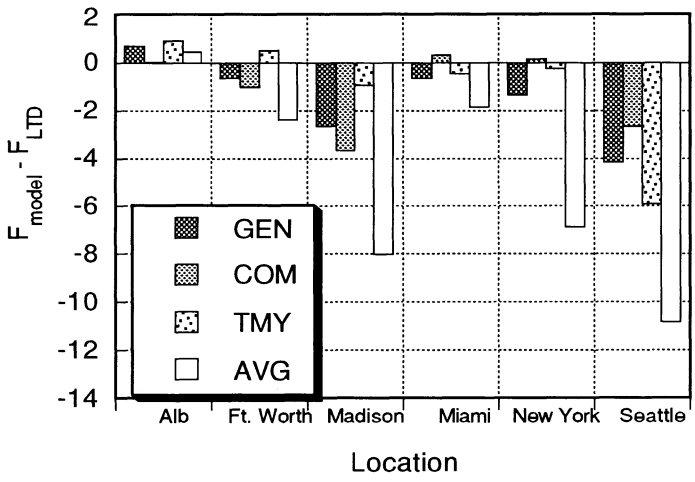

Figure 3.40 Difference in Solar Fractions, $F_R U_L$=15 kJ/m^2-K-hr, Collector Area Set A

When a higher loss collector ($F_R U_L$=30 kJ/m^2-K-hr), but with the same collector area as before is used in the system, the differences between the models increase. Figure 3.41 displays these results. For some of the locations, the model choice does not seem to matter. However, for some locations, the differences become much more noticeable. COM tends to indicate lower performance than GEN.

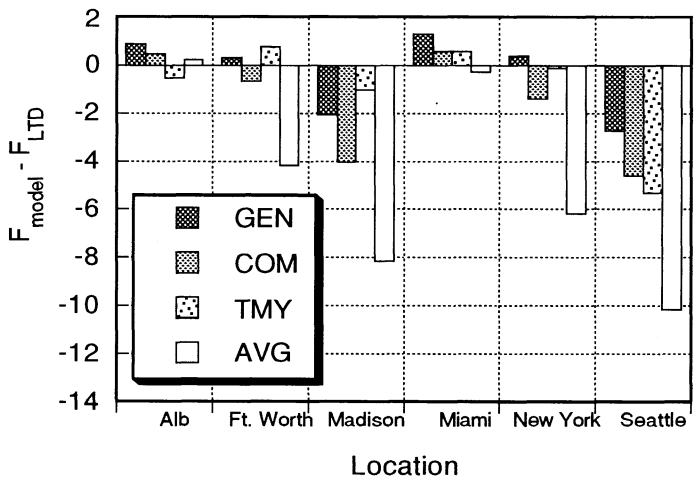

Figure 3.41 Difference in Solar Fractions, F_RU_L=30 kJ/m^2-K-hr, Collector Area Set A

Additional simulations were performed with a different solar fraction target. The collector sizes were adjusted so that an annual solar fraction of 75% was achieved. The flow rate per unit collector area was maintained as was the size of the storage tank. Additionally, a higher value of F_RU_L was used but with the same collector size as for the 75% target.

TMY seems to represent the long term performance better than the other models. GEN does an admirable job, and COM does well, though it tends to underpredict performance. All of the models have difficulty in producing accurate results for Seattle. AVG results show the greatest differences when compared to the LTD performance.

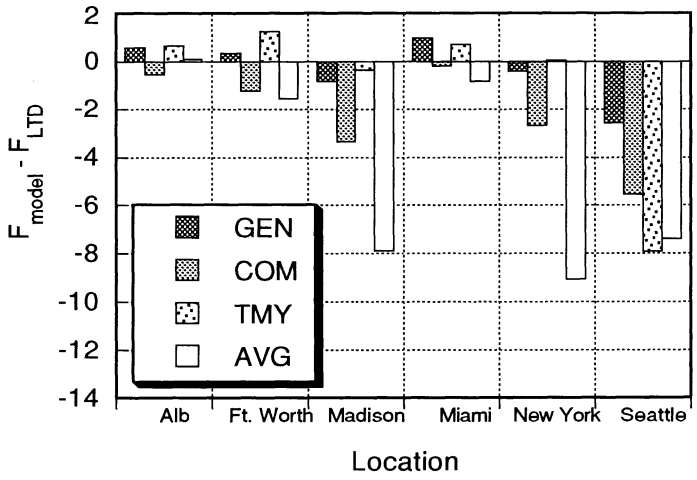

Figure 3.42 Difference in Solar Fractions, $F_R U_L$=15 kJ/m^2-K-hr, Collector Area Set B

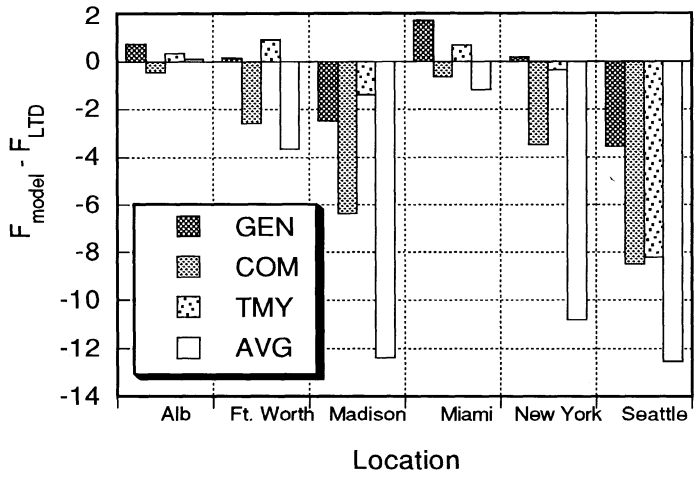

Figure 3.43 Difference in Solar Fractions, $F_R U_L$=30 kJ/m^2-K-hr, Collector Area Set B

CHAPTER 4. Minute Radiation

4.1 Introduction

Simulation studies have traditionally been performed using hourly data. Data for shorter time periods are generally unavailable for extended periods. Hourly data are appropriate for systems that respond linearly to solar radiation input. However, for a system that responds non-linearly, the variation of radiation as well as temperature within an hour could have significant effects upon system performance. More non-uniformity in solar radiation leads to higher utilizability and consequently better system performance. Variation within an hour has been typically determined by two methods; linear interpolating between two hourly values or following the variation of extraterrestrial radiation. However, analysis of minute-by-minute data shows that there can be a great deal of non-uniformity of minute clearness indices, c_t, within a given hour.

4.2 Analysis of Previous Work

Suehrcke [1991] has proposed a model in which minute radiation behaves markedly different from the average hourly values. The model introduces the concept of a bimodal shape to a cumulative frequency distribution curve. When plotted as a cumulative frequency distribution, hourly values will usually follow a Bendt distribution about their average k_t. When such hours are grouped on the basis of airmass and are compared to minutes corresponding to that airmass range, distinct differences can be observed. Suehrcke found this behavior in data that he collected for Perth, Australia. From these results, he derived a mathematical model to explain the bimodal shape of the minute curve.

Suehrcke proposed that there are three regions in which the clearness indices of minute radiation lie. Suehrcke uses k to represent the minute clearness index and $\bar{k}$ to represent the hourly clearness index. Suehrcke's model is as follows:

$$q(k)= \begin{cases} q_1 \text{ for } k_0 \le k \le k_1 \\ q_2 \text{ for } k_1 \le k \le k_2 \\ q_3 \text{ for } k_2 \le k \le k_3 \end{cases} \qquad (4.1)$$

By fitting the data, he found

$$q_1 = 1.0 \qquad (4.2)$$

$$q_2 = 0.14 \qquad (4.3)$$

$$q_3 = 1.831\ e^{-0.202\ m} \qquad (4.4)$$

and

$$k_0 = 0.03 \qquad (4.5)$$

$$k_1 = 0.550\ e^{-0.129\ m} \qquad (4.6)$$

$$k_2 = 0.857\ e^{-0.103\ m} \qquad (4.7)$$

$$k_3 = 0.905\ e^{-0.074\ m} \qquad (4.8)$$

$$P(k)=C\ q(k)\ e^{\gamma k} \qquad (4.9)$$

$$f(k)=\int_{k_{min}}^{k} P(k)\ dk \qquad (4.10)$$

The values of C and γ were fitted by using the data. γ is in the form of a transcendental function, as it was in the case of the Bendt distribution. Suehrcke approximated γ as a function of $\bar{k}$ and m.

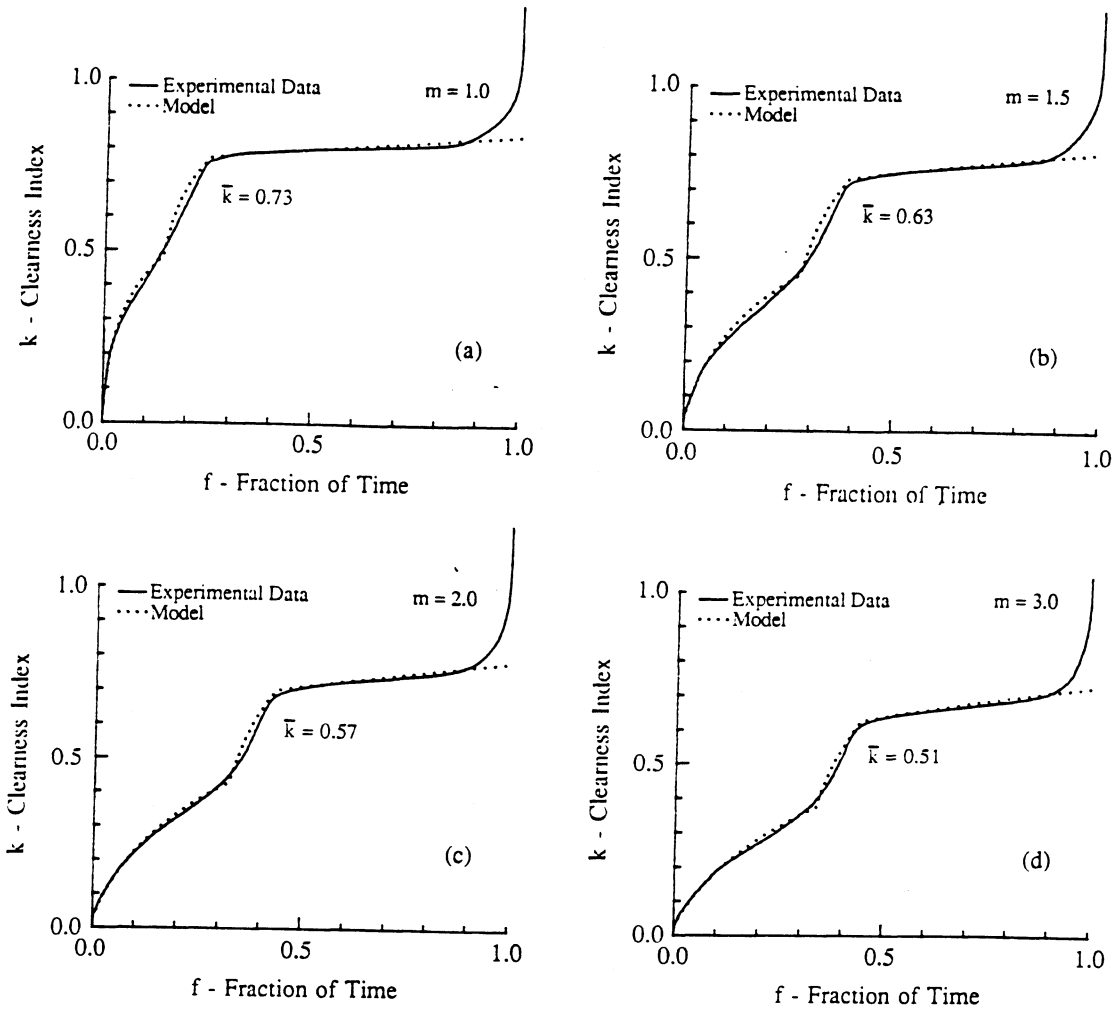

Figure 4.1 Suehrcke's Results for Perth, Australia

$$C = \frac{\gamma}{\sum_{i=1}^{3} q_i \left[e^{\gamma k_i} - e^{\gamma k_{i-1}} \right]} \qquad (4.11)$$

The model proposes that intermediate clearness indices (values between k_1 and k_2) do not often occur a hourly timescale. Rather, they are a result of averaging over the period of an hour. Clearness indices are assumed to behave in more of an "on-off" fashion - it is either cloudy or sunny in a given minute. Only high and low clearness indices exist on a minute time scale. As a consequence, a cumulative frequency distribution of minute clearness indices should show that there is a very small part of the fractional time spent in the intermediate clearness index range.

Suehrcke's model was derived exclusively from the results for Perth, Australia although he believes that the algorithm should be applicable to any location. The model reproduces his data very well (see Figure 4.1). However, this model does not hold true for other locations. Data for other locations have shown that, while there can be some bimodal shape to minute cumulative frequency distributions, the behavior is not as marked as Suehrcke found for Perth nor does his model accurately represent the bimodal shape in those other locations.

Figures 4.2 through 4.4 show the results for data collected at Georgia Tech for Atlanta, Georgia. [SEMRTS, 1991] While there is some evidence of bimodality at lower airmasses, the effect decreases as the airmass increases. The two curves do not have exactly the

same average clearness index. This difference can be attributed to the fact that not all of the minutes that comprise a given hour will fall into the same airmass range that their hour does. In addition, the minute clearness indices, c_t, were calculated from

$$c_t = G/G_0 \qquad (4.12)$$

while

$$k_t = \sum_{1}^{60} G \Big/ \sum_{1}^{60} G_0 \qquad (4.13)$$

The hourly curves generally behave as the Bendt distribution would indicate.

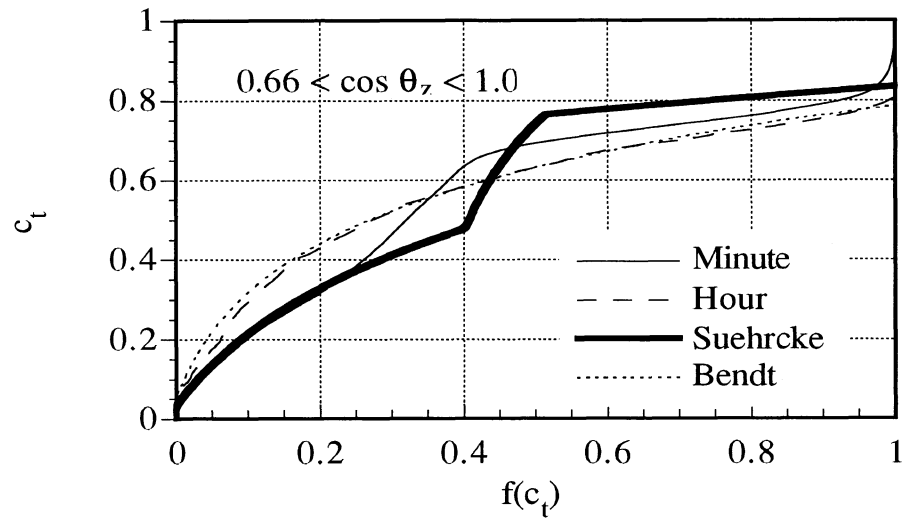

Figure 4.2 Low Airmass Cumulative Frequency Distribution, Atlanta

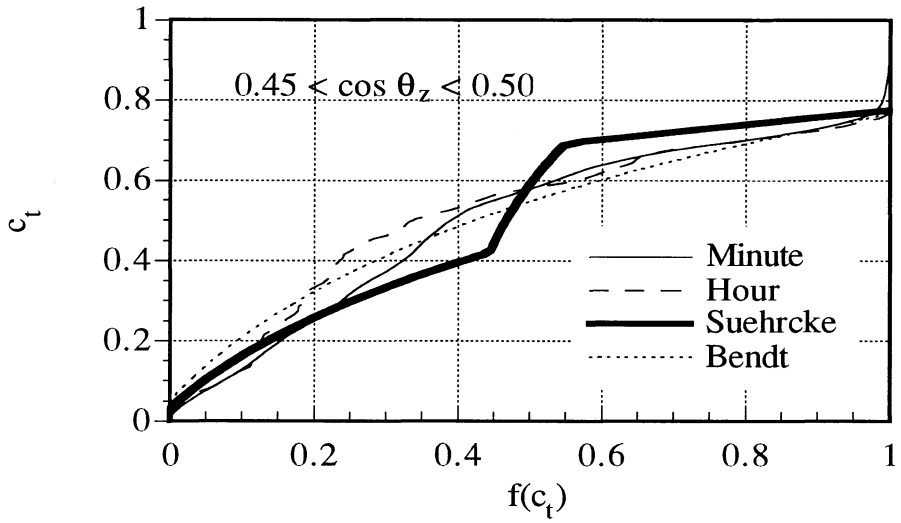

Figure 4.3 Medium Airmass Cumulative Frequency Distribution, Atlanta

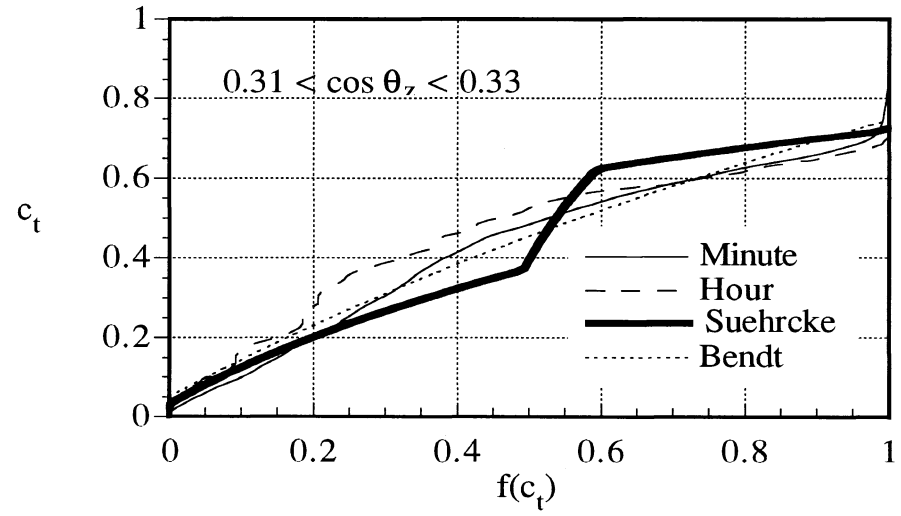

Figure 4.4 High Airmass Cumulative Frequency Distribution, Atlanta

4.3 Distribution of Clearness Indices Within Hours

It would be convenient if the distribution of minute clearness indices within an hour of a given k_t would follow the Bendt

distribution curves. However, the distributions of minutes within hours do not seem to exhibit the same behavior. The c_t distributions for San Antonio, Texas; Albany, New York; and Atlanta, Georgia are shown in Figure 4.5. Data are shown for an entire year for each location. Minute clearness indices were grouped according to their hourly k_t. A CFD curve was then plotted for a number of ranges of k_t. The figure shows that there is a definite order to the c_t distributions. The curves for the given hourly clearness index ranges are nearly identical for the three locations. There are some differences at the extremes of the curves - at very low and very high fractional times.

4.4 Modeling of Minute Clearness Indices

The shapes of minute clearness indices distributions were very similar to those of relative humidity curves plotted by Erbs [1984]. He used a Weibull distribution to fit the curves. Using the data from Atlanta and San Antonio, a two-parameter model was fitted to the data. The model was fitted for hourly clearness indices of 0.3 to 0.7. The results of the fitting were

$$f(c_t) = \frac{\left(1 - \exp\left[-(c_t/\theta_1)^{\theta_2}\right]\right)}{\left(1 - \exp\left[-(1/\theta_1)^{\theta_2}\right]\right)} \qquad (4.14)$$

$$\theta_1 = 0.223 + 2.21\ k_t - 1.211\ k_t^2 \qquad (4.15)$$

$$\theta_2 = 5.948 \times 10^{-9}\ e^{30.054\ k_t} + 1.587\ e^{1.815\ k_t} \qquad (4.16)$$

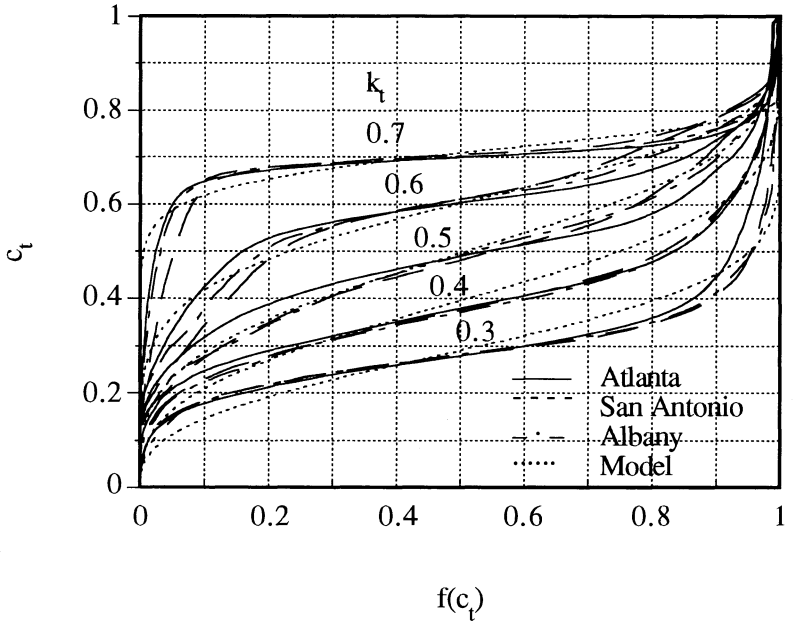

Figure 4.5 Model versus Data Cumulative Frequency Distribution of Minute Clearness Indices Within Hours

Figure 4.5 shows the result of the fit with the addition of the data from Albany. The fit is not perfect. Nonetheless, the model produces a shape that does represent the data much better than a Bendt or a uniform distribution would. Figure 4.6 shows the difference between a model and a Bendt distribution.

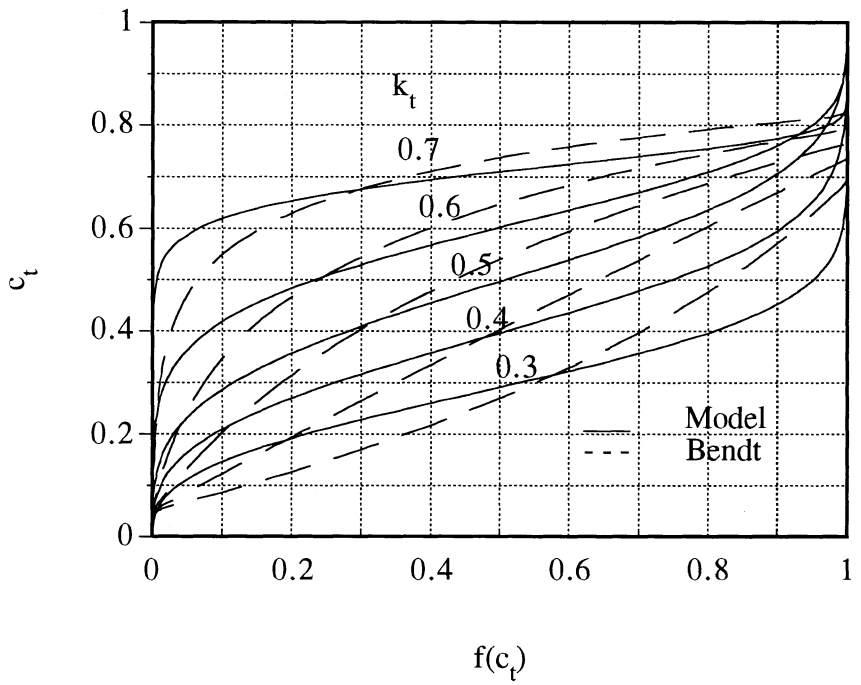

Figure 4.6 Comparison of Model and Bendt Distributions

4.5 Zenith Angle Dependencies

The model of Equations 4.14-4.16 was generated using annual data from each location. However, there might be some seasonal variation. In addition, there is almost certain to be some variation with solar position. To investigate the latter influence, the hourly airmass at the midpoint of the hour was selected as an independent variable. This was done for all three locations and for three airmass ranges; (1.0-1.5), (2.0-2.5), and (3.0-3.5). These airmass ranges corresponded to $\cos \theta_z$ ranges of (0.66-1.0), (0.40-0.50), and (0.28-0.33). Figures 4.7-4.9 show the results of c_t distributions about the hourly clearness index as a function of airmass.

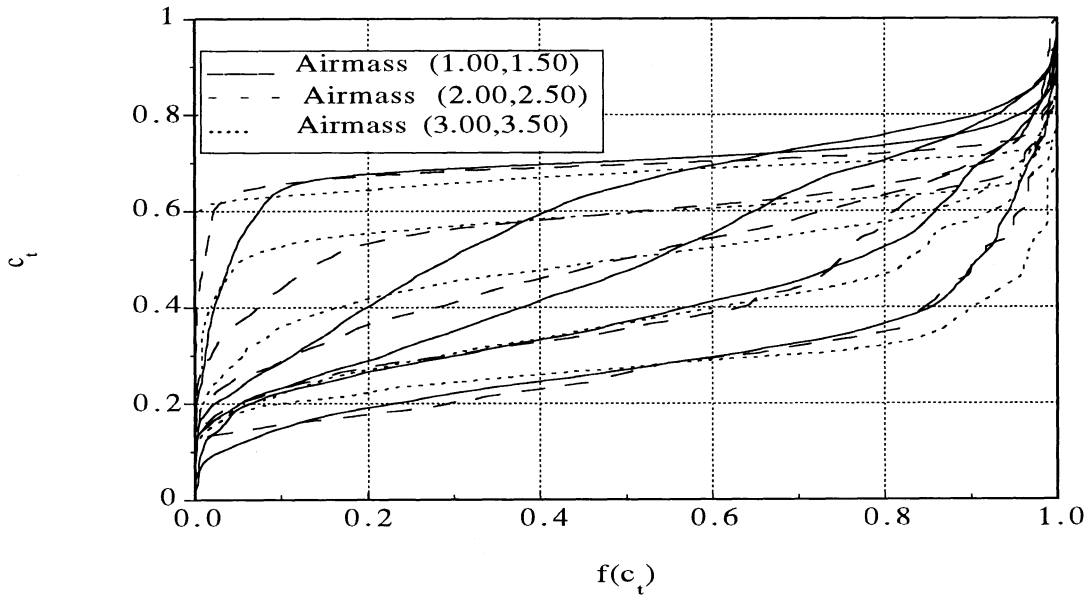

Figure 4.7 Airmass Cumulative Frequency Distributions, Atlanta

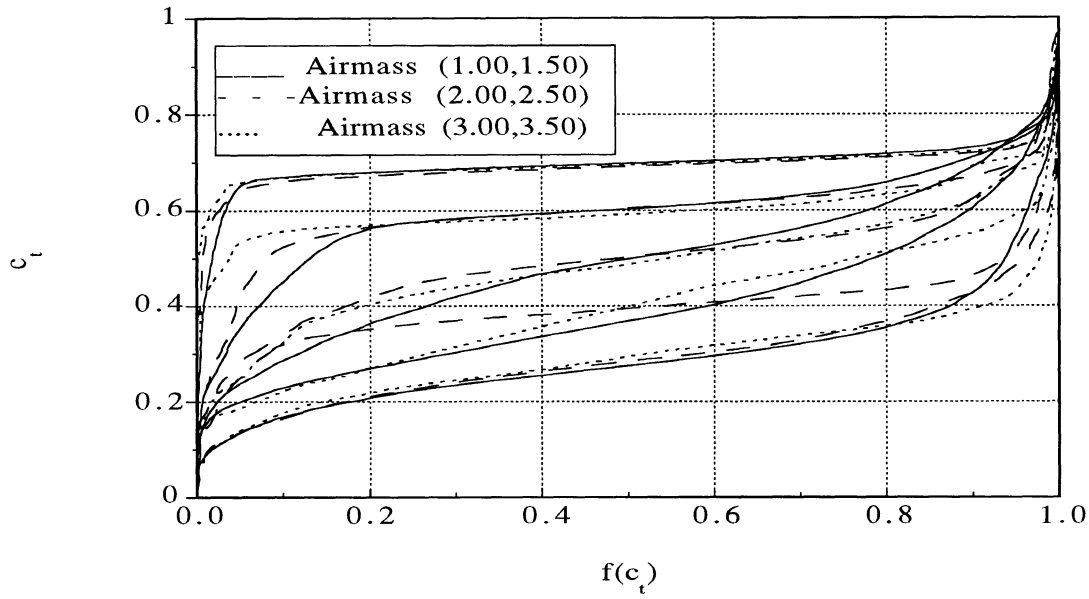

Figure 4.8 Airmass Cumulative Frequency Distributions, Albany

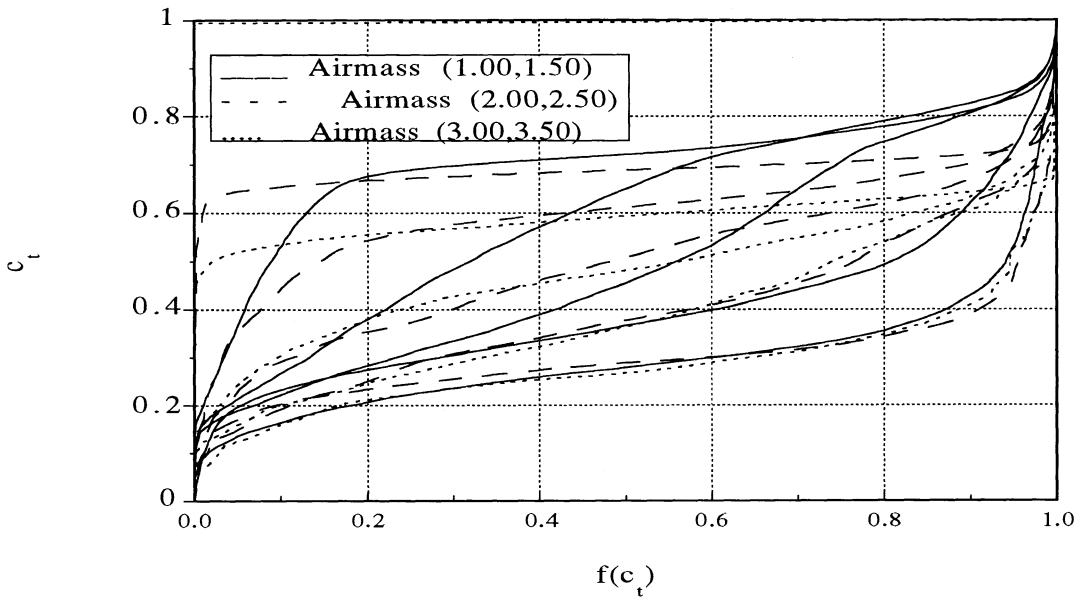

Figure 4.9 Airmass Cumulative Frequency Distributions, San Antonio

There are noticeable differences at hourly clearness indices of 0.4 to 0.6. At low airmass, the distributions differ markedly from those of higher airmass. In fact, the distributions at low airmass are very much like those a Bendt distribution would produce. This apparent discrepancy has a physical explanation. Consider, for example, a day with partly cloudy conditions. At high airmass (i.e. at large solar zenith angles), it is unlikely that there will be clouds moving sporadically in front of the sun to give a wide distribution of minute clearness indices within the hour. Rather, it is more likely clouds will completely block the sun during the hour. At a low airmass, it is more likely that clouds will be causing the sun to be occasionally hidden within the hour. At high and low hourly clearness indices,

the curves exhibit little dependence on airmass. Thus, the model of minute clearness indices should be modified to be $f(c_t)=F(k_t, \cos\theta_z)$ and not just $f(c_t)=F(k_t)$.

Zenith angle dependent cumulative frequency distribution curves are shown in Figures 4.10-4.18. Three-dimensional probability plots of $0.25 \leq k_t \leq 0.30$; $0.45 \leq k_t \leq 0.50$; and $0.65 \leq k_t \leq 0.70$. The value of $\cos(\theta_z)$ was also varied. Minute clearness indices were sorted by their hourly clearness index into bins with a k_t width of 0.05, a c_t width of 0.05, and a $\cos(\theta_z)$ width of 0.10. The size of each bin was then normalized so that the sum of the bins for given values of k_t and $\cos(\theta_z)$ was 100. At the lower and higher ends of the k_t spectrum, there is little difference in the probability plots. The characteristics are location-independent. That is, the distributions peak very sharply around the value of k_t. In addition, those peaks are smaller in magnitude and the distributions are wider as the values of $\cos(\theta_z)$ approaches unity. For small zenith angles, the distribution of c_t is wider. The peaks are larger at the higher values of k_t.

However, at intermediate values of k_t, quite different behavior is displayed. At low values of $\cos(\theta_z)$, the c_t distributions remain centered around the value of k_t. However, the peaks are nowhere near as large as in the lower and higher k_t distributions. Furthermore, the peaks flatten out as $\cos(\theta_z)$ increases.

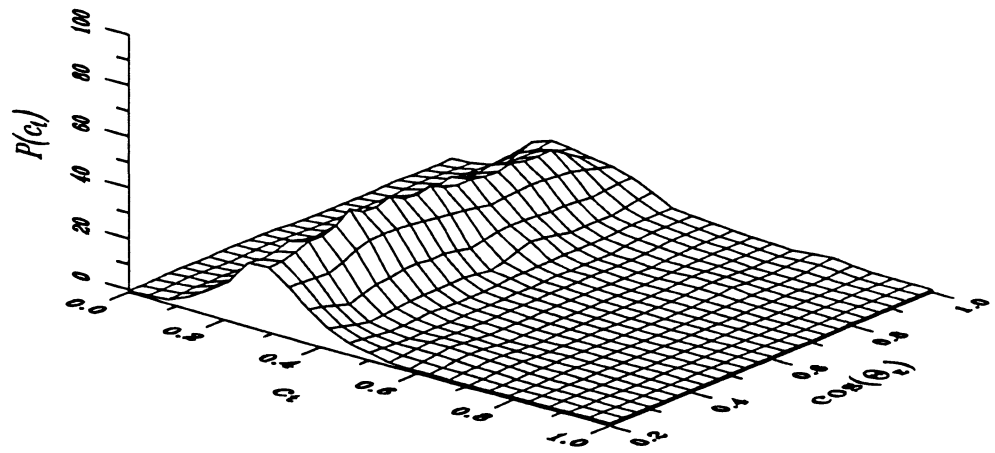

Figure 4.10 Probability Plot, $0.25 \leq k_t < 0.30$, Albany

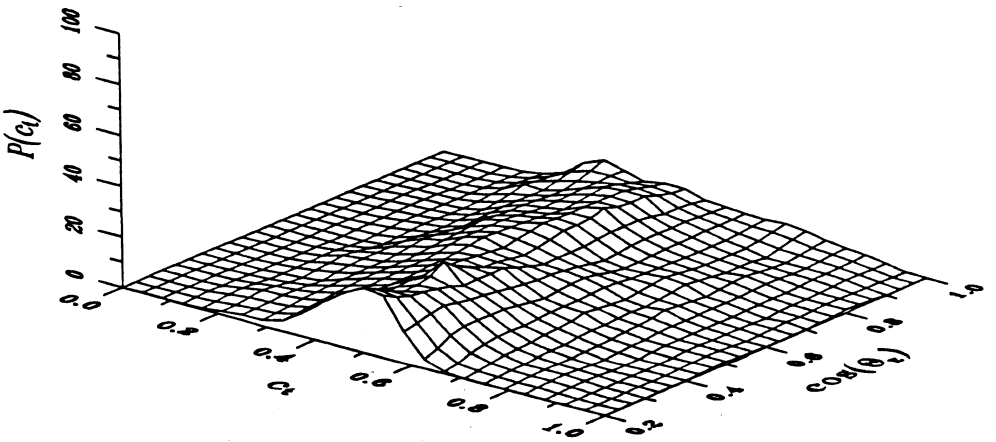

Figure 4.11 Probability Plot, $0.45 \leq k_t < 0.50$, Albany

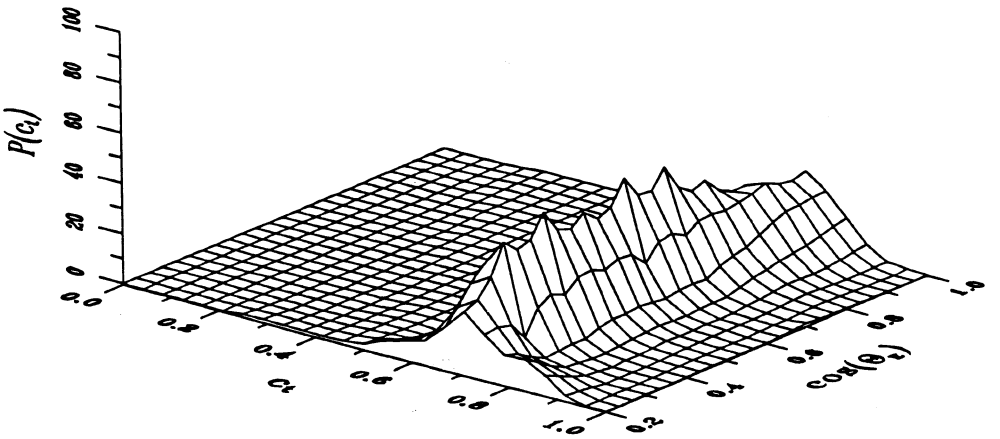

Figure 4.12 Probability Plot, $0.65 \leq k_t < 0.70$, Albany

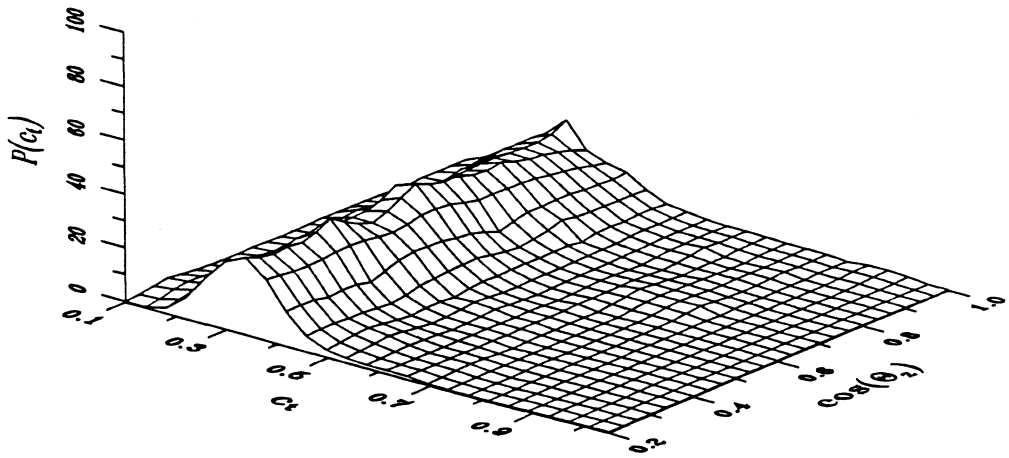

Figure 4.13 Probability Plot, $0.25 \leq k_t < 0.30$, Atlanta

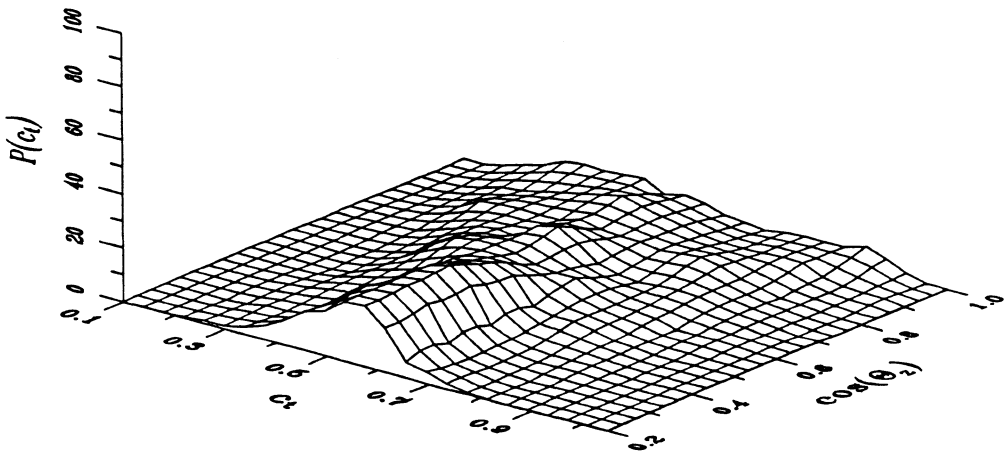

Figure 4.14 Probability Plot, $0.45 \leq k_t < 0.50$, Atlanta

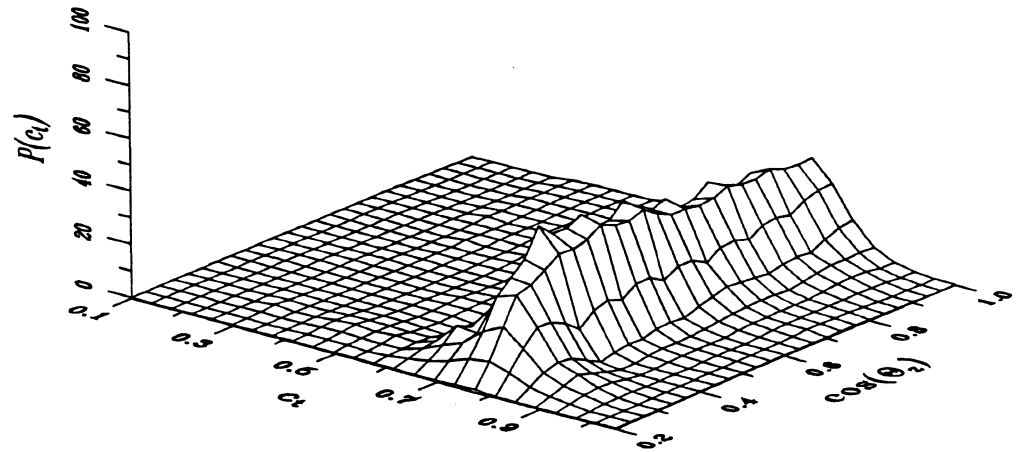

Figure 4.15 Probability Plot, $0.65 \leq k_t < 0.70$, Atlanta

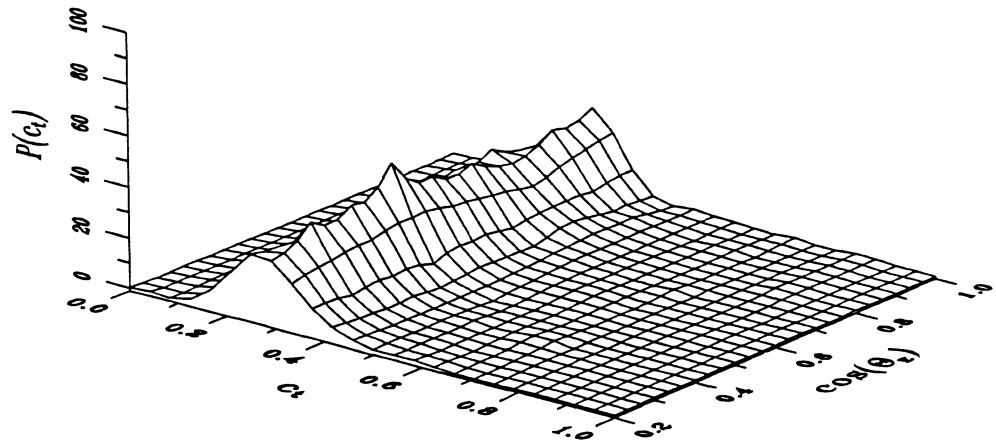

Figure 4.16 Probability Plot, $0.25 \leq k_t < 0.30$, San Antonio

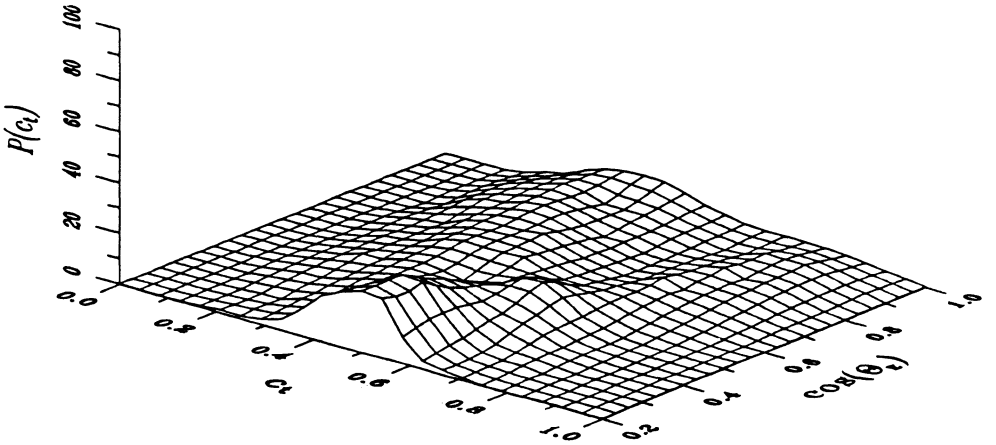

Figure 4.17 Probability Plot, $0.45 \leq k_t < 0.50$, San Antonio

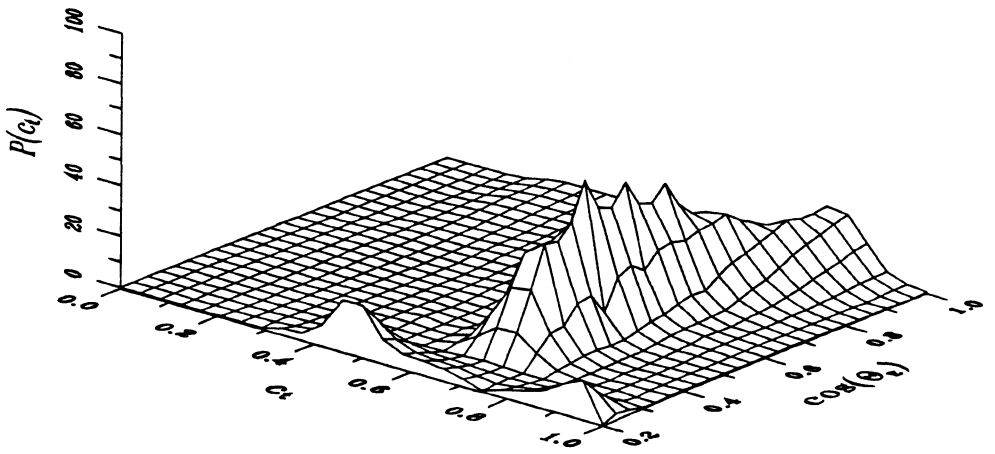

Figure 4.18 Probability Plot, $0.65 \leq k_t < 0.70$, San Antonio

All of these probability distributions could be integrated to produce cumulative frequency distributions. Then there would be a set of curves of $f(c_t)=F(k_t,\theta_z)$. Then a curve fitting process could be undertaken in order to empirically determine θ_1 and θ_2 as functions of $\cos(\theta_z)$ and k_t. Such a procedure has not been undertaken here; it would be wise to accumulate more data in order to do an accurate fitting. In addition, perhaps a different distribution should be used in the modeling because of the large difference in curve shape with $\cos(\theta_z)$.

Of all the probability plots shown, there is only one noticeable occurrence of bimodality. In Figure 4.18, there is a distinct bimodal shape at $\cos(\theta_z)=0.2$. One possible explanation of the lack of bimodal shape in Figures 4.2-4.4 was that they had lower average clearness indices than did those of Suehrcke. However, Figures 4.11,4.15,and 4.18 are for high average clearness indices, and there is only the one distinct representation of bimodal behavior, suggesting that intermediate clearness indices do exist on a minute timescale. Figures 4.14 and 4.17, which represent intermediate values of k_t, show some evidence of bimodality, especially at high values of $\cos(\theta_z)$. However, the bimodality is not as marked as Suehrcke suggests.

4.6 Minute Autocorrelation

The autocorrelation of minute clearness indices should be quite high. The weather typically does not change much from one minute to the next. For the three locations, the hourly average lag-one autocorrelation coefficient was calculated for each hour for all twelve months by the following formula:

$$\overline{\varnothing}_{1\ m,h} = \frac{1}{N}\sum_{1}^{N} \frac{\sum_{i=1}^{59} (c_{t_{h,i}} - k_{t_h})\ (c_{t_{h,i+1}} - k_{t_h})}{\sum_{i=1}^{60} (c_{t_{h,i}} - k_{t_h})^2} \qquad (4.17)$$

where m is the month, N is number of days in the month and h is the hour. The effect of clearness indices in the previous hour are neglected, even though the first minute clearness index of a given hour will be somewhat dependent on the last few minute clearness indices of the preceding hour.

The lag-one autocorrelation coefficients for the annual series of K_t were determined for each location . They were 0.41 (San Antonio), 0.32 (Atlanta), and 0.33 (Albany). These values are around the accepted value of 0.30.

The three-dimensional plots are similar for all three locations as shown in Figures 4.19-4.21. The values of $\overline{\varnothing}_1$ ranged from 0.68 to 0.93. There seems to be a seasonal trend in that $\overline{\varnothing}_1$ for a given hour is higher in the winter months than in the summer months. Another general trend that appears is with respect to the hour of the day. The central hours of the day typically have a lower value of $\overline{\varnothing}_1$ than do the early and late hours of the day.

The autocorrelation behavior corresponds the the behavior of minute clearness indices within an hour. At low zenith angles (which correspond to the central hours of the day), the c_t distributions show a Bendt-like shape. This type of shape implies less uniformity of the minute clearness indices than the modeled shape. Less uniformity will translate to lower autocorrelation while more uniformity will lead to higher autocorrelation.

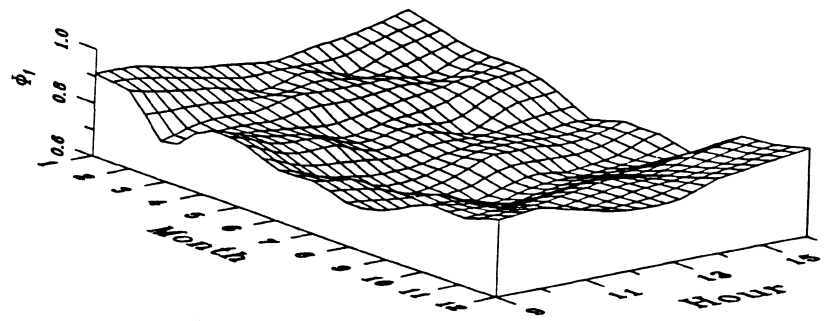

Figure 4.19 Hourly Lag-One Autocorrelation Coefficients, Albany

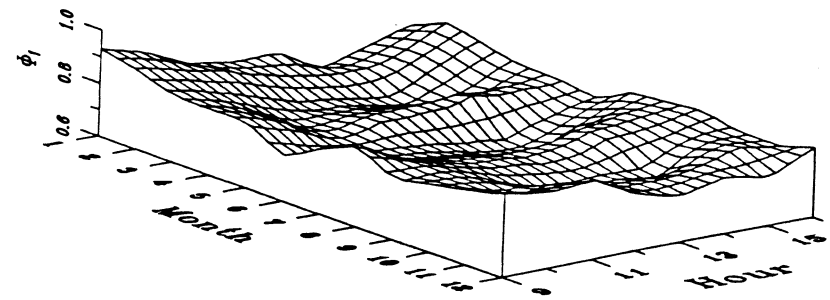

Figure 4.20 Hourly Lag-One Autocorrelation Coefficients, Atlanta

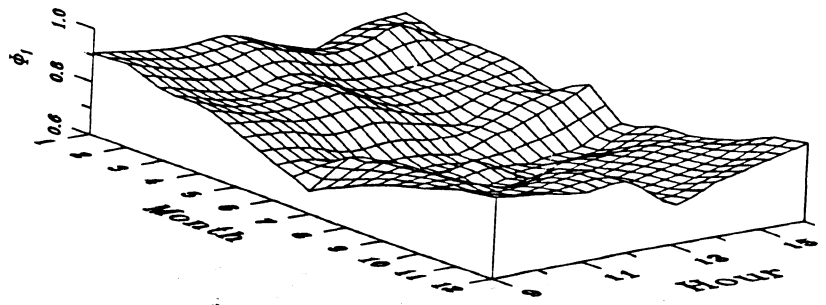

Figure 4.21 Hourly Lag-One Autocorrelation Coefficients, San Antonio

The preceding analysis involved mixing the data to some degree. The value of $\overline{\varnothing}_1$ was calculated for each hour from the distribution of c_t about k_t. These $\overline{\varnothing}_1$ values were grouped by month and hour and averaged. Each grouping would have a large range of values of k_t. As seen in the long term radiation data, hourly distributions are different for different values of K_t and $\cos(\theta_z)$. This behavior would lead one to assume that the distribution of c_t would vary in a somewhat similar manner with k_t and $\cos(\theta_z)$. The θ_z dependence will probably not be that important because its effects will be taken care of in the grouping by hour. Once again looking at Figure 3.41, the variation of $\cos(\theta_z)$ for an hour in a given month will not be that great. However, grouping the hours together, irrespective of k_t, may be hiding what the lag-one autocorrelation coefficient really is by mixing together cloudy hours with clear hours. Such an investigation would be time consuming because it would entail determining three-dimensional distributions for each hour for each of the twelve months. In addition, the autocorrelation of minute radiation might not be adequately described by only the lag-one autocorrelation coefficient. Higher order autocorrelation coefficients (comparing a value of c_t to that of two minutes before, three minutes before, *et al*) may not be insignificant as they are for daily radiation.

Skartveit and Olseth [1992] have developed their own model of generating autocorrelated radiation on time scales of less than one hour. They found that radiation on a time scale of five minutes gave significant differences from hourly average values. However, they noted that a reduction to one minute data produced only slightly more information than five minute data. Their investigations agreed with Suehrcke's in that they found distinct bimodal behavior in minute radiation. However, they used a broadband model with

which to compare the measured radiation. The broadband model is intended to account for absorption in the ozone, water vapor, nonvariable gases and aerosols, as well as scattering on air molecules an aerosols and even for multiple backscattering of radiation reflected from the surface, in order to give a clear sky value of radiation. Thus,

$$c_t = G/G_{clear\ sky} \qquad (4.18)$$

It must be noted that most of the aforementioned atmospheric effects in the calculation of $G_{clear\ sky}$ are modeled and not measured. Thus, their analysis is not exactly the same as the one undertaken in this study.

4.7 Minute Versus Hourly Modeled Diffuse Radiation

In the simulations of a solar domestic hot water system (see Section 5.7), the solar fractions achieved by using hourly average values of horizontal radiation were higher than those achieved by using the actual minute values. After investigation, it was determined that the hourly average values gave a higher value of tilted radiation than what the minute values gave for tilted radiation. The problem was corrected by using the hourly average value of tilted radiation, as determined by the minute values, for the hourly average simulations. The question of why the two values of tilted radiation were different still remained. Obviously, the correlation that was used to determine tilted radiation was insufficient when applied to minute radiation.

The correlations that were used were the Erbs' hourly diffuse model along with the Perez anisotropic model. The diffuse correlation was investigated as the likely source of the discrepancies.

Tilted radiation models are for the most part only geometric representations. Thus, incorrect input into the model will lead to incorrect output.

An analysis was undertaken so see if all diffuse models would produce differences between minute and hourly radiation. The models included the Erbs hourly, Boes, and the reduced Reindl correlations. The Boes correlation is:

$$I_{dn} = (1.3304\ k_t - .3843)\ G_{sc}$$
$$I_{dn} = \max [I_{dn}, 0]$$
$$I_{dn} = \min [I_{dn},\ 0.739\ G_{sc}]$$
$$I_b = \min [I_{dn} \cos(\theta_z),\ I]$$
$$I_d = I_{dn} - I_b \qquad (4.19)$$

where I_{dn} is the direct normal radiation.

The reduced Reindl correlation is:

for $k_t < 0.3$

$$D = 1.02 - 0.254\ k_t + 0.123 \cos(\theta_z)$$
$$I_d = \min [I,\ DI]$$

for $0.3 < k_t < 0.78$

$$D = 1.4 - 1.479\ k_t + 0.177 \cos(\theta_z)$$
$$D = \min [D,\ 0.97]$$
$$D = \max [D,\ 0.10]$$
$$I_d = DI$$

for $k_t > 0.78$

$$D = 0.486\ k_t - 0.182 \cos(\theta_z)$$
$$D = \min [D,\ 0.97]$$
$$D = \max [D,\ 0.10]$$

$$I_d = DI \tag{4.20}$$

Hourly diffuse radiation values were calculated from

$$I_{d,hour} = D(k_t)\, I \tag{4.21}$$

The hourly total of the minute diffuse radiation was determined from

$$I_{d,min} = \sum_{i=1}^{60} G_i\, D(c_{t_i}) \tag{4.22}$$

The difference was expressed as

$$\Delta = \frac{I_{d,hour} - I_{d,min}}{I_{d,hour}} \tag{4.23}$$

The error for each value of k_t was the average of the differences for all hours of $(k_t - 0.04, k_t)$.

$$error(k_t) = \frac{\sum \Delta}{N} \tag{4.24}$$

This error term was calculated for each of the three models for different values of k_t. In Figures 4.22 and 4.23, the results are shown for the San Antonio and Atlanta. The analysis was done for the entire year at both locations. There will probably be some zenith angle dependencies in the errors, but these were not investigated. The figures show that there is a definite dependence in the errors on k_t.

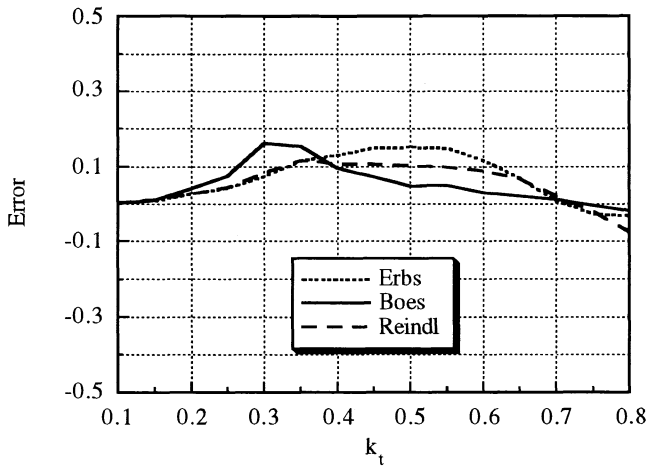

Figure 4.22 Average Hourly Error in Calculating Diffuse Radiation, Atlanta

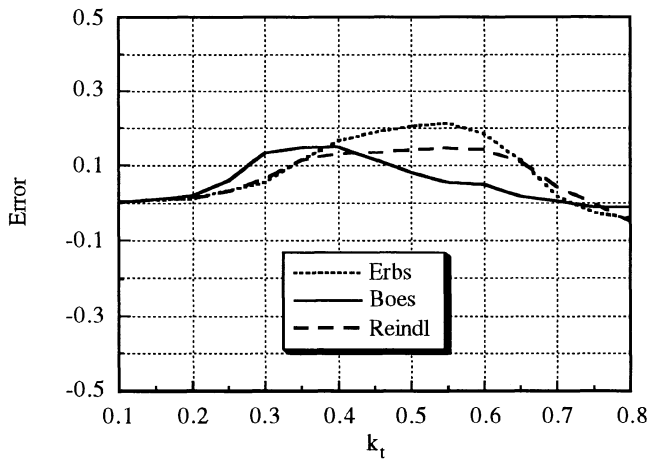

Figure 4.23 Average Hourly Error in Calculating Diffuse Radiation, San Antonio

4.8 Minute Diffuse and Tilted Radiation

In the preceding section, it was demonstrated that that existing

correlations for hourly diffuse fractions were inadequate for minute radiation. Applying the correlations to the minute radiation and then summing up the calculated minute diffuse radiation values did not lead to the same value as applying the correlations to the average hourly horizontal value. This effect was observed for both San Antonio and Atlanta. The correlations tended to give higher values for diffuse radiation calculated from the hourly average as opposed to the sum of the minute values. The question is if the correlations truly are inapplicable for such small time scales or if the differences were only a result of the imperfect way in which the correlations model diffuse radiation. Thus, an investigation was undertaken to see how the correlations performed by comparing calculated minute diffuse radiation to actual minute diffuse radiation data.

All three diffuse models were applied to the minute horizontal data. Results for each month in San Antonio were generated on the basis of c_t. The error for each value of c_t was the average of the differences for all minutes of $(c_t - 0.04, c_t)$.

$$\Delta_d = \frac{G_{d,\ model} - G_d}{G_d} \tag{4.25}$$

$$error(c_t) = \frac{\sum \Delta_d}{N} \tag{4.26}$$

In Figures 4.24 and 4.25, the curves for January and June are represented. It is clear that the differences are greater in January than in June. Boes' correlation seems to perform the best of the three models. It must be noted that while the percent relative errors may be great in terms of percentage at high c_t, the actual difference in terms of insolation is quite small since diffuse radiation decreases with increasing clearness index. At intermediate clearness indices,

the errors are generally quite large.

These large errors did not bode well for the calculation of tilted radiation on a minute-by-minute time scale. Two efforts were made in the area of gauging the performance of existing correlations for tilted radiation. First, comparisons were made between measured minute tilted radiation data (at a tilt equal to latitude) and calculated tilted values via actual horizontal and actual diffuse data. Second, the actual tilted values were compared to calculated values in which only the actual horizontal data were used. In this case, the diffuse values were calculated by the three diffuse correlations and then the tilted surface correlations were applied. The error for each value of c_t was the average of the differences for all minutes of $(c_t - 0.04, c_t)$.

$$\Delta_T = \frac{G_{T,\,model} - G_T}{G_T} \qquad (4.27)$$

$$error(c_t) = \frac{\sum \Delta_T}{N} \qquad (4.28)$$

Figures 4.26 and 4.27 show the results of the first effort. The errors are clearly much less in June than they are in January. In the case of January, the models range from +8% to -20%. In contrast, June data exhibit errors only from +5% to -5%. It seems that there must be other meteorological factors to be taken into account in the tilted models. Pure geometry is not enough. The Hay and Davies model and the Reindl model give almost identical results. These two models give the best results in both months. The Perez anisotropic model performs surprisingly poorly in both months. In June, the isotropic sky model performs well, but it suffers greatly in January.

Figures 4.28-4.33 display the results of tilted radiation calculated

from actual horizontal and modeled diffuse radiation. All of the models encounter problems at high values of c_t in January. Once again, the models perform better in June than they do in January. It is difficult to tell which diffuse model works best in helping to determine tilted radiation. With only one data set studied here, no generalized conclusion can be made. However, in the case of San Antonio, the Reindl diffuse correlation seems to operate the best in terms of calculating minute tilted radiation values from horizontal data.

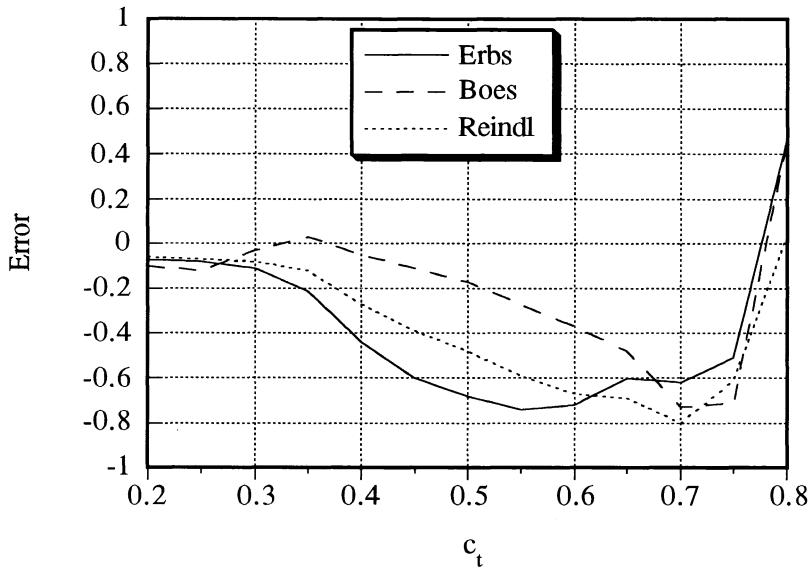

Figure 4.24 Error in Diffuse Fraction via Hourly Correlations, January

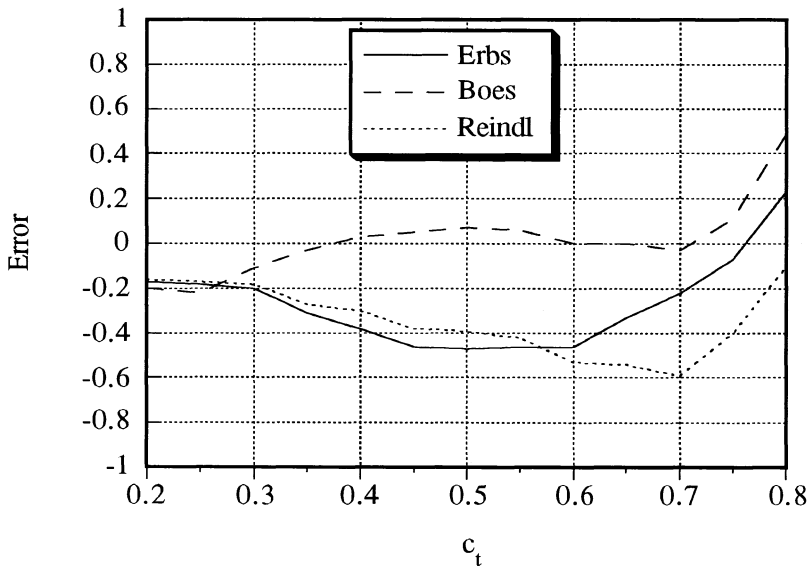

Figure 4.25 Error in Diffuse Fraction via Hourly Correlations, June

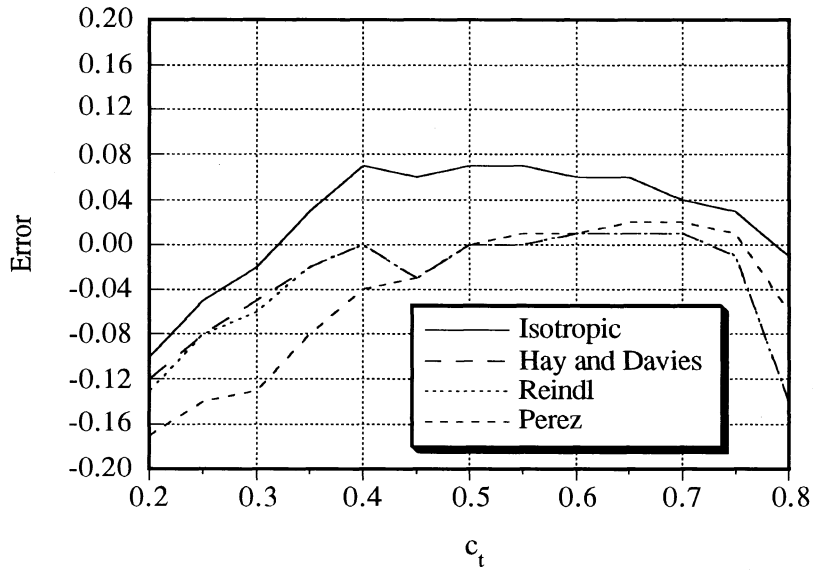

Figure 4.26 Error in Tilted Surface Radiation, January

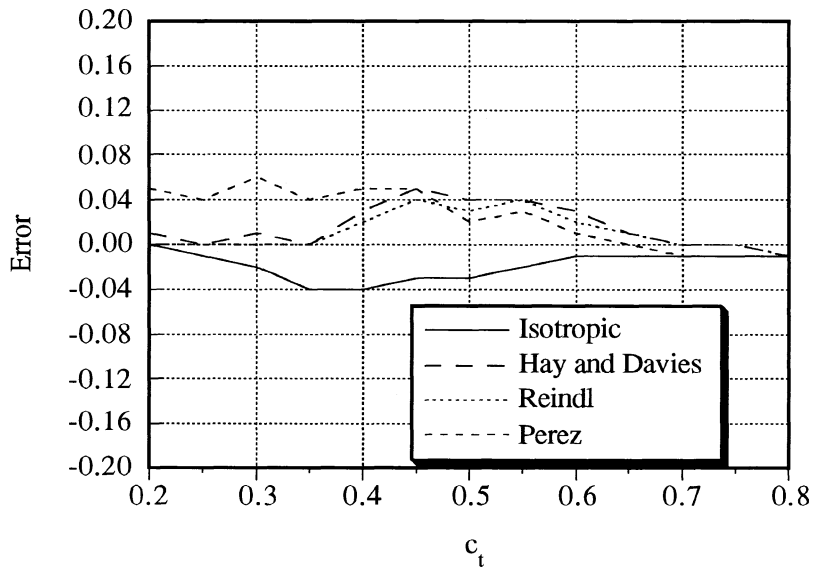

Figure 4.27 Error in Tilted Surface Radiation, June

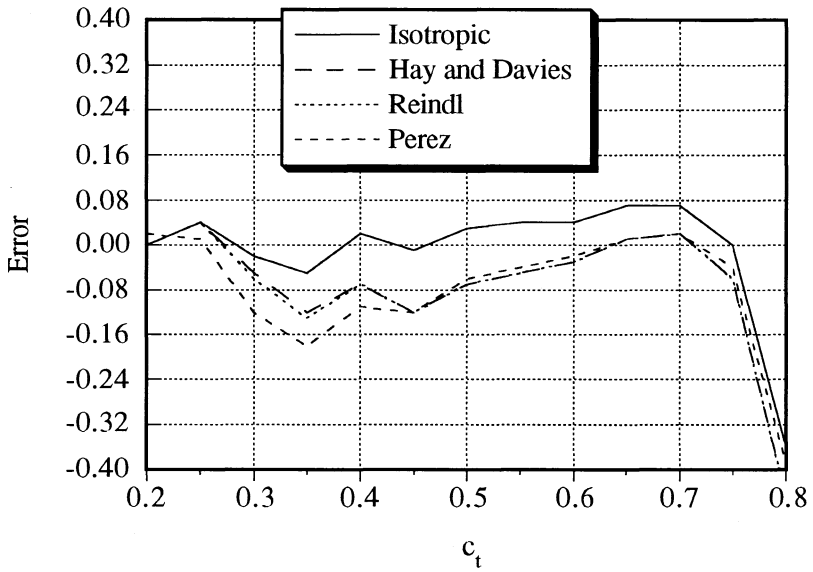

Figure 4.28 Error in Tilted Surface Radiation, Diffuse via Boes, January

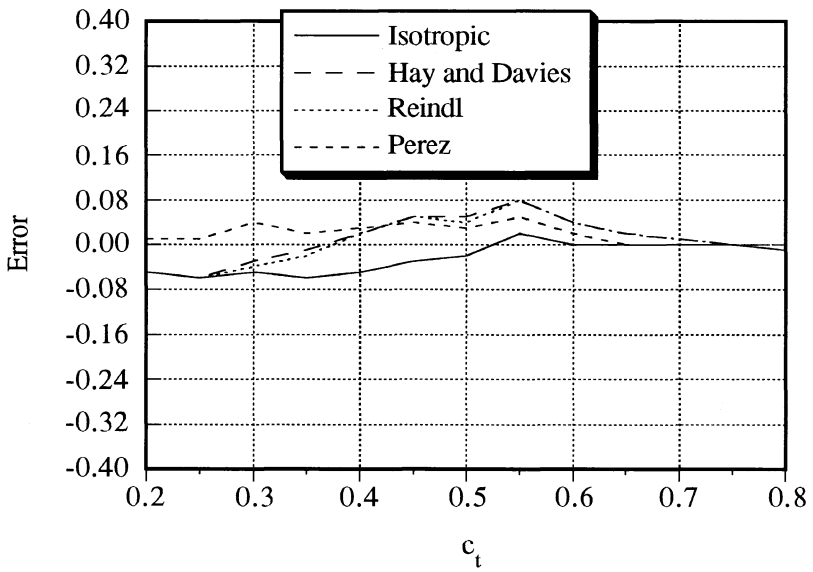

Figure 4.29 Error in Tilted Surface Radiation, Diffuse via Boes, June

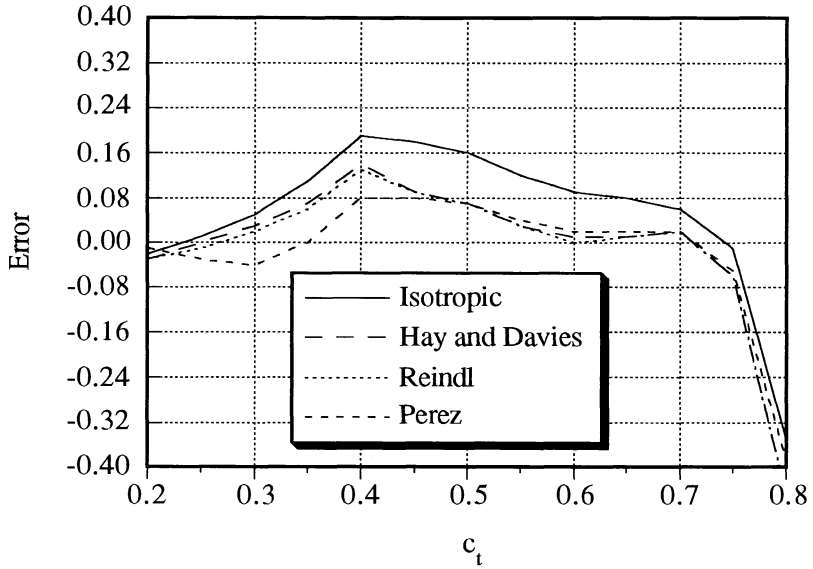

Figure 4.30 Error in Tilted Surface Radiation, Diffuse via Erbs, January

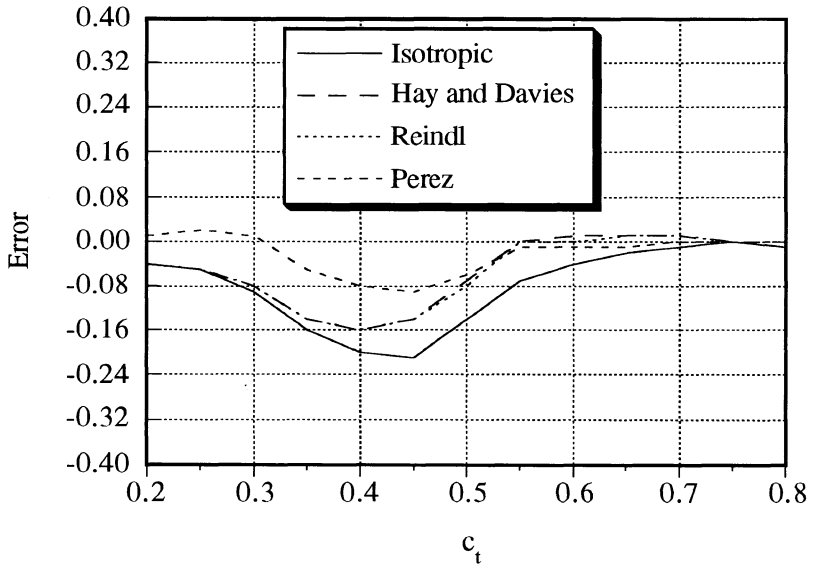

Figure 4.31 Error in Tilted Surface Radiation, Diffuse via Erbs, June

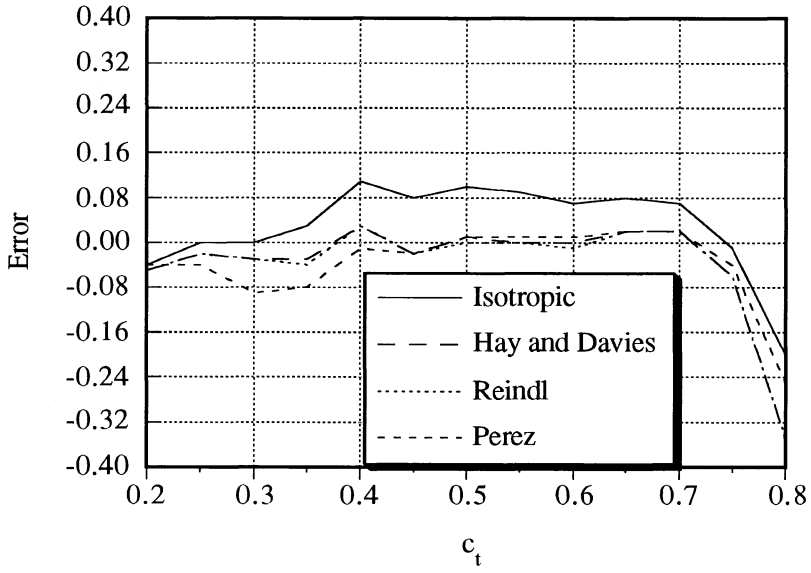

Figure 4.32 Error in Tilted Surface Radiation, Diffuse via Reindl, January

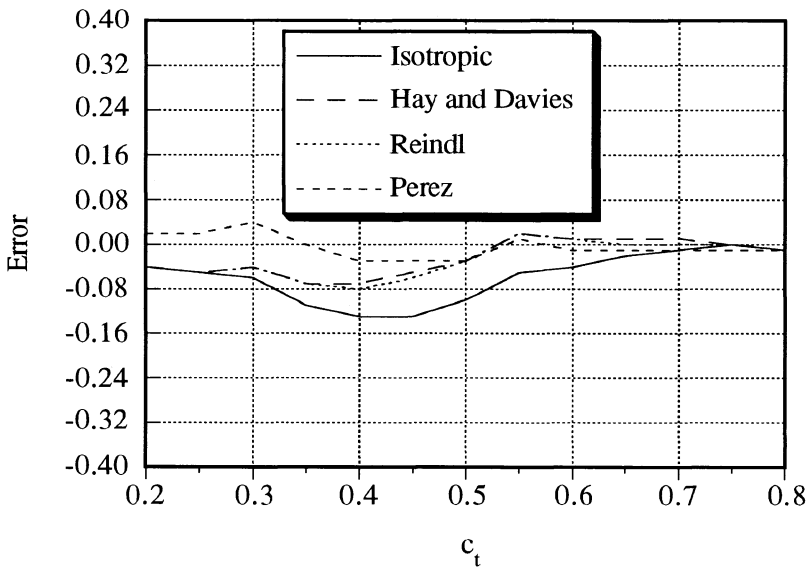

Figure 4.33 Error in Tilted Surface Radiation, Diffuse via Reindl, June

4.9 Correlations for Minute Diffuse Radiation

Figures 4.22 and 4.23 show that a model for minute diffuse radiation is needed. The differences when using correlations to determine hourly diffuse values from minute and hourly horizontal values are sizeable, especially at intermediate values of k_t. A model of the form $d=F[c_t,\cos(\theta_z)]$ was attempted, where $d=G_d/G$ is the minute diffuse fraction. Since airmass effects have been important in other things concerning minute radiation, the minute value of $\cos(\theta_z)$ was included to see if it had any effect. Regressions of the San Antonio and Atlanta data were performed separately using MINITAB.

Stepped regression of the San Antonio data resulted in good fits. The fit of $d=F(c_t)$ ($d=1.1214 - 1.2115c_t$) had an R^2 of 0.8047. Adding additional terms raised the value of R^2 to 0.84 (see Table 4.1; The R^2 value is the regression result using that predictor with all the predictors above it). The stepwise regression did not turn out as well for the Atlanta data. The value of R^2 never exceeded 0.70. When a four term regression using the same predictors as those determined for San Antonio was performed, the resulting R^2 was only 0.63. (see Table 4.2) Nonetheless, in the regressions for both locations, a zenith angle term was always an important predictor. However, even the inclusion of zenith angle dependence was not enough to produce a good fit of the data. It seems apparent that additional factors need to be taken into account, perhaps using those that are included in the full Reindl correlation for hourly diffuse fractions - relative humidity and ambient temperature.

Predictor	R-squared
c_t	0.8047
$[c_t \cos(\theta_z)]^2$	0.8089
c_t^2	0.8099
c_t^3	0.8432
$\cos(\theta_z)$	0.8434

Table 4.1 Stepwise Regression Results for San Antonio

Predictor	R-squared
c_t	0.6017
$\cos(\theta_z)$	0.6370
c_t^2	0.6462
c_t^3	0.6617
$[c_t \cos(\theta_z)]^2$	0.6693

Table 4.2 Stepwise Regression Results for Atlanta

To produce a accurate minute diffuse model, data for other locations and data for longer time periods should be used. The computing effort necessary for such an endeavor would be extreme considering that there are about 200,000 minutes for each location-year. Existing diffuse fraction correlations show a great deal of scatter. Other meteorological factors must play a part in the scattering of radiation in the atmosphere. The three locations do not represent the multitude of climates that are represented in the United States in particular or the world in general so more data must be utilized in order to determine what meteorological factors are important.

CHAPTER 5. Simulations and Minute Radiation

5.1 Introduction

The previous chapter discussed the differences between minute and hourly average radiation. Minute clearness indices follow trends dictated by hourly clearness index and zenith angle. The question then arises if these distributions are of any importance to solar energy systems. Solar heating simulations have always ignored variation of radiation within an hour. However, for a photovoltaic (PV) application, the variation of radiation within an hour could make a difference in system performance because of the way PV cells respond to incident solar radiation.

5.2 Photovoltaic Performance

A photovoltaic panel converts solar energy into electrical energy. Photovoltaic cells can respond in a non-linear fashion to solar radiation; solar water heating applications exhibit linear behavior. Photovoltaic system performance is also dependent on cell temperature. This temperature is affected by the incoming solar radiation, the ambient temperature, and the power output. The relationship between power output and cell temperature is implicit and both are related to ambient temperature and irradiation. With the non-linearity that can be involved, the choice of inputs that are used in evaluating the performance of certain photovoltaic systems could be crucial.

As in most solar heating applications, simulations of photovoltaic systems are typically done on an hourly basis. However, the time constant of a PV cell is very small. Thus, variation of the meteorological inputs, ambient temperature and irradiation, could be

very important in determining the true performance of a PV system. Utilizing hourly values may not give an accurate representation of what actually occurs in that hour. The working assumption has been that weather variables do not change in an significant manner within the time of an hour. However, common experience says that there can be significant changes of weather within an hour. Furthermore, it has been shown in the preceding sections that the distribution of minute clearness indices within an hour is not uniform. This distribution of clearness indices will cause a number of insolation values to occur within the hour. It might be advantageous to use this distribution in order to produce a more accurate picture of PV system performance.

5.3 Photovoltaic One-Day Simulations

Hourly average values have typically been used in the simulation of PV performance. However, it has been shown in Section 4.5 that radiation values can vary significantly within an hour. Since PV cells react almost instantly to insolation level, these varying levels of insolation might predict different system performance than if an average value were present for the entire hour. To investigate this, a photovoltaic system was simulated using EES [Klein, 1992], an equation-solving program The modified SEL method (Equations 1.18-1.30) was utilized as the governing equations of the PV cell's response. The system setup and the parameters used in the simulation were given in Section 1.5. A number of different systems were run using both the minute weather data and the hourly average data.

The first system considered was a maximum power point tracking system. Only one day (specifically October 1, 1981, San Antonio) was simulated. As Figure 5.1 shows, on an hourly basis, there were virtually no differences between the minute and the hourly average simulations. The difference was defined as:

$$\text{difference} = \frac{P_{hour} - P_{minute}}{P_{minute}} \qquad (5.1)$$

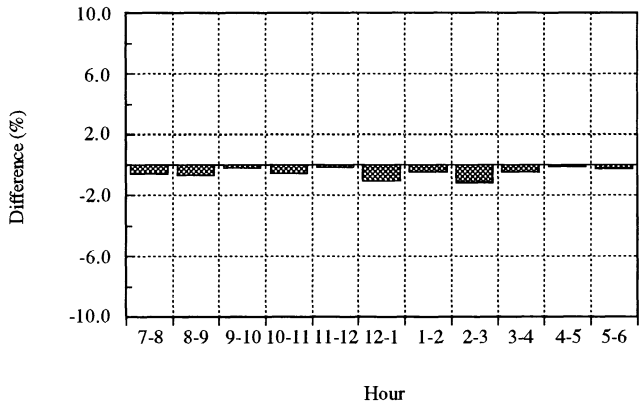

Figure 5.1 Difference between Hourly and Minute, Maximum Power Point Tracking

Maximum power point tracking causes the response of a PV cell to be nearly linear with the incident radiation. Thus, it is not surprising that the minute and hourly simulations gave nearly the same results. The small differences might be attributable to the rounding errors in calculating the hourly radiation from the minute data.

The other systems that were used contained a load resistance. Three different resistive loads were applied to the array; 5, 10, and 18 ohms, which corresponded to the resistances at maximum power point tracking at three different hours of the day. Figure 5.2 depicts the results of these one-day simulations. At a low resistance, the hourly averages underpredict the system performance noticeably. At a high resistance, the hourly average method also performs poorly but surprisingly so. The hourly average method actually overpredicts the system performance. This result was completely

unexpected since a utilizability analysis on the irradiation indicates that the minute weather should always give higher performance. The minutes are by nature non-uniform when compared to their hourly average. Thus, it would seem impossible for the hourly averages to exhibit higher performance.

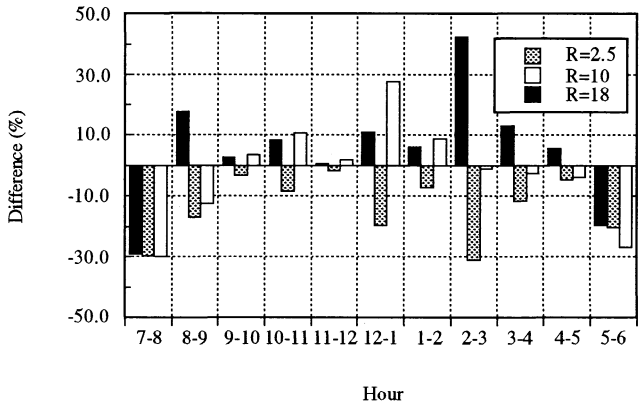

Figure 5.2 Differences between Hourly and Minute, Constant Resistive Load

5.4 Explanations for Discrepancies in Power Output

One possible explanation for the increased performance using hourly weather data rather than minute data was due to the variation in temperature during the hour. This explanation was discarded when the simulations were redone using the hourly average temperatures instead of the minute ones. The results did not change. Thus, the incoming solar flux was the only difference between the two simulations. Somehow, the system was responding more favorably to the hourly average values.

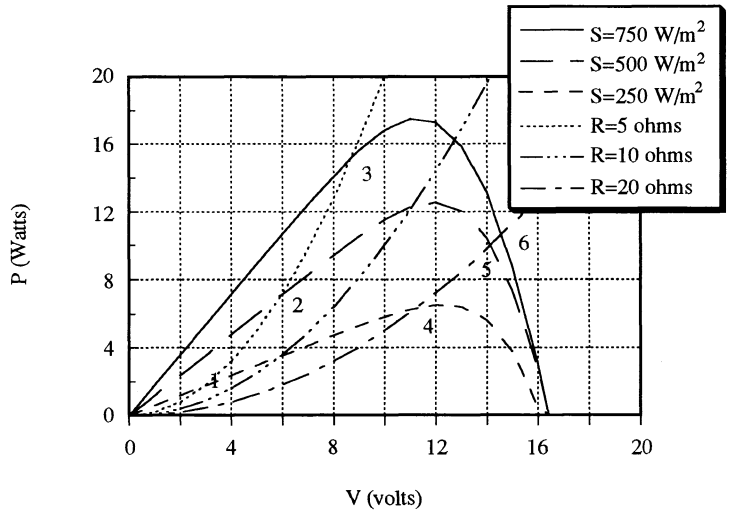

Figure 5.3 Voltage versus Power Curves of a PV Cell

The power-voltage plot in Figure 5.3 provides an answer to this apparent discrepancy. Three PV power curves are displayed in Figure 5.3 at various insolation levels but all at 25C. Also included are three curves describing the power at a constant resistance ($P=V^2/R$) While the three insolation curves cover a wide range of radiation, such a range is physically possible within an hour. The key is to look at the intersection of the high and low insolation curves (750 and 250 W/m^2) with the load curves and to compare the power output at the extremes versus the average insolation value of 500 W/m^2. At a low resistance, the average of point (1) and point (3) is lower than point (2). This point indicates a lower performance using hourly average. At a high resistance, the voltage-power curves are close together as the power decreases to zero at open circuit voltage. Point (5) is greater than the average of points (4) and (6). This point shows that average insolation level will produce more power than the average of the extremes does.

5.5 Photovoltaic Yearly Simulations

If there were only minor variation of radiation within the hour, the use of hourly average radiation for PV systems would still be legitimate because the differences between the curves would be negligible. However, the weather can exhibit drastic changes within an hour. This effect will probably be damped out over a longer simulation so minute and hourly simulations will yield similar results. Nonetheless, the power output for individual hours could be drastically wrong even though they are supposed to be the same.

Year-long simulations of the same PV system used previously were run by a FORTRAN program. To solve the inherently non-linear, implicit set of equations, the secant method was used. A value of current, I, was guessed for each time step. A tolerance of 0.001 amperes was used. When the calculated current was within 0.001 amperes of the guessed current, the time step was considered solved.

The simulations were performed for the three locations using the actual minute radiation and the hourly average radiation. The average hourly power was computed for each hour for each data set. Since there were gaps in the minute data, certain precautions had to be taken so that the analysis was valid. The value of k_t was calculated from only those minutes that had measured radiation.

Simulations were performed at three different resistances; 5, 10, and 18 ohms. Maximum power point tracking was not used since it has been established that the choice of model has no significant effect on system performance. For each month, the hourly average power was calculated. The error term computed for each hour of each month from the following equation:

$$\text{error} = \frac{\bar{P}_{hour} - \bar{P}_{minute}}{\bar{P}_{minute}} \qquad (5.2)$$

Figures 5.4 and 5.5 show the results for the months of January and June in Atlanta for resistances of 5 and 18 ohms. Figures 5.6 and 5.7 show the same results for San Antonio. A positive error implies that the use of hourly average radiation values overpredicted the PV performance as compared to the minute data while a negative value indicates that the hourly average radiation underpredicted.

For the low resistance, the hourly average radiation consistently underpredicts in January while it does better in June. In fact, it slightly overpredicts around noon in June. At the high resistance, the use of hourly average radiation seems appropriate enough for January; the errors are small except in early morning and late afternoon (where the radiation values are small). However, for June, the hourly average radiation consistently and noticeably overpredicts the PV cell output. The errors are not as large as were seen in the one-day simulation. Nonetheless, they are significant.

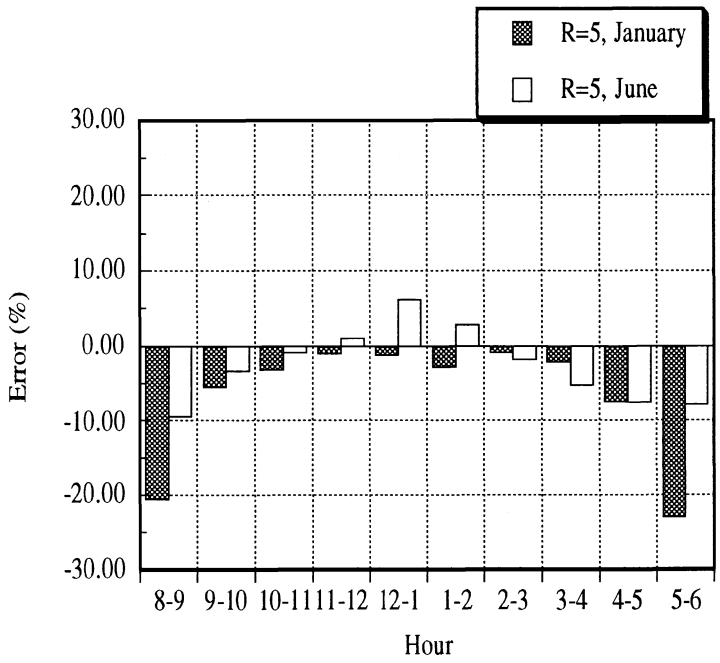

Figure 5.4 Hourly Error of PV Cell Output, Atlanta, R=5 ohms

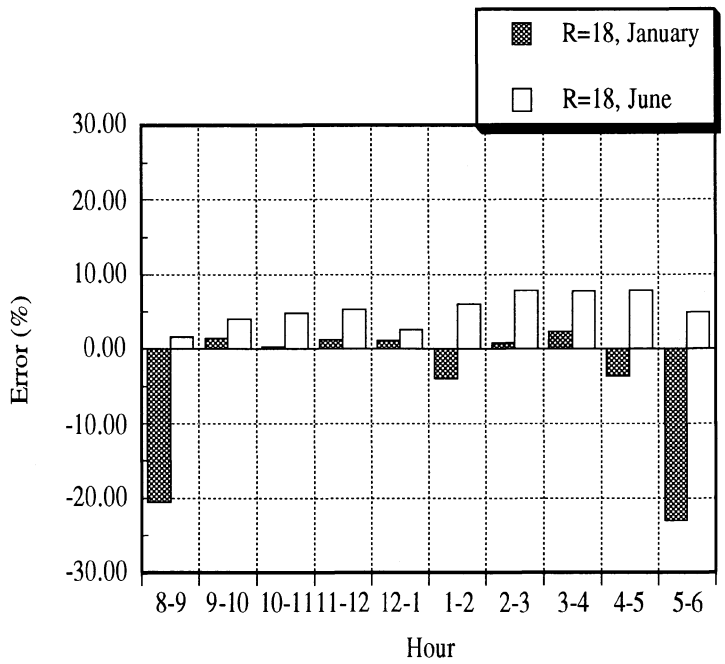

Figure 5.5 Hourly Error of PV Cell Output, Atlanta, R=18 ohms

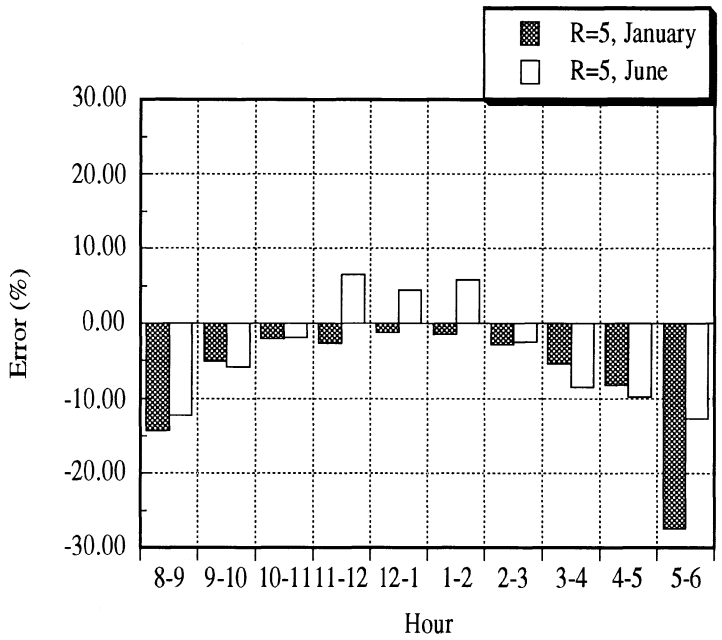

Figure 5.6 Hourly Error of PV Cell Output, San Antonio, R=5 ohms

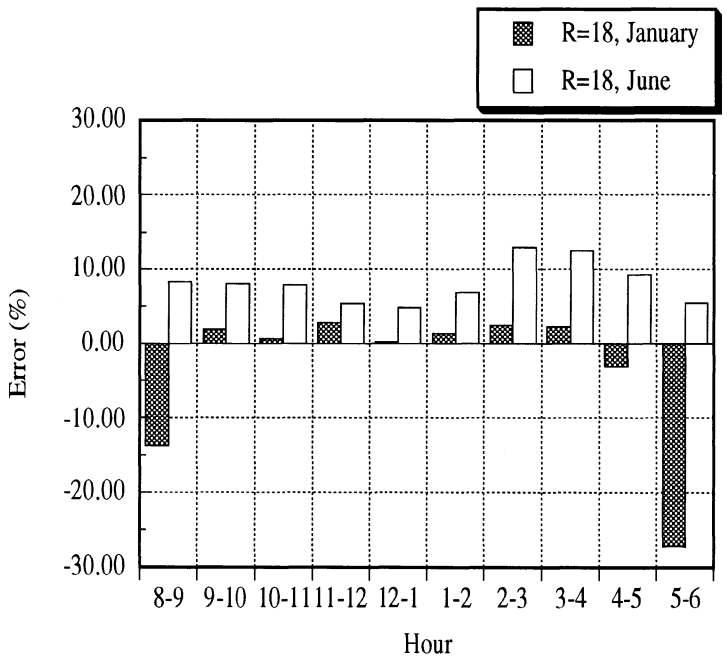

Figure 5.7 Hourly Error of PV Cell Output, San Antonio, R=18 ohms

5.6 Impact of Radiation Distribution

Hourly radiation values are highest during the central hours of the day of the summer months. Section 4.6 showed that the autocorrelation of minute clearness indices is lowest during these same time periods. With such high radiation values and high variability, photovoltaic system performance estimates can be in error by the use of hourly average values. Furthermore, PV systems have been touted as a way to reduce the peak demands upon utilities for electricity. These peak demands happen in the same time frame as the high value, highly variable radiation, suggesting that the use of hourly average values could lead to problems in sizing PV systems for such an application.

The variability of radiation within the hour implies that there are cloud effects. The presence of clouds can change the spectral distribution of the radiation as well as its magnitude. PV cells have a specific spectral response. As minute clearness indices vary within the hour, there must be changes in cloud position with respect to the sun. The cloud position will change the spectral distribution which could lead to different response of the PV cell to incident solar radiation.

5.7 Solar Domestic Hot Water Minute and Hourly Simulations

5.7.1 Introduction

Hourly weather data has traditionally been used for the simulation of solar domestic hot water (SDHW) systems. It has been argued that the transient behavior of a SDHW system and the

variation of meteorological phenomena within an hour would be insignificant or would be "averaged out" over the course of the simulation. It has been shown that the distribution of radiation within an hour is not uniform. It remains to be proven that such a real distribution would not affect system performance and thus justify the use of hourly average quantities to perform simulations.

5.7.2 System Setup

The same system design (see Figure 1.4) that was used previously in the comparison of the different hourly weather models to the long term data (see Section 1.4) was used in this analysis. In contrast to the yearly simulations which were performed for the weather models, only a one-month simulation was performed here. The minute data for March 1981 in Atlanta were used. The simulations were performed using both the minute and hourly average (calculated from the minute) of ambient temperature and horizontal radiation. The system was designed with collector having a tilt angle equal to the latitude of Atlanta. Since only horizontal radiation was used as input, the tilted radiation had to be calculated. The calculation of the tilted radiation was accomplished in the TRNSYS Type 16 Radiation Processor using the Erbs' hourly diffuse correlation and the Perez anisotropic model to generate the tilted radiation from the horizontal and diffuse.

5.7.3 Results

Surprisingly, Figure 5.8 shows that the hourly simulations gave noticeably higher solar fractions than the minute simulations for all system configurations. From a utilizability analysis, this result would seem impossible since the minute values of radiation are by nature

more non-uniform than their hourly average. There is an explanation for this apparent discrepancy. Due to the non-linearity in the correlations that are were used in the calculation of the diffuse values and the subsequent calculation of the tilted values, the two simulations do not receive the same inputs. That is, using the correlations with the hourly average horizontal gave a higher hourly average tilted radiation value than the average of the minute tilted radiation values

$$I = \sum_{i=1}^{60} G_i \qquad (5.2)$$

but

$$I_t > \sum_{i=1}^{60} G_{t_i} \qquad (5.3)$$

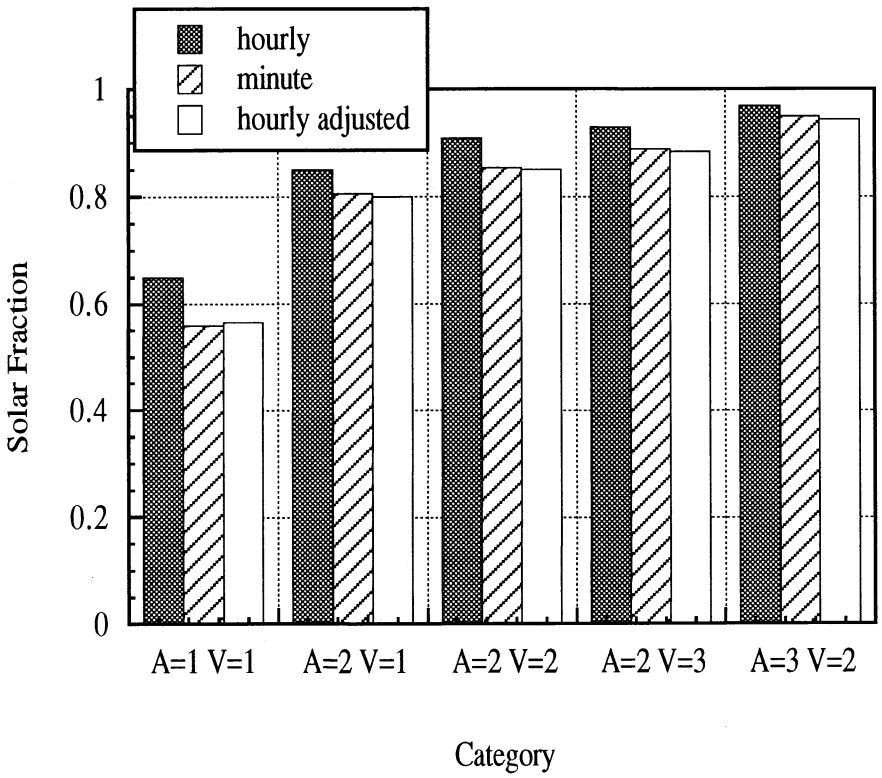

Figure 5.8 Simulation Results of Different Systems

To perform a fair comparison, the two simulations needed to have the same tilted radiation over an hour. Consequently, the hour simulations were reformulated so that $I_t = \sum_{i=1}^{60} G_{t_i}$. Figure 5.8 shows the results of the month-long simulations with the hourly adjusted data. The values of collector area "A" and storage tank volume "V" are given in Table 5.1. The minute simulations gave only marginally higher solar fractions than those in which hour adjusted values were used.

This indistinguishability of the results held on a daily basis. Figure 5.9 shows the daily solar fractions over a month for one system configuration. There are no significant differences between

the simulations performed using the two data sets.

Other simulations were performed to see if the nearly identical results were due to the selected system parameters. Two of those parameters, the collector loss coefficient F_RU_L and the storage tank loss coefficient U_L, were varied. These results are in Figures 5.10 and 5.11. As the collector F_RU_L is increased, the system's solar fraction was reduced. However, no difference appeared between the two data sets. When the tank's U_L was increased, there was a small decrease in solar fraction. Once again, the results of the minute simulations matched those of the hourly.

The conclusion from this analysis is that hourly average meteorological values and hourly simulation time steps are acceptable for the simulation of solar domestic hot water systems.

A	Collector Area [m^2]
1	3.25
2	6.50
3	13.00

V	Tank Volume [m^3]
1	0.195
2	0.390
3	0.780

Table 5.1 Values of A and V

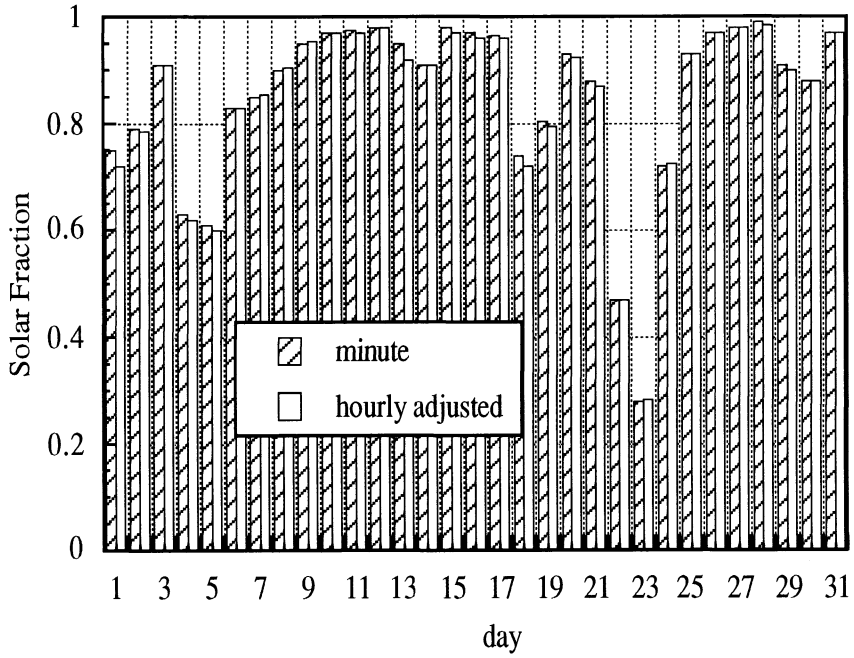

Figure 5.9 Daily Solar Fractions

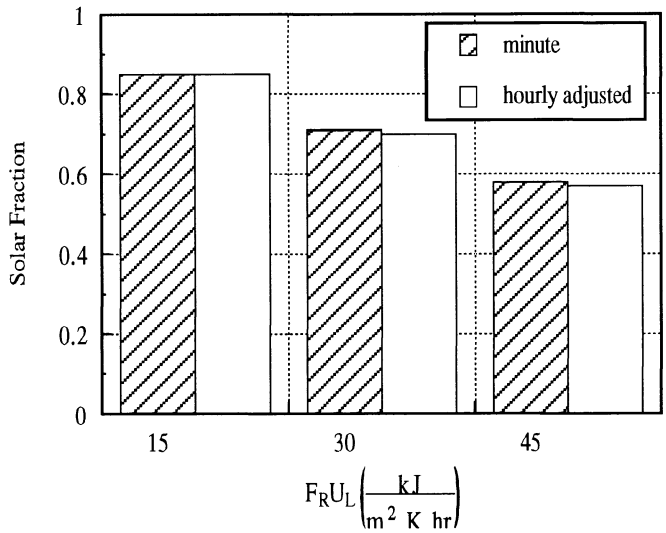

Figure 5.10 Solar Fractions with Different Collector F_RU_L

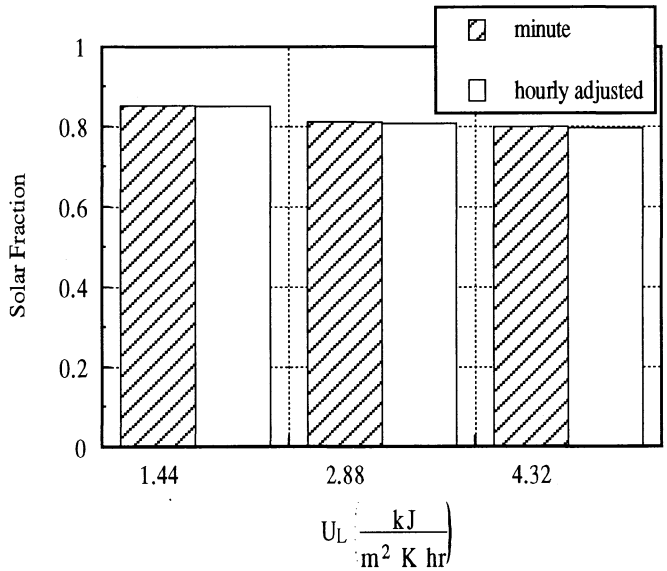

Figure 5.11 Solar Fractions with Different Tank Loss Coefficients

5.7.4 Capacitance Effects

The analysis of Section 5.6 neglected the effects of thermal capacitance upon the performance of the system. It is conceivable that the inclusion of capacitance could result in differences between the use of hourly average as opposed to minute weather data. To investigate this possibility, a model was developed to look specifically at the collector using EES. The same governing equations that were used in the TRNSYS representation of the collector were used here. Specifically, there are four energy flows in the collector. There is the water flow into the collector, the water flow out of the collector, the incident solar radiation, and the losses from the collector. These are shown in Figure 5.12. The mathematical form of the collector equation with storage is:

$$MC\frac{dT_m}{dt} = \dot{m}c_p(T_{in} - T_{out}) + AF_R(\tau\alpha)G_T - AF_RU_L(T_{in} - T_a) \quad (5.3)$$

where

$$T_m = \frac{1}{2}(T_{in} + T_a) \quad (5.4)$$

$$\frac{dT_m}{dt} = \frac{T_m^i - T_m^{i-1}}{\Delta t} \quad (5.5)$$

where i is the current time and i-1 is the previous time period.

Two simulations were run with a minute time step. In the first simulation, the hourly average value was used for every minute in one case and the actual minute data was used in the other. The simulation was performed for two hours in which there were a large variations in the radiation as well as a significant step change from one hourly average value to the next. For the collector capacitance, a typical value of 8000 J/(m^2 K) was chosen. [Duffie and Beckman, 1991] A constant fluid inlet temperature of 50C was used. The radiation and temperature profiles are shown in Figures 5.13 and 5.14. Table 5.2 contains the results of the simulation. The useful energy delivered by the collector in the two simulations were nearly identical. The minute curves are different, but the end results are the same. As can be seen in Figure 5.15, using the hourly average data results in a steady-state being achieved quite rapidly. Even though the radiation varied considerably during the hour, it did not affect the water heating system on an hourly basis. Thus, the use of hourly average meteorological data, as opposed to minute data, is justified.

Simulation	Useful Energy (W)
Hourly	777.802
Minute	777.820

Table 5.2 Collector Output with Capacitance Included

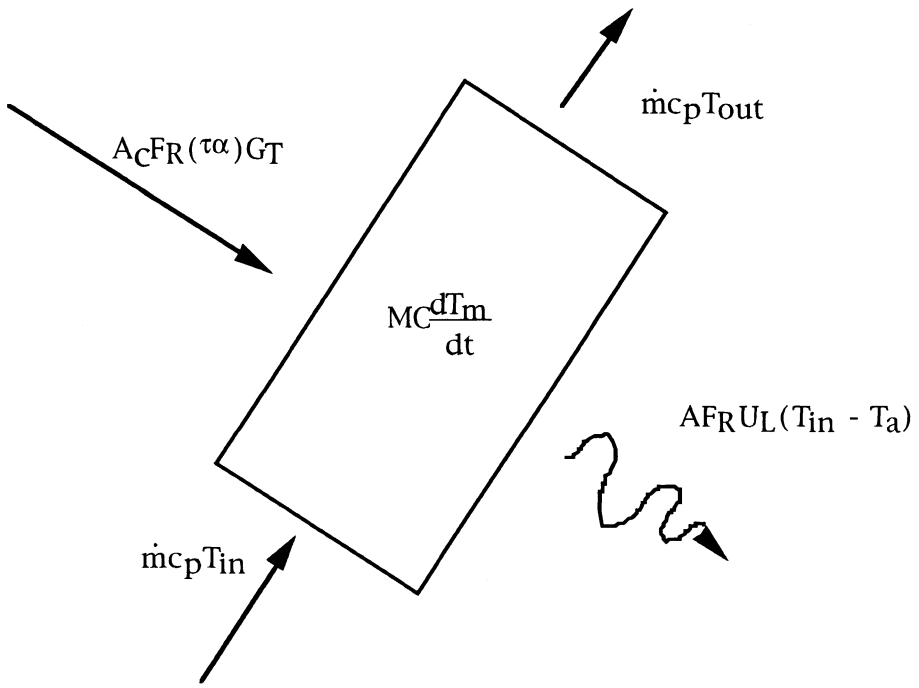

Figure 5.12 Energy Flows In Collector Subsystem

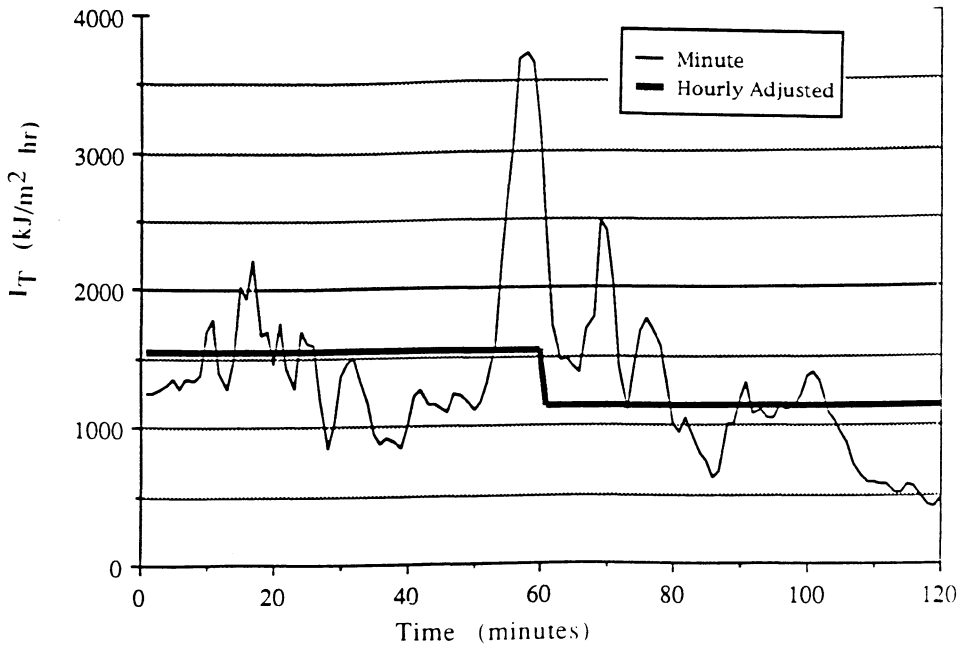

Figure 5.13 Radiation Profile

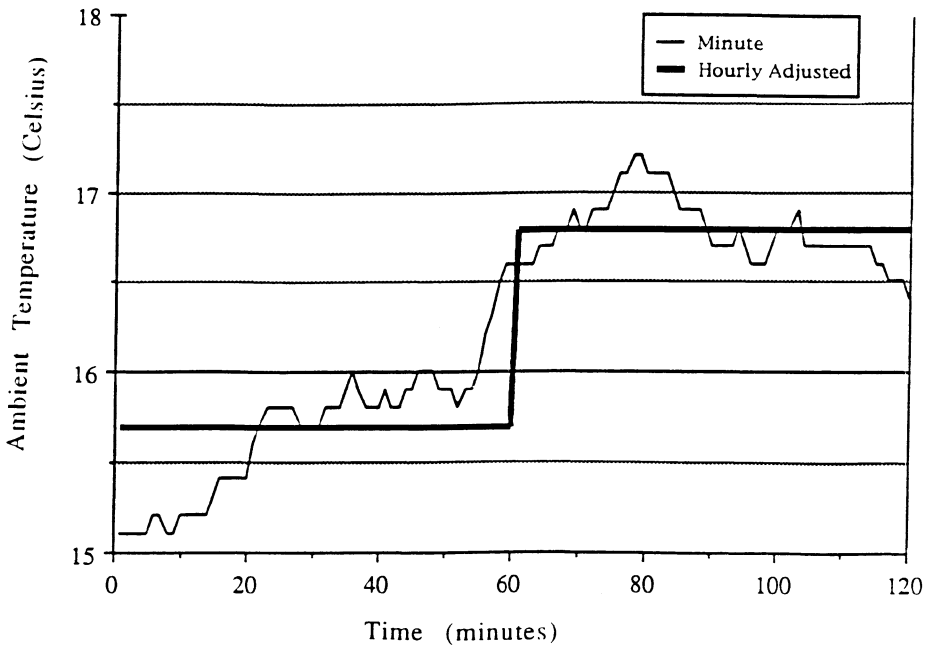

Figure 5.14 Temperature Profile

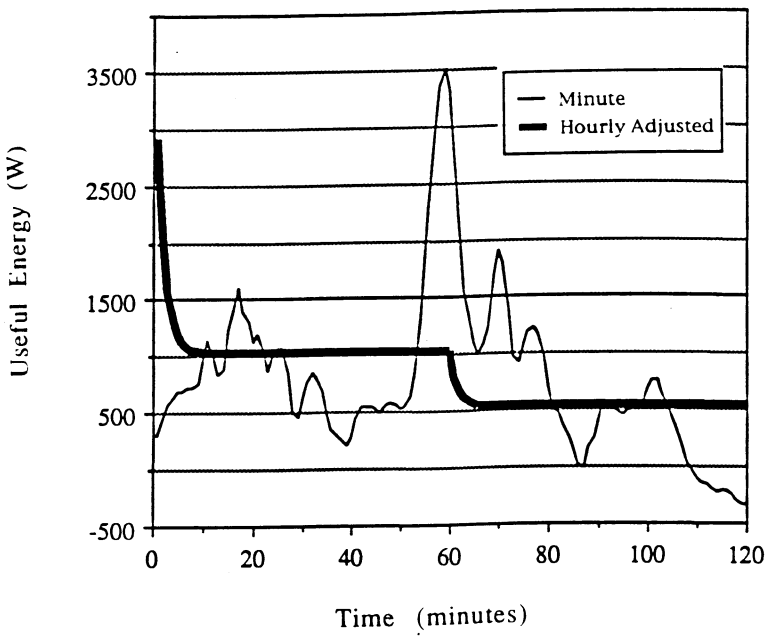

Figure 5.15 Useful Energy Profile

CHAPTER 6 Conclusions and Recommendations

6.1 Conclusions

No model will be able to perfectly reproduce the long term behavior of the multitude of meteorological phenomena and all of their interrelations. The Type 54 Weather Generator and Type 75 Compressed Weather Generator are attempts to produce quick and accurate representations of actual weather conditions. When compared on a strict meteorological basis, both compare very well to the long term, sometimes even better than the typical meteorological year. When the models are compared on a simulation basis, the mathematical models stand up very well against the LTD, once again, better than TMY sometimes. This indicates that the two weather generators can be used for solar energy simulations.

The method in which weather in generated in GEN and COM may not be universally applicable. Collares-Pereira and Aguiar show very sharp peaks at $k_t/k_{tm} = 1$ for high values of K_t in their data. These peaks are not as sharp for the U.S. data. It could be that the method used in GEN for determining k_t from k_{tm} is sufficient for U.S. locations but that the different behavior does not allow GEN to accurately reproduce European weather. This behavior suggests that other meteorological quantities are important in the distribution of radiation. The algorithms that are used in GEN were developed from U.S. data. Thus, they may not be applicable to locations outside of the U.S.

Some of the data that will be used in the new National Solar Radiation Database will have been taken from the old SOLMET data and rehabilitated by new meteorological algorithms. This might lead to different distributions than those that were developed from the

old data and used in GEN and COM. When the NSRDB and its associated TMY files are released, it will be necessary to compare the performance of the weather generators against them. It has been reported that the new data has annual daily horizontal radiation values from +18% higher to -11% lower than the SOLMET averages [Marion and Myers, 1992]. The new data should be investigated on a statistical as well as simulation basis as was performed here.

Minute radiation can display marked differences from hourly average values. However, the distribution of minute radiation does not seem to correspond to the universal model that Suehrcke has proposed. Nonetheless, there is a difference between minute and hourly, especially at low airmasses. Furthermore, the distributions of minute clearness indices about an hourly average value are quite smooth and regular. Thus, it should be possible to develop algorithms to generate minute values from hourly average values such as those produced by the two weather generators.

To incorporate minute-by-minute generation of data is of extreme importance in photovoltaic simulations. Because of the non-linear response of such devices to insolation, hourly simulations can give erroneous results when there is non-uniformity in the distribution of minutes within a given hour.

PV performance is characterized not only by the incident radiation but also by the spectral distribution of that radiation. Data on the spectral distribution of radiation is available on minute time scales. PV applications should be investigated on the basis of the spectral distribution.

Other applications in which minute-by-minute data could be crucial could be daylighting and building cooling. In daylighting applications, the purpose is to let natural illuminence provide the lighting needs of the structure. These systems usually operate in an

on-off fashion. Electric lights will activate only when the solar illuminence falls below a set threshold. The use of hourly average values might indicate that the electric lights were not necessary while the minute values would show the need for artificial lighting.

While building cooling systems do not respond as fast as a minute, they do respond markedly faster than the hourly time steps upon which simulations of systems are traditionally performed. In addition, some utilities charge electrical rates on the basis of the peak rate within a quarter-hour time period. In this case, hourly radiation values could be misrepresented the cooling loads and costs. If a PV cell were to be used to help meet these cooling loads, the variation of radiation within the hour might tell a completely different story than the hourly averages would.

6.2 Recommendations

There are a number of improvements that could be made in the area of weather generation. If the distributions presented in Section 3.6 can be shown to have bearing on solar energy system performance, then the dependence of the distribution of k_t about k_{tm} on zenith angle and K_t should be incorporated. Since it has been shown that the variation of radiation within an hour to be important in certain solar energy applications, synthetic weather programs should include the capability of generating radiation on timesteps of less than an hour. In particular, the generation of short-term radiation should feature dependence on hourly clearness index and zenith angle. In addition, the autocorrelation behavior of minute clearness indices should also be included.

Appendix A: Average Daily Profiles

This appendix contains the average daily profiles of horizontal radiation for the six locations.

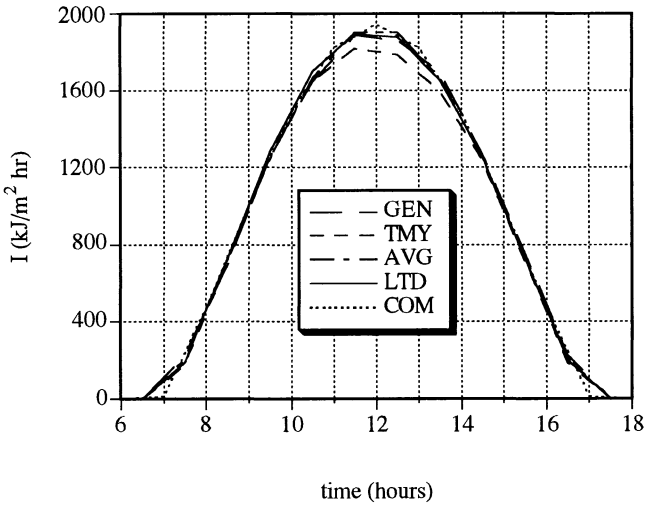

Figure A.1 Average Daily Profile, January, Albuquerque

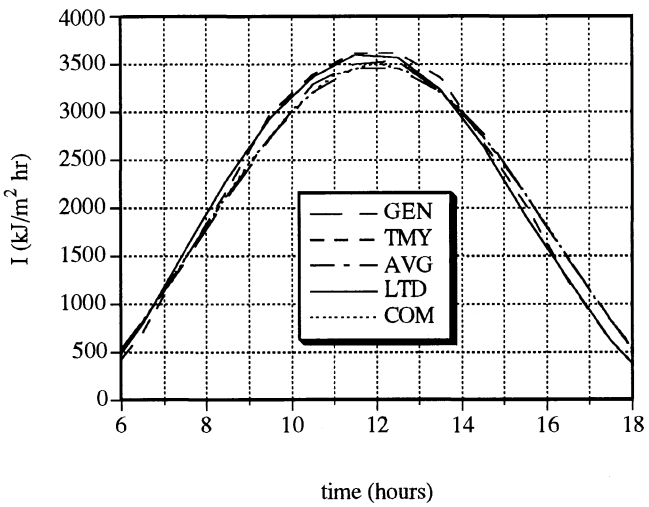

Figure A.2 Average Daily Profile, July, Albuquerque

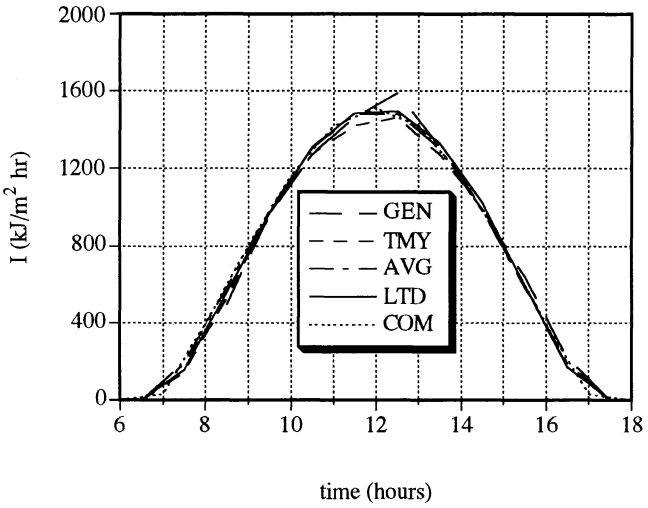

Figure A.3 Average Daily Profile, January, Fort Worth

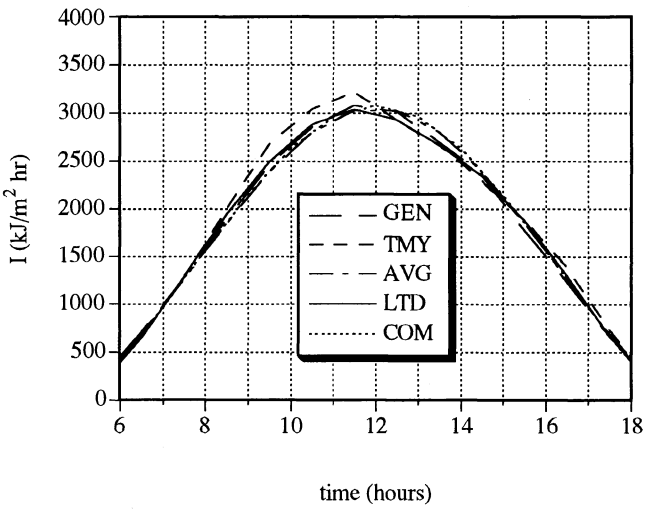

Figure A.4 Average Daily Profile, July, Fort Worth

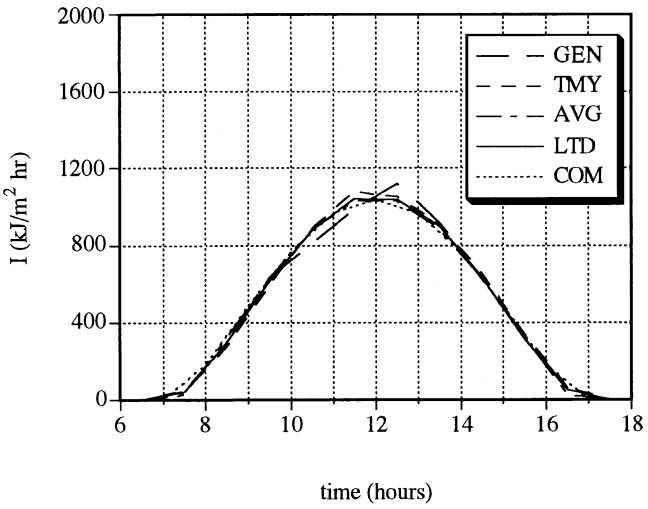

Figure A.5 Average Daily Profile, January, Madison

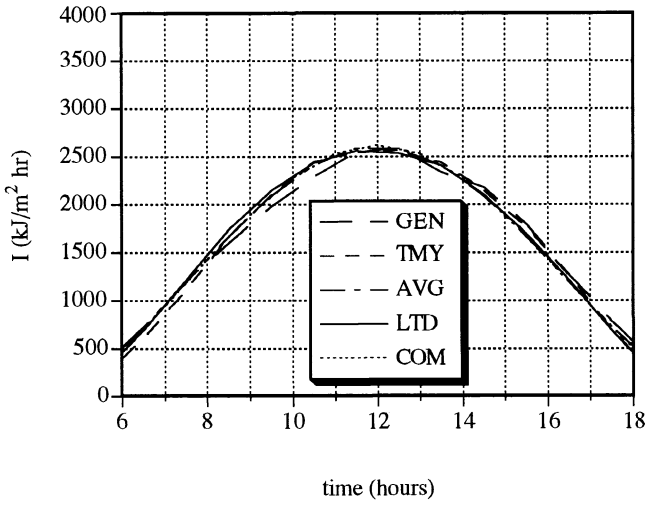

Figure A.6 Average Daily Profile, July, Madison

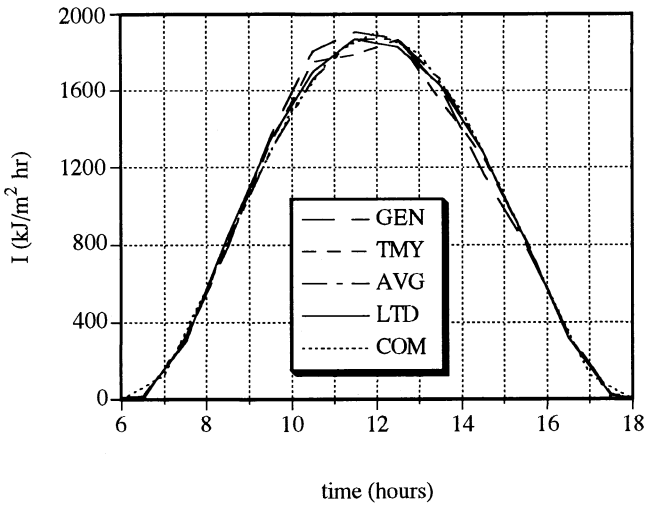

Figure A.7 Average Daily Profile, January, Miami

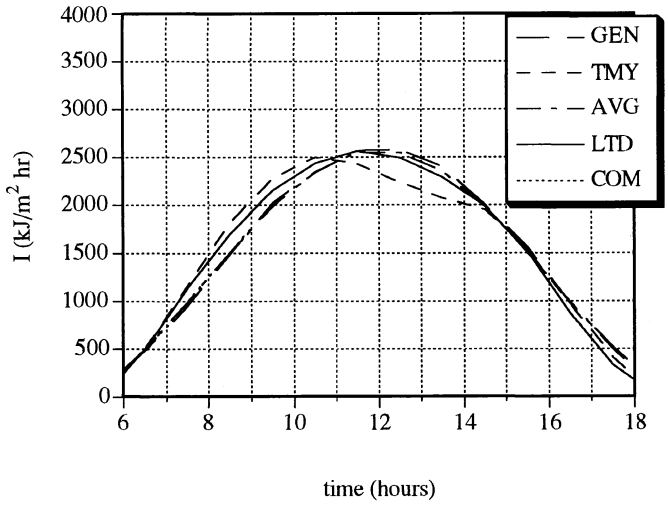

Figure A.8 Average Daily Profile, July, Miami

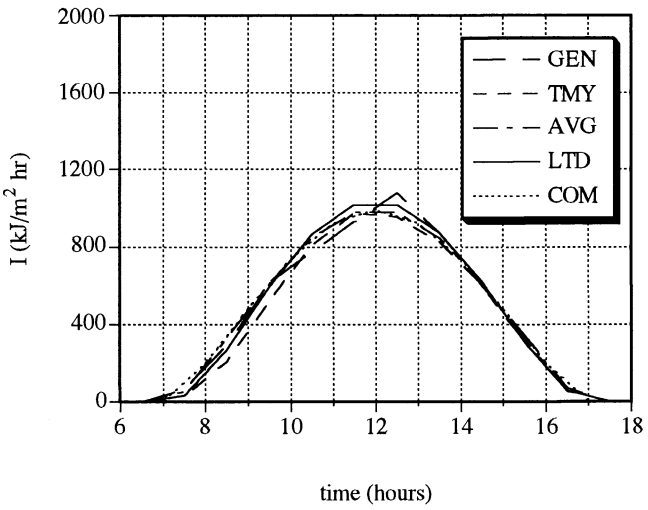

Figure A.9 Average Daily Profile, January, New York City

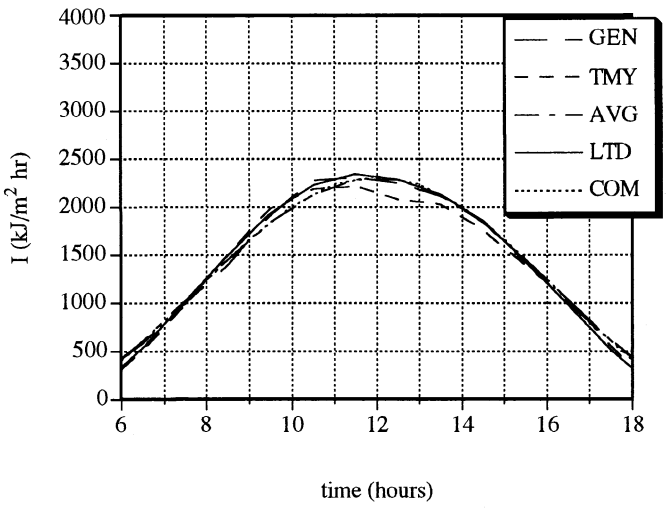

Figure A.10 Average Daily Profile, July, New York City

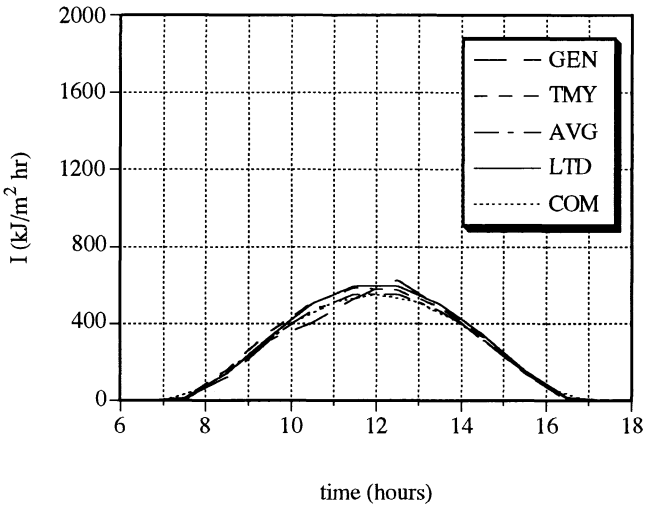

Figure A.11 Average Daily Profile, January, Seattle

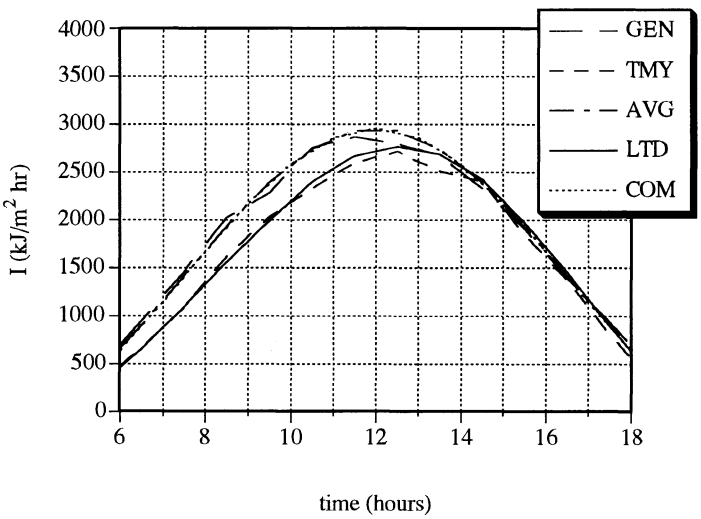

Figure A.12 Average Daily Profile, July, Seattle

Appendix B: Monthly Utilizability Bias

This appendix contains the monthly utilizability bias graphs for each of the four hourly models. This was done for each of the six locations investigated in Chapter 3. The bias for each month was calculated from

$$\text{Bias} = \sum_{i=1}^{100} \varnothing_{\text{model, } c_i} - \varnothing_{\text{LTD, } c_i} \qquad \text{(B.1)}$$

where c_i is the critical level,

$$c_i = 40\ (i\text{-}1)\ \frac{\text{kJ}}{\text{m}^2\ \text{hr}} \qquad \text{(B.2)}$$

and i ranges from 1 to 100.

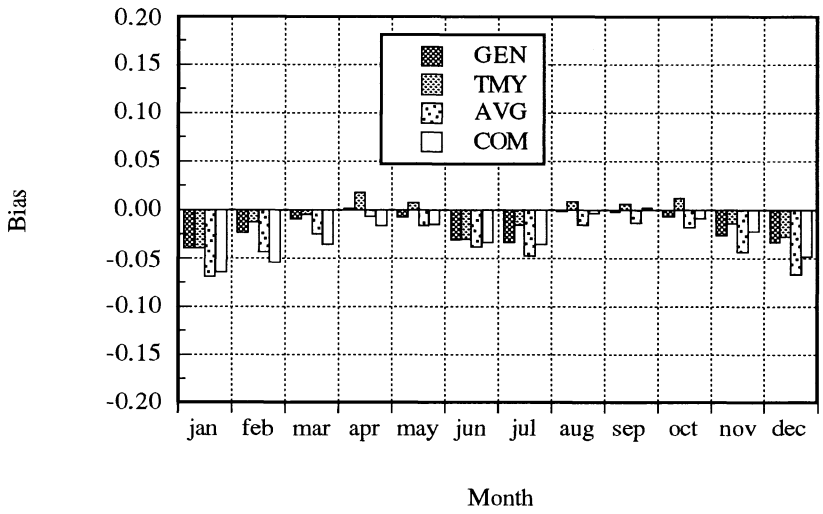

Figure B.1 Monthly Utilizability Bias, Albuquerque

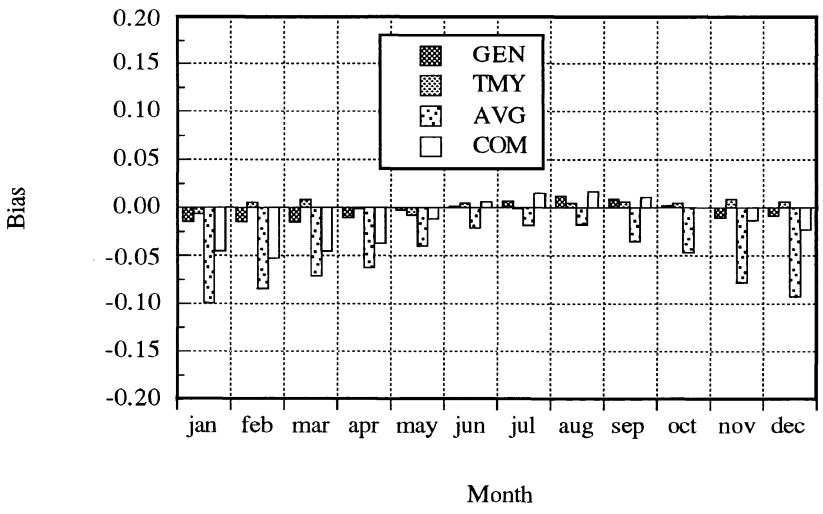

Figure B.2 Monthly Utilizability Bias, Fort Worth

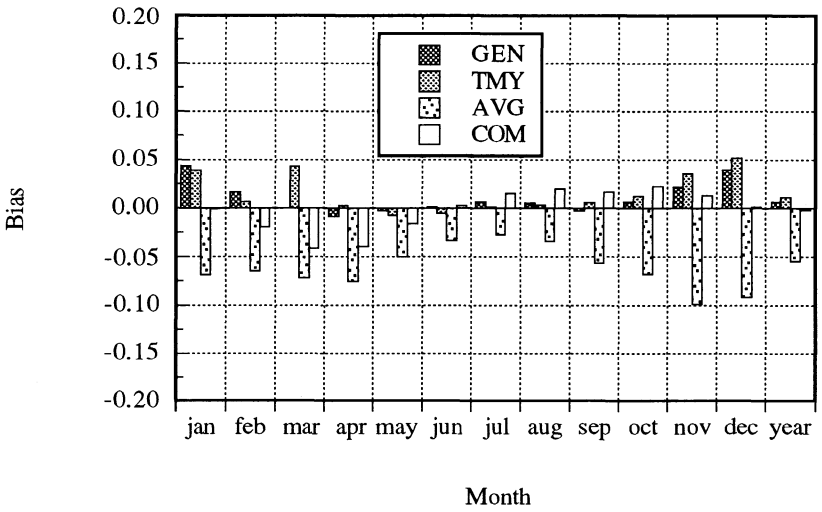

Figure B.3 Monthly Utilizability Bias, Madison

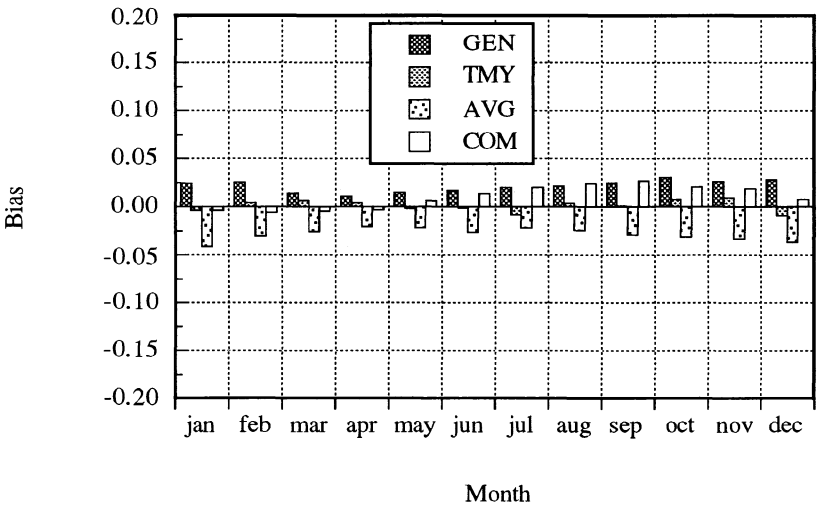

Figure B.4 Monthly Utilizability Bias, Miami

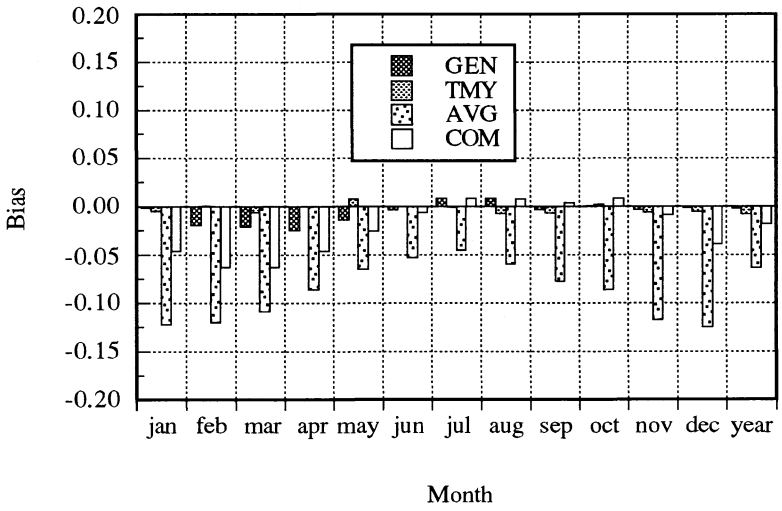

Figure B.5 Monthly Utilizability Bias, New York City

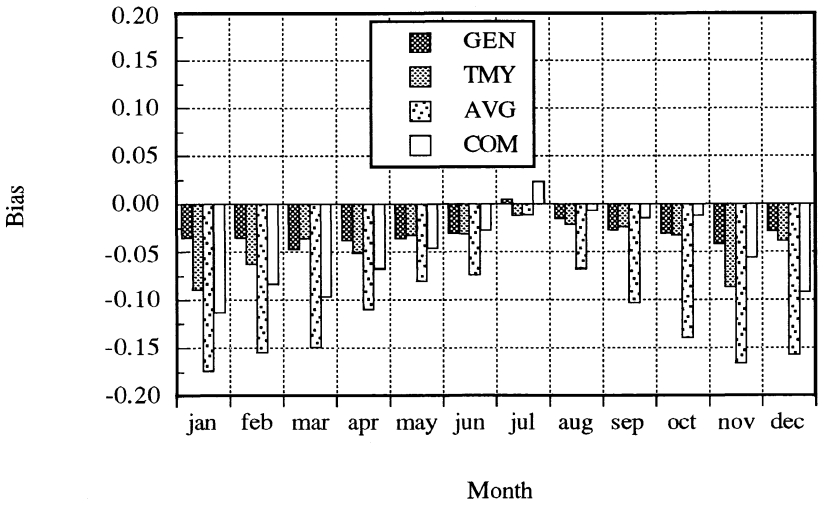

Figure B.6 Monthly Utilizability Bias, Seattle

Appendix C: Computer Codes

This appendix contains some of the computer codes that were written for the purposes of this study

C.1 FAKE: Generation of a Year of Monthly Average Days

```
      program fake
*     This program generates a year's worth of data by taking the
*     average values for the Type 75 Compressed Weather Generator.
*     It uses the standard rt method to find Ibar from Hbar and the
*     same stochastic model as the Type 54 Generator to find the monthly
*     average hourly temperature and hourly horizontal radiation
*     for each month
*
*     See Knight MS 1988 for a full description of the temperature
*     model.  See Duffie and Beckman for the radiation model
**********************************************************************
*********
*HBAR   Monthly average horizontal radiation (kJ/m2 hr)
*CBAR    Monthly average daily clearness index
*TBAR    Monthly average daily ambient temperature
**********************************************************************
*********
*rt ratio of hourly to daily radiation (rt=I/H)

      integer  mon(12)
      real   day(12),Tbar(12),Hbar(12),cbar(12)
      real  ai(12,24),at(12,24)
      open  (UNIT=6,file='weather.dat',STATUS='OLD')
      open  (UNIT=7,file='fake54.fak',STATUS='OLD')
```

```
data  mon  /31,28,31,30,31,30,31,31,30,31,30,31/
data  day  /17,47,75,105,135,162,198,228,258,288,318,344/
pi=acos(-1.0)
degrad=pi/180
      read  (6,*)  xlat,x1,x2
      read  (6,*)  y1,y2,y3,y4
      read  (6,*)  (Hbar(i),  i=1,12)
      read  (6,*)  (cbar(i),  i=1,12)
      read  (6,*)  (tbar(i),  i=1,12)
phi=xlat*degrad
do 10, i=1,12
  DELTA=23.45*degrad*sin(360*degrad*(284+day(i))/365)
      cosws=-tan(delta)*tan(phi)
      ws=acos(cosws)
      sinws=sin(ws)
do 20, j=1,24
      w=(j-.5-12)*15*degrad
      if  (abs(w).lt.abs(ws))  then
      cosw=cos(w)
      a=.409+0.5016*sin(ws-60*degrad)
      b=.6609-.4767*sin(ws-60*degrad)
      rt=(pi/24.0)*(a+b*cosw)*(cosw-cosws)/(sinws-ws*cosws)
      Ai(i,j)=max(hbar(i)*rt*1000,0.0)
      else
      rt=0
      Ai(i,j)=0
      endif
      tstar=2*pi*(real(j)-1)/24
      A=25.8*cbar(i)-5.21
```

```
        t1=0.4632*cos(tstar-3.805)
        t2=0.0984*cos(2*tstar-0.360)
        t3=0.0168*cos(3*tstar-0.822)
        t4=0.0138*cos(4*tstar-3.513)
        at(i,j)=tbar(i)+A*(t1+t2+t3+t4)
20 continue
10 continue

   ii=ai(1,1)
   ti=at(1,1)
   write (7,110) i1,ik,ii,ti
   do 50, i=1,12
        ik=1
        do 45, id=1,mon(i)
              do 40, j=1,24
            ii=Ai(i,j)
              ti=At(i,j)
              write (7,110) i,ik,ii,ti
              ik=ik+1
40      continue
45      continue
50 continue

100    format (14x,f4.0,1x,f4.0)
110    format (1x,i2,1x,i3,7x,i5,1x,f5.1)
   stop
   end
```

C.2 KMCFD: Generation of Suehrcke and Bendt Cumulative Frequency Distributions

```
*    Program  KMCFD
*    This program reads in a value of kbar and airmass
*    and produces a Suehrcke minute cfd curve
*    It also generates a probability curve and a Bendt
*    cumulative frequency distribution
**********************************************************
*********
Suehrcke
*kbar    average clearness index
*mass    airmass
*k0,k1,k2,k3,kmid     from Suehrcke's thesis
*Q1,Q2,Q3       from Suehrcke's thesis
*C0          from Suehrcke's thesis
*g           gamma from Suehrcke's thesis

Bendt
*bkmax          Kmax
*bkmin          Kmin
*bg       gamma

      PROGRAM KMCFD
      REAL KMIN,KMAX,KMID,KPRIME,KPRIME2
      REAL K0,K1,K2,K3
      REAL MASS,CO,G,DUMB
      REAL Itc
      REAL  Ktbar(20),M(20),F(0:200),p(200),k(0:200)
      real  fb(0:200)
```

```
      real  kbar
      OPEN (6,FILE='kmCFD.DAT',STATUS='OLD')
      OPEN (7,FILE='kmCFD.OUT',STATUS='OLD')
      k(0)=0
      f(0)=0
      fb(0)=0
      pi=acos(-1.0)
      degrad=pi/180
      read  (6,*)  inum
      KMIN=.03
      K0=KMIN
      Q1=1
      Q2=.14
      DO  10,  I=1,inum
            read  (6,*)  kbar
            read  (6,*)  mass
            KPRIME=.55*EXP(-.129*MASS)
            KPRIME2=.857*EXP(-.103*MASS)
            KMAX=.905*EXP(-.074*MASS)
            bkmin=.05
            K1=KPRIME
            K2=KPRIME2
            K3=KMAX
            Q3=1.831*EXP(-.202*MASS)
            CO=1/(Q1*(KPRIME-KMIN)+Q2*(KPRIME2-KPRIME)+
     1            Q3*(KMAX-KPRIME2))
            KMID=.5*CO*(Q1*(K1**2-K0**2)+Q2*(K2
     1                  **2-K1**2)+Q3*(K3**2-K2**2))
            G=(KBAR-KMID)*(6.6*KBAR**2+(.39*MASS-3.79)*
     1            KBAR-2.4)/((KBAR-KMIN)*(KBAR-KMAX))
```

```
write  (7,*)
write  (7,*)
WRITE  (7,*)  'Airmass=',MASS,'kbar=',kbar
write  (7,*)  'k"',kprime,'k""',kprime2,'kmax',kmax
C1=Q1*(EXP(G*K1)-EXP(G*K0))
C2=Q2*(EXP(G*K2)-EXP(G*K1))
C3=Q3*(EXP(G*K3)-EXP(G*K2))
C=G/(C1+C2+C3)
     one=q1*(exp(g*k1)-exp(g*k0))
two=q2*(exp(g*k2)-exp(g*k1))
three=q3*(exp(g*k3)-exp(g*k2))
FK1=C*ONE/G
FK2=C*(TWO+ONE)/G
    fk3=c*(one+two+three)/g
PK1=C*Q1*EXP(G*K1)
PK2=C*Q2*EXP(G*K2)
pk3=c*q3*exp(g*k3)
IN=1
      bkmax=.6313+.267*kbar-11.9*(kbar-.75)**8
       zi=(bkmax-bkmin)/(bkmax-kbar)
           bg=-1.498+(1.184*zi-27.182*exp(-1.5*zi))/(bkmax-bkmin)

write  (7,*)  'Bendt  Kmax=',bkmax
write (7,*) '    k         fs(k)     fb(k)      Ps(k)'
count=0
do 90, z=.05,1,.0125
   in=in+1
   k(in)=z
        fb(in)=(exp(bg*bkmin)-exp(bg*z))/(exp(bg*bkmin)-exp(bg*
```

```
     1                                                        bkmax))

        if (fb(in).gt.1) fb(in)=1
      IF (Z.GT.KMAX) THEN
        F(IN)=G/C
        P(IN)=0
      ELSE IF ((Z.LE.KMAX).AND.(Z.GT.KPRIME2)) THEN
         F(IN)=one+two+Q3*(EXP(G*z)-EXP(G*K2))
          P(in)=c*q3*exp(g*z)
      ELSE IF ((Z.LE.KPRIME2).AND.(Z.GT.KPRIME)) THEN
          F(IN)=one+Q2*(EXP(G*z)-EXP(G*K1))
          p(in)=c*q2*exp(g*z)
      ELSE
          F(IN)=Q1*(EXP(G*Z)-EXP(G*K0))
          P(IN)=C*Q1*EXP(G*Z)
      ENDIF
55      F(IN)=F(IN)*C/G
        IF ((F(IN).ge.1).AND.(fb(IN).ge.1)) THEN
          count=count+1
        endif
        if (count.le.1) then
          WRITE (7,500) K(IN),F(IN),fb(in),p(in)
      ENDIF
90  CONTINUE
     WRITE (7,502) K1,FK1,PK1
     WRITE (7,502) K2,FK2,PK2
     write (7,502) k3,fk3,pk3
     write (7,*)
10  CONTINUE
500  FORMAT (F10.4,F10.4,F10.4,f10.4)
```

```
 502   format (f10.4,f10.4,10x,f10.4)
       STOP
       END
```

C.3 PVSYS: Modeling of PV system

```
       subroutine  pvsys(g,htot,gmod,xnum,hcount,m,id,ih)
       common  /pow/  act(12,31,24),avg(12,31,24),rag(12,31,24)
*S   solar  flux
*G   minute  radiation  values
*HTOT    hourly  average  radiation  value
*GMOD    modeled  minute  radiation  values
*XNUM    number  of  minutes  of  data  in  hour
*M  month
*ID  day
*IH  hour



*ACTTOT  minute  power  output
*AVGTOT hourly  power  output
*RAGTOT  modeled  minute  power  output

       real  g(60),gmod(60)
       acttot=0
       ragtot=0
       do 10, i=1,60
            curract=.8
            currmod=.8
```

```
            curravg=.8
            s=g(i)
            if (s.gt.0.0) call solve(s,power,curract)
            acttot=acttot+power
            s=gmod(i)
            if (s.gt.0.0) call solve(s,power,currmod)
            ragtot=ragtot+power
 10 continue
 50 format (3f10.3)

      s=htot
      call  solve(s,power,curravg)

      act(m,id,ih)=acttot/hcount
      pmax=18
      if (act(m,id,ih).gt.pmax) then
            act(m,id,ih)=0
            avg(m,id,ih)=0
            rag(m,id,ih)=0
      else
            avg(m,id,ih)=power
            rag(m,id,ih)=ragtot/xnum
      endif

      return
      end

      subroutine  solve(s,power,curr)

*     Secant method to solve for the current
```

```
*power  power
*curr   current

      epsilon=1e-3
      xi0=0.0
      xi1=curr
      call  solve2(s,power,xi0,q0)
      call  solve2(s,power,curr,q1)
 10   curr=curr-q1*(xi1-xi0)/(q1-q0)

      call  solve2(s,power,curr,qqq)
      if (abs(qqq).lt.epsilon) goto 20
      xi0=xi1
      xi1=curr
      q0=q1
      q1=qqq
      goto 10
 20   return
      end

      subroutine  solve2(s,power,curr,qqq)
*     See Al-Ibrahim Modified SEL model for description of PV terms
      real  iscref,impref,ilref,ioref,i,il,io
      real  muvov,muisc
      real  k,inew

      iscref=2.353
      vocref=19.3
```

```
muvoc=-0.08820
muisc=0.001968
vmpref=13.8
impref=1.985
area=0.5
aokdev=2.387e6
ego=1.155
k=8.62e-5
t=25+273

tcref=25+273
sref=1000
ilref=iscref
ioref=area*aokdev*tcref**3*exp(-ego/(k*tcref))
aref=vocref/log(iscref/ioref)
rs=(aref*log(1-impref/ilref)-vmpref+vocref)/impref

r=18
tau=0.9
tcnoct=46+273
UL=tau*800.0/(tcnoct-20.0)

i=curr
power=i*i*r
v=i*r
eta=power/s
tcell=t+(s*tau/UL)*(1-eta/tau)
a=aref*tcell/tcref
io=area*aokdev*tcell**3*exp(-ego/(k*tcell))
il=(s/sref)*(ilref+muisc*(tcell-tcref))
```

```
      inew=il-io*(exp((v+i*rs)/a)-1)
      qqq=inew-i
      return
      end
```

C.4 SUPER: Generation and Sorting of Minute and Hourly Clearness Indices

```
      PROGRAM super
*
*
*
*************************************************
* INSTANTANEOUS RADIATION PROGRAM CLEARNESS PROGRAM
*
* This program reads in instantaneous radiation data
* and calculates the corresponding instantaneous clearness
* index.  Hourly average clearness indices are computed as well
* The data are binned into three files
*
* Ibin contains the instantaneous clearness index airmass
*    distributions.
*
* Hbin contains the hourly clearness index airmass
*     distributions
*
* Hibin contains the instantaneous clearness index distributions
*      around their hourly clearness index
```

```
**************************************************
*
*     Am        contains the values of airmass
*     Ibin      contains the values for IBIN.DAT
*        Hbin     contains the values for HBIN.DAT
*        Hibin    contains the values for HIBIN.DAT
**************************************************************

      real  am(62)
      real   ibin(62,100),hbin(62,100),hibin(100,100)
      real  abin(3,100,100)
         open (10,file='KandAM.dat',status='old')
      open   (20,file='ibin.all',status='old')
      open   (21,file='hbin.all',status='old')
      open   (22,file='hibin.all',status='old')
      open   (23,file='abin1s.all',status='old')
      open   (24,file='abin2s.all',status='old')
      open   (25,file='abin3s.all',status='old')

      do 12, i=1,62
        read (10,*) am(i)
      do 15, j=1,100
           ibin(i,j)=0
           hbin(i,j)=0
           hibin(i,j)=0
           abin(1,i,j)=0
           abin(2,i,j)=0
           abin(3,i,j)=0
   15 continue
   12 continue
```

```
OPEN  (6,file='jul.s',status='old')
open  (11,file='jul.dat',status='old')
call  doit(am,ibin,hbin,hibin,abin)
open  (6,file='aug.s',status='old')
open  (11,file='aug.dat',status='old')
call  doit(am,ibin,hbin,hibin,abin)
open  (6,file='sep.s',status='old')
open  (11,file='sep.dat',status='old')
call  doit(am,ibin,hbin,hibin,abin)
open  (6,file='oct.s',status='old')
open  (11,file='oct.dat',status='old')
call  doit(am,ibin,hbin,hibin,abin)
open  (6,file='nov.s',status='old')
open  (11,file='nov.dat',status='old')
call  doit(am,ibin,hbin,hibin,abin)
open  (6,file='dec.s',status='old')
open  (11,file='dec.dat',status='old')
call  doit(am,ibin,hbin,hibin,abin)
open  (6,file='jan.s',status='old')
open  (11,file='jan.dat',status='old')
call  doit(am,ibin,hbin,hibin,abin)
open  (6,file='feb.s',status='old')
open  (11,file='feb.dat',status='old')
call  doit(am,ibin,hbin,hibin,abin)
open  (6,file='mar.s',status='old')
open  (11,file='mar.dat',status='old')
call  doit(am,ibin,hbin,hibin,abin)
open  (6,file='apr.s',status='old')
```

```
      open  (11,file='apr.dat',status='old')
      call  doit(am,ibin,hbin,hibin,abin)
      open  (6,file='may.s',status='old')
      open  (11,file='may.dat',status='old')
      call  doit(am,ibin,hbin,hibin,abin)
      open  (6,file='jun.s',status='old')
      open  (11,file='jun.dat',status='old')
      call  doit(am,ibin,hbin,hibin,abin)
      call  printit(ibin,hbin,hibin,abin)
      stop
      end

      subroutine  doit(am,ibin,hbin,hibin,abin)
*     This subroutine calculates the clearness indices as well
*    as the airmasses
************************************************************
*
*     G is the instantaneous solar flux
*          G0 is the instantaneous extraterrestrial solar flux
*          IKT are the instantaneous clearness indices
*                              IAM  are  the  instantaneous  airmasses

*        XLAT is location's latitude
*        XLONG is the location's longitude
*         XLST is the longitude of the standard meridian of the time zone
*        E is the equation of time
*        DELTA is the sun's declination
*        COSTZ is the cosine of the sun's zenith angle
*        HTOT is the hourly total radiation
*     HAM is the airmass at the midpoint of the hour
```

```
*        EXTOT is the hourly total extraterrestrial radiat
*     HCOUNT is the number of minutes of data in the hour
*        HKT is the hourly clearnes index
*****************************************************************
*
      REAL KT,AIRMASS
      REAL G(100)
      real  ikt(60),iam(60)
      real  ibin(100,100),hbin(100,100),hibin(100,100)
      real  abin(3,100,100)
      z=0
      read  (11,*)  xmonth
      READ (11,*) DAY1,DAY2
       READ (11,*) xlong
      read  (11,*)  xlst
      xlat=33.77
      m=int(xmonth)
      pi=acos(-1.0)
      degrad=pi/180
      bad=9900
      phi=xlat*degrad
      DO 100, DAY=DAY1,DAY2
          daymon=day-day1+1
       DO 200, HOUR=1,24
          do 202, ix=1,10
            ij=(ix-1)*6+1
            READ (6,333) (G(I),I=ij,ij+5)
 202     continue
        ihour=int(hour)
        B=(day-1)*360*degrad/365
```

```
      E1=.000075
       E2=.0018688*cos(B)
       E3=-.032077*sin(B)
       e4=-.014615*cos(2*B)
       e5=-.04089*sin(2*B)
       E=229.2*(e1+e2+e3+e4+e5)
        Shour=real(hour-1)+(E+4*(xlst-xlong))/60
         w=(Shour-12)*15*degrad
       wdeg=w/degrad
        DELTA=23.45*degrad*sin(360*degrad*(284+day)/365)
      htot=0
       hcount=0
      extot=0
     do 300, im=1,60
       if  ((g(im).ge.0.0).and.(g(im).lt.bad))  then
*************      15 degrees per hour * 1/60 of an hour= 1/4
         w=w+degrad/4
              COSTZ=cos(phi)*cos(delta)*cos(w)+sin(phi)*sin(delta)
        GO=1367*(1+0.033*COS(360*DEGRAD*DAY/365))*COSTZ
        iKT(im)=G(Im)/GO
         iam(im)=1/costz
         if  (ikt(im).ge.0.0)  then
             if  ((iam(im).lt.100).and.(iam(im).gt.0.0))  then
           hcount=hcount+1
          htot=htot+g(im)
        extot=extot+GO
        endif
       endif
      else
```

```
            ikt(im)=0
            iam(im)=0
          endif
 300    CONTINUE

              if        ((hcount.gt.0).and.(htot.gt.0))        then

            htot=htot/hcount
            extot=extot/hcount
                hShour=real(hour-.5)+(E+4*(xlst-xlong))/60
             hw=(hShour-12)*15*degrad
              hCOSTZ=cos(phi)*cos(delta)*cos(hw)+sin(phi)*sin(delta)
           xIO=1367*(1+0.033*COS(360*DEGRAD*DAY/365))*hcostz
           ham=1/hcostz
*          hKT=htot/xIO
            hkt=htot/extot
                     call    BIN(am,ikt,hkt,iam,ham,hcount,ibin,hbin,hibin,abin)

          endif

 200    CONTINUE
 100    CONTINUE
  333     format (6f10.5)
        close  (6)
        close  (11)
        return
        end

*************************************************
```

```
* INSTANTANEOUS RADIATION BIN PROGRAM
* This program puts the clearness indices into the appropriate
* bins for use in the three main output files
*
* NNHK is the pointer for the hourly clearness index
* NNHAM is the pointer for the hourly airmass
* NNIK is the pointer for the instantaneous clearness index
* NNIAM is the pointer for the instantaneous airmass
************************************************
      subroutine   BIN(am,ikt,hkt,iam,ham,hcount,ibin,hbin,hibin
     1 ,abin)
      real  am(62)
      real  iam(60)
      real  ikt(60)
      integer  ibin(62,100),hbin(62,100),hibin(100,100)
      nhk=0
      if  ((hkt.gt.0.0).and.(ham.ge.1.0))  then
      do 400, i=1,61
            if  ((ham.ge.am(i)).and.(ham.lt.am(i+1)))  then
           nnham=i
           goto 401
          endif
 400      continue
          nnham=62
 401       nnhk=int(hkt*100)
          if  (nnhk.gt.100)  nnhk=100
          if  (nnhk.ne.0)  then
                    hbin(nnham,nnhk)=hbin(nnham,nnhk)+1
        endif
      endif
```

```
      do 200, j=1,60
           if ((iam(j).lt.1.0).or.(ikt(j).le.0.0)) goto 200
        do 300, i=1,61
              if ((iam(j).ge.am(i)).and.(iam(j).lt.am(i+1))) then
            nniam=i
            goto 301
           endif
 300      continue
          nniam=62
 301       nnik=int(ikt(j)*100)
          if (nnik.gt.100) nnik=100
               ibin(nniam,nnik)=ibin(nniam,nnik)+1
           if ((nnhk.ne.0).and.(nnik.ne.0)) then
               hibin(nnhk,nnik)=hibin(nnhk,nnik)+1
*          write (*,*) ham,nnhk,nnik
                                call bin2(abin,ham,nnhk,nnik)

         endif
 200  CONTINUE
      return
      END

      subroutine bin2(abin,ham,nnhk,nnik)
* This subroutine isn't really necessary.  It puts the minute
* clearness indices into bins based on hourly clearness index and
* airmass.  The program SUPERB does this much better
**********************************************************
***
```

```
      integer  abin(3,100,100)
      if  ((ham.gt.1.5).and.(ham.lt.2.0))  then
            abin(1,nnhk,nnik)=abin(1,nnhk,nnik)+1
      else  if  ((ham.gt.2.5).and.(ham.lt.3.0))  then
            abin(2,nnhk,nnik)=abin(2,nnhk,nnik)+1
      else  if  ((ham.gt.3.5).and.(ham.lt.4.0))  then
            abin(3,nnhk,nnik)=abin(3,nnhk,nnik)+1
      else
      endif
      return
      end

      subroutine   Printit(ibin,hbin,hibin,abin)
*     This subroutine writes the output files
*************************************************************88
      integer  ibin(62,100),hbin(62,100),hibin(100,100)
      integer  abin(3,100,100)
      do 500, i=1,62
            write  (20,9)  (ibin(i,j),  j=1,10)
            write  (20,9)  (ibin(i,j),  j=11,20)
            write  (20,9)  (ibin(i,j),  j=21,30)
            write  (20,9)  (ibin(i,j),  j=31,40)
            write  (20,9)  (ibin(i,j),  j=41,50)
            write  (20,9)  (ibin(i,j),  j=51,60)
            write  (20,9)  (ibin(i,j),  j=61,70)
            write  (20,9)  (ibin(i,j),  j=71,80)
            write  (20,9)  (ibin(i,j),  j=81,90)
            write  (20,9)  (ibin(i,j),  j=91,100)
            write  (20,9)
            write  (21,9)  (hbin(i,j),  j=1,10)
```

```
      write (21,9) (hbin(i,j), j=11,20)
      write (21,9) (hbin(i,j), j=21,30)
      write (21,9) (hbin(i,j), j=31,40)
      write (21,9) (hbin(i,j), j=41,50)
      write (21,9) (hbin(i,j), j=51,60)
      write (21,9) (hbin(i,j), j=61,70)
      write (21,9) (hbin(i,j), j=71,80)
      write (21,9) (hbin(i,j), j=81,90)
      write (21,9) (hbin(i,j), j=91,100)
      write (21,9)
      write (22,9) (hibin(i,j), j=1,10)
      write (22,9) (hibin(i,j), j=11,20)
      write (22,9) (hibin(i,j), j=21,30)
      write (22,9) (hibin(i,j), j=31,40)
      write (22,9) (hibin(i,j), j=41,50)
      write (22,9) (hibin(i,j), j=51,60)
      write (22,9) (hibin(i,j), j=61,70)
      write (22,9) (hibin(i,j), j=71,80)
      write (22,9) (hibin(i,j), j=81,90)
      write (22,9) (hibin(i,j), j=91,100)
      write (22,9)
500   continue
    do 501, i=63,100
      write (22,9) (hibin(i,j), j=1,10)
      write (22,9) (hibin(i,j), j=11,20)
      write (22,9) (hibin(i,j), j=21,30)
      write (22,9) (hibin(i,j), j=31,40)
      write (22,9) (hibin(i,j), j=41,50)
      write (22,9) (hibin(i,j), j=51,60)
      write (22,9) (hibin(i,j), j=61,70)
```

```
      write (22,9) (hibin(i,j), j=71,80)
      write (22,9) (hibin(i,j), j=81,90)
      write (22,9) (hibin(i,j), j=91,100)
      write (22,9)
501 continue

    do 601, L=1,3
      LU=L+22
    do 602, i=1,100
      write (LU,9) (Abin(L,i,j), j=1,10)
      write (LU,9) (Abin(L,i,j), j=11,20)
      write (LU,9) (Abin(L,i,j), j=21,30)
      write (LU,9) (Abin(L,i,j), j=31,40)
      write (LU,9) (Abin(L,i,j), j=41,50)
      write (LU,9) (Abin(L,i,j), j=51,60)
      write (LU,9) (Abin(L,i,j), j=61,70)
      write (LU,9) (Abin(L,i,j), j=71,80)
      write (LU,9) (Abin(L,i,j), j=81,90)
      write (LU,9) (Abin(L,i,j), j=91,100)
      write (LU,9)
602 CONTINUE
601 CONTINUE

 9  format (10i6)
    return
    end
```

C.5 SUPERDIFF: Comparison of Measured and Calculated Minute Diffuse and Tilted Radiation Values

Note:SUPERDIFF calls this subroutine. The main program is virtually the same as SUPER.

```
      subroutine  doit(am,ibin,hbin,hibin,abin)
*     This subroutine calculates the clearness indices as well
*     as the airmasses
*
*     DIFFUSE and TILTED subroutines adapted from TRNSYS Type 16
*     Radiation Processor

************************************************************
*
*     G is the instantaneous solar flux
*          Gd is the instantaneous diffuse via correlation
*     Gdreal is the actual instantaneous diffuse
*          G0 is the instantaneous extraterrestrial solar flux
*     GTREAL is the actual tilted data
*     GTGGD is the tilted calculated from G and Gdreal
*     GTG is the tilted calculated from G only
*          IKT are the instantaneous clearness indices
*                              IAM  are  the  instantaneous  airmasses

*        XLAT is location's latitude
*        XLONG is the location's longitude
*         XLST is the longitude of the standard meridian of the time zone
*        E is the equation of time
*        DELTA is the sun's declination
```

```
*       COSTZ is the cosine of the sun's zenith angle
*       HTOT is the hourly total radiation
*     HAM is the airmass at the midpoint of the hour
*       EXTOT is the hourly total extraterrestrial radiat
*     HCOUNT is the number of minutes of data in the hour
*       HKT is the hourly clearnes index
*************************************************************
*
      REAL KT,AIRMASS
      REAL  G(60),gd(4,60),d(4),Gdreal(60)
      real  gtreal(60)
      real  gt(3,4,100)
      real  ikt(60),iam(60)
      real  tbad(4,3)
      real  ibin(100,100),hbin(100,100),hibin(100,100)
      real  abin(3,100,100),tilt(4)
      real  gtdata(4,60)
      real  gdg(100,3,2)
      real  gtg(100,3,4,2)
      real  gtggd(100,4,2)
      real  xnum(20)
      z=0
      do 27, i=1,20
           xnum(i)=0
27    continue
      do 57, i=1,100
      do 58, j=1,3
      do 59, k=1,4
      do 60, L=1,2
           gdg(i,j,L)=0
```

```
          gtg(i,j,k,L)=0
          gtggd(i,k,L)=0
60      continue
59    continue
58      continue
57      continue
      read  (11,*)  xmonth
      READ (11,*) DAY1,DAY2
       READ (11,*) xlong
      read  (11,*)  xlst
      xlat=29.46
      xlong=98.49
      xlst=90
      m=int(xmonth)
      write  (*,*)  m
      write  (22,*)  m
      write  (23,*)  m
      write  (24,*)  m
      write  (25,*)  m
      write  (27,*)  m
      pi=acos(-1.0)
      degrad=pi/180
      bad=9900
      phi=xlat*degrad
      DO 100, DAY=DAY1,DAY2
          daymon=day-day1+1
       DO 200, HOUR=1,24
          do 202, ix=1,10
            ij=(ix-1)*6+1
             READ (6,333,err=200) (G(I),I=ij,ij+5)
```

```
          read (7,333,err=200) (Gdreal(i), i=ij,ij+5)
          read (8,333,err=200) (Gtreal(i), i=ij,ij+5)
202     continue

        do 203, i=1,60
          do 204, j=1,4
                gd(j,i)=0
                gtdata(j,i)=0
          do 205, k=1,3
                gt(k,j,i)=0
205       continue
204       continue
203       continue

        ihour=int(hour)
        B=(day-1)*360*degrad/365
       E1=.000075
        E2=.0018688*cos(B)
        E3=-.032077*sin(B)
        e4=-.014615*cos(2*B)
        e5=-.04089*sin(2*B)
        E=229.2*(e1+e2+e3+e4+e5)
         Shour=real(hour-1)+(E+4*(xlst-xlong))/60
          w=(Shour-12)*15*degrad
        wdeg=w/degrad
        DELTA=23.45*degrad*sin(360*degrad*(284+day)/365)


      do 300, im=1,60
```

```
          rad=g(im)
           dif=gdreal(im)
           til=gtreal(im)
          if (rad.gt.9000) rad=0
          if (dif.gt.9000) dif=0
          if (til.gt.9000) til=0

           if (rad*dif*til.le.0) goto 300
**********          15 degrees per hour * 1/60 of an hour= 1/4
          w=w+degrad/4
               COSTZ=cos(phi)*cos(delta)*cos(w)+sin(phi)*sin(delta)
         GO=1367*(1+0.033*COS(360*DEGRAD*DAY/365))*COSTZ
         iKT(im)=G(Im)/GO
          ct=ikt(im)

          air=1/costz


           if ((ct.lt.0.0).or.(ct.gt.1)) goto 300
           if ((air.gt.100).or.(air.lt.0.0)) goto 300

* Calculate Gd from G
              call diffuse(d,rad,ct,costz,w)
           do 167, id1=1,3
             gd(id1,im)=d(id1)
             diff=d(id1)
            coszen=costz

* Calculate Gt from G
                                call    tilted(tilt,rad,diff,GO,phi,coszen,delta,W)
```

```
            do 455, it1=1,4
                gt(id1,it1,im)=tilt(it1)
455             continue
167             continue

* Calculate Gt from G and Gd
            do 467, it1=1,4
                                                diff=gdreal(im)

                                        call    tilted(tilt,rad,diff,GO,phi,coszen,delta,W)

                gtdata(it1,im)=tilt(it1)
467             continue

* Group by minute clearness index and add to running totals

              ndex1=real(ct*20)
                xnum(ndex1)=xnum(ndex1)+1
            do 486, id=1,3
                gdg(ndex1,id,1)=gdg(ndex1,id,1)+
     *       (gdreal(im)-gd(id,im))/gdreal(im)
                gdg(ndex1,id,2)=gdg(ndex1,id,2)+
     *       abs(gdreal(im)-gd(id,im))/gdreal(im)
            do 487, it=1,4
                gtg(ndex1,id,it,1)=gtg(ndex1,id,it,1)+
     *       (gtreal(im)-gt(id,it,im))/gtreal(im)
                gtg(ndex1,id,it,2)=gtg(ndex1,id,it,2)+
     *       abs(gtreal(im)-gt(id,it,im))/gtreal(im)
```

```
487          continue
486         continue
     do 488, it=1,4
               gtggd(ndex1,it,1)=gtggd(ndex1,it,1)+
   *       (gtreal(im)-gtdata(it,im))/gtreal(im)
               gtggd(ndex1,it,2)=gtggd(ndex1,it,2)+
   *       abs(gtreal(im)-gtdata(it,im))/gtreal(im)
488 continue

 300   CONTINUE

 200   CONTINUE
 100   CONTINUE

* give monthly output by minute clearness index

      do 801, ndex1=2,16
       ct=real(ndex1)/20
      n=ndex1
        if (xnum(ndex1).eq.0) goto 801
      do 804, ij=1,2
      do 803, id=1,3
            gdg(ndex1,id,ij)=gdg(ndex1,id,ij)/xnum(ndex1)
      do 802, it=1,4
                        gtg(ndex1,id,it,ij)=gtg(ndex1,id,it,ij)/xnum(ndex1)

  802     continue
  803     continue
     do 805, it=1,4
```

```
            gtggd(ndex1,it,ij)=gtggd(ndex1,it,ij)/xnum(ndex1)
 805 continue
 804     continue
       write  (22,336)  ct,(gtg(n,1,ix,1),  ix=1,4),
      *        (gtg(n,1,iy,2),  iy=1,4),xnum(ndex1)
       write  (23,336)  ct,(gtg(n,2,ix,1),  ix=1,4),
      *        (gtg(n,2,iy,2),  iy=1,4),xnum(ndex1)
       write  (24,336)  ct,(gtg(n,3,ix,1),  ix=1,4),
      *        (gtg(n,3,iy,2),  iy=1,4),xnum(ndex1)
          write  (25,335)  ct,(gdg(n,ix,1),  ix=1,3),
      *        (gdg(n,iy,2),  iy=1,3),xnum(ndex1)
       write  (27,336)  ct,(gtggd(n,ix,1),  ix=1,4),
      *        (gtggd(n,iy,2),  iy=1,4),xnum(ndex1)
 801     continue
       write  (22,*)
       write  (23,*)
       write  (24,*)
       write  (25,*)
       write  (27,*)

  333     format (6f10.5)
  334     format (5f10.3)
  335     format (7f7.2,1x,f6.0)
  336     format (9f7.2,1x,f6.0)
       close  (6)
       close  (11)
       return
       end

       subroutine   diffuse(d,rad,clear,costz,w)
```

```
      real  d(4)
      sc=1367
      clear=min(clear,1.0)

*     ERBS correlation
      if  (clear.le.0.22)  then
            d(1)=(1-.09*clear)*rad
      else  if  (clear.le.0.80)  then
             d(1)=(.9511+clear*(-0.1604+clear*(4.388+clear*
     *           (-16.638+12.336*clear))))*rad
      else
          d(1)=.165*rad
      endif

*     Boes
      dn=(1.3304*clear-.3843)*sc
      dn=max(dn,0.0)
      dn=min(dn,0.739*sc)
      b=min(dn*costz,rad)
      d(2)=rad-b

*     Reindl
      if  (clear.lt.0.3)  then
           dh=1.020-.254*clear+.0123*costz
          dh=min(1.0,dh)
          d(3)=dh*rad
      else  if  (clear.lt.0.78)  then
           dh=1.4-1.749*clear+.177*costz
          dh=min(dh,0.97)
          dh=max(dh,.10)
```

```
      d(3)=dh*rad
    else
      dh=.486*clear-.182*costz
      dh=min(dh,0.97)
      dh=max(dh,.10)
      d(3)=dh*rad
    endif


    return
    end

    subroutine  tilted(tilt,hor,diff,extra,phi,coszen,decl,W)

                                        dimension     p11(8),p12(8)

    DIMENSION P13(8), P21(8), P22(8), P23(8)
      dimension  hdiff(4),tilt(4)

  INTEGER UNITS

     DATA  IUNIT/0/,RDCONV/0.0174533/,DGCONV/57.2958/,PI/3.1415927/
C
C DATA FOR PEREZ MODEL REPORTED IN SANDIA REPORT, 1988.
C
     DATA P11 /-0.196,0.236,0.454,0.866,1.026,0.978,0.748,0.318/
     DATA P12 /1.084,0.519,0.321,-0.381,-0.711,-0.986,-0.913,-0.757/
     DATA P13 /-0.006,-0.18,-0.255,-0.375,-0.426,-0.35,-0.236,0.103/
     DATA P21 /-0.114,-0.011,0.072,0.203,0.273,0.28,0.173,0.062/
```

```
      DATA P22 /0.18,0.02,-0.098,-0.403,-0.602,-0.915,-1.045,-1.698/
      DATA P23 /-0.019,-0.038,-0.046,-0.049,-0.061,-0.024,0.065,0.236/

    do 150, i=1,4
          tilt(i)=0
150 continue

     slope=phi
    AZM = 0
    RHO = .2
     zenith=acos(coszen)
     COSHR=COS(W)
     sinhr=sin(w)

     alat=phi
     SINLAT=sin(slope)
    COSLAT=cos(slope)
     TANLAT=tan(slope)
   SINDEC = SIN(DECL)
  COSDEC = COS(DECL)
  TANDEC = SINDEC/COSDEC
   WS = ACOS(-TANDEC*TANLAT)
  CC = COSLAT*COSDEC
   SS = SINLAT*SINDEC
C
C      FIND POSITION OF THE SUN
      SAZM = 0.
     COSZEN = CC*COSHR + SS
      COSZEN = SIGN(AMAX1(ABS(COSZEN),1.E-06),COSZEN)
     ZENITH = ACOS(COSZEN)
```

```
      SINZEN = SIN(ZENITH)
     TANZEN = SINZEN/COSZEN

      IF (ABS(SINZEN) .GE. 1E-06) THEN
      SINAZM = COSDEC*SINHR/SINZEN
        SINAZM=SIGN(AMIN1(ABS(SINAZM),1.),SINAZM)
      SAZM = ASIN(SINAZM)

C     DETERMINE IF THE ABSOLUTE VALUE OF THE SOLAR AZIMUTH
C     IS GREATER THAN 90 DEGREES BY COMPARING THE HOUR
C     ANGLE WITH THE HOUR ANGLE AT WHICH THE SOLAR AZIMUTH IS
C     +/- 90 DEGREES
     CWEW = TANDEC/TANLAT
      CWEW = SIGN(AMIN1(ABS(CWEW),1.),CWEW)
      WEW = PI
      IF(ALAT*(DECL-ALAT) .LE. 0.0) WEW = ACOS(CWEW)
        IF((ABS(W)-ABS(WEW))*ALAT*(DECL-ALAT) .LE. 0.)
     .    SAZM = SIGN(PI,SAZM) - SAZM

C     DON'T ALLOW THE ABSOLUTE VALUE OF THE SOLAR AZIMUTH
C     TO BE GREATER THAN 180 DEGREES.
        IF(ABS(SAZM) .GT. PI) SAZM = SAZM - SIGN((2.*PI),SAZM)
     ENDIF

C     INPUTS ARE TOTAL (HORIZONTAL) AND DIFFUSE (HORIZONTAL)
      Beam = hor - Diff
       Beam = max(beam,0.0)

227    COSSLP = COS(SLOPE)
```

```
      SINSLP  =  SIN(SLOPE)
     COSTT = COSSLP*COSZEN + SINSLP*SINZEN*COS(SAZM - AZM)

     IF (COSTT.GT.1.) COSTT=1.

C         BEAM AND GROUND REFLECTED RADIATION INDEPENDENT OF TILTED
SURFACE
C        MODEL

     RB = AMAX1(COSTT,0.)/COSZEN
      HBEAM = Beam*RB
       HGRF  = hor*RHO*0.5*(1. - COSSLP)

          if (hor.eq.0) write (*,*) 'hor'
          if (extra.eq.0) write (*,*) 'extra'
          if (coszen.eq.0) write (*,*) 'coszen'

C        ISOTROPIC SKY MODEL FOR TILTED SURFACE DIFFUSE
228         HDIFF(1) = Diff*0.5*(1. + COSSLP)

C        HAY MODEL FOR TILTED SURFACE DIFFUSE
229         AI = Beam/EXTRA
            HDIFF(2) = diff * (0.5*(1.-AI)*(1.+COSSLP) + AI*RB)

C        REINDL TILTED SURFACE MODEL
230         AI = Beam/EXTRA
           F  = SQRT(beam/hor)
          SCUBE = (SIN(SLOPE*0.5))**3
       HDIFF(3) = Diff*(0.5*(1.-AI)*(1.+COSSLP)*(1.+F*SCUBE) + AI*RB)
```

```
C       PEREZ POINT SOURCE MODEL (SANDIA REPORT OCT, 1988)
231      HDN = Beam/COSZEN
         IF ( Diff .LT. 0.00001 ) THEN
          EPS = 99999.
        ELSE
           EPSILN = ( Diff + HDN ) / diff
            EPS = ( EPSILN+1.041*ZENITH**3 )/( 1.+1.041*ZENITH**3 )
        ENDIF
        SKYB = Diff/EXTRA
        IF (EPS .GT. 0.0 .AND. EPS .LE. 1.065) THEN
         NBIN = 1
        ELSEIF (EPS .GT. 1.065 .AND. EPS .LE. 1.230) THEN
         NBIN = 2
        ELSEIF (EPS .GT. 1.230 .AND. EPS .LE. 1.500) THEN
         NBIN = 3
        ELSEIF (EPS .GT. 1.500 .AND. EPS .LE. 1.950) THEN
         NBIN = 4
        ELSEIF (EPS .GT. 1.950 .AND. EPS .LE. 2.800) THEN
         NBIN = 5
        ELSEIF (EPS .GT. 2.800 .AND. EPS .LE. 4.500) THEN
         NBIN = 6
        ELSEIF (EPS .GT. 4.500 .AND. EPS .LE. 6.200) THEN
         NBIN = 7
        ELSE
         NBIN = 8
        ENDIF

          P1 = P11(NBIN) + P12(NBIN)*SKYB + P13(NBIN)*ZENITH
         IF ( P1 .LT. 0.0 ) P1 = 0.0
          P2 = P21(NBIN) + P22(NBIN)*SKYB + P23(NBIN)*ZENITH
```

```
          A1 = AMAX1(COSTT,0.0)
          B1 = AMAX1(COS(85.0*RDCONV),COSZEN)
           HDIFF(4) = Diff*(0.5*(1.-P1)*(1.+COSSLP)+P1*A1/B1+P2*SINSLP)
           IF ( HDIFF(4) .LT. 0.0 ) HDIFF(4) = 0.0
C
C        OUTPUT TOTAL (FLAT SURFACE)
           do 100, i=1,4
           Tilt(i) = HBEAM + HDIFF(i) + HGRF
 100       continue
       return
     END
```

C.6 UTILTD: Generation of Monthly and Annual Utilizability from Long Term Data

```
      program  UtiLTD
**************************************************************
***********
      XI     The  hourly  tilted  radiation
      XIC    The  critcal  levels  of  radiation
      TOT(i)         The  total  amount  of  radiation  in  month  i,
             month(13)  is  the  yearly  total
      TOP(i,j)  The  total  amount  of  radiation  in  month  i  above  critical
             level  j
      PHI(i,j)  Utilizability  at  critical  level  j  in  month  i
**************************************************************
***********
      open   (6,file='ltrad.swh',status='old')
      call   doit(ipoints)
```

```
      stop
      end

      subroutine   doit(ipoints)
      dimension   xIc(100),top(13,100)
      dimension   tot(13)
      dimension   phi(13,100)
      dimension   mon(12)
      data  mon  /31,28,31,30,31,30,31,31,30,31,30,31/
      do 4, i=1,13
           tot(i)=0
           do 5, j=1,100
                top(i,j)=0
5          continue
4     continue

      do 6, i=0,99
           xic(i+1)=real(i)*40
6     continue

      do  10,  year=1,23
      do 11, i=1,12
      do  12,  days=1,mon(i)
           read  (6,*)  ia,xi
                do 20, j=1,100
                     sub=xi-xic(j)
                     diff=max(sub,0.0)
                     top(i,j)=top(i,j)+diff
                     top(13,j)=top(13,j)+diff
20              continue
```

```
                tot(i)=tot(i)+xi
                tot(13)=tot(13)+xi
 12 continue
 11 continue
 10 continue

    do 30, j=1,100
        do 25, i=1,13
                phi(i,j)=top(i,j)/tot(i)
 25     continue
 30 continue

    do 40, i=1,13
    do 50, j=1,100
        write  (i+10,120)  xic(j),phi(i,j)
 50 continue
 40 continue
 120   format (4x,f8.0,2x,f8.4)
    return
    end
```

C.7 ZENDEP: Generation of k_t/k_{tm} distributions based on K_t and zenith angle

```
      Program ZENDEP
*     ZENith DEPendence
*     This program reads in the hourly clearness indices ,kt,  from LTRAD.SWH
*     and the daily clearness indices, Kt, from LTRAD.KDAY. It calculates
*     the mean hourly clearness, ktm, for each hour of the day based on
```

```
*     Kt and finds the ratio of kt/ktm.  These ratios are sorted into twenty
*     files depending on Kt.  Inside each file, the kt/ktm are binned by the
*     cosine of the zenith angle at the midpoint of the hour.  The bins are
*     then normalized so that for a given cos(theta z), the sum of the bins
*     is 100.

*cday    Daily clearness index (Kt)
*ch Hourly clearness index (kt)
*zenSolar zenith angle (theta z)

*kd Matrix index for Kt
*kh Matrix index for kt
*kz Matrix index for cos(theta z)

      real  bin(20,20,10),tot(20,10)
      open  (6,file='ltrad.swh',status='old')
      open  (7,file='ltrad.kday',status='old')
      open  (8,file='years.dat',status='old')
      open  (11,file='zen.1',status='old')
      open  (12,file='zen.2',status='old')
      open  (13,file='zen.3',status='old')
      open  (14,file='zen.4',status='old')
      open  (15,file='zen.5',status='old')
      open  (16,file='zen.6',status='old')
      open  (17,file='zen.7',status='old')
      open  (18,file='zen.8',status='old')
      open  (19,file='zen.9',status='old')
      open  (20,file='zen.10',status='old')
      open  (21,file='zen.11',status='old')
      open  (22,file='zen.12',status='old')
```

```
      open  (23,file='zen.13',status='old')
      open  (24,file='zen.14',status='old')
      open  (25,file='zen.15',status='old')
      open  (26,file='zen.16',status='old')
      open  (27,file='zen.17',status='old')
      open  (28,file='zen.18',status='old')
      open  (29,file='zen.19',status='old')
      open  (30,file='zen.20',status='old')


      read  (8,*)  years

      do 5, k=1,10
      do 6, j=1,20
            tot(j,k)=0
      do 7, i=1,10
            bin(i,j,k)=0
7     continue
6     continue
5     continue

      pi=3.141529
      do  10,  i=1,years
      write  (*,*)  i
      do 15, j=1,365
            read  (7,*)  x,cday
            kd=int(cday*20)+1
            kd=min(20,kd)
            kd=max(kd,0)
```

```
      do 20, k=1,24
            read (6,*) x,ch,zen
            kh=int(ch*20)+1
            kh=min(20,kh)
            kh=max(kh,0)
            if (zen.gt.90) goto 20
            kz=int(cos(zen*pi/180)*10)+1
*           kz=int(zen/10)+1
            bin(kd,kh,kz)=bin(kd,kh,kz)+1
 20     continue
 15  continue
 10  continue

     do 35, kd=1,20
     do 36, kh=1,20
     do 37, iz=1,10
          tot(kd,iz)=tot(kd,iz)+bin(kd,kh,iz)
 37  continue
 36  continue
 35    continue

     do 40, kd=1,20
     LU=kd+10
     do 50, kh=1,20
          ch=real(kh)/20
     do 60, iz=1,10
          if(tot(kd,iz).gt.0)  then
              bin(kd,kh,iz)=100*bin(kd,kh,iz)/tot(kd,iz)
          endif
 60  continue
```

```
      write (LU,100) ch,(bin(kd,kh,iz), iz=1,10)
50  continue
40  continue
100 format (f6.2,10f5.0)
    stop
    end
```

References

Aguiar, R. and M. Collares-Pereira, "Statistical Properties of Hourly Global Radiation", *Solar Energy*, Volume 48, pp. 157-167, 1992.

Aguiar, R. and M. Collares-Pereira, "TAG: A time-dependent, autoregressive, Gaussian model for generating synthetic Hourly Radiation", *Solar Energy*, Volume 49, pp. 167-174, 1992.

Al-Ibrahim, A.M., "New Models for Photovoltaic Systems", Ph.D. Thesis, University of Wisconsin-Madison, 1993.

Bendt, P., T. Hollands and R.G. Huget, "The Frequency Distribution of Daily Insolation Values", *Solar Energy*, Volume 27, pp. 1-5, 1981.

Boes, E.C., "Estimating the Direct Component of Solar Radiation", Sandia Report SAND 75-0565, 1975.

Duffie, J.A. and W.A. Beckman, *Solar Engineering of Thermal Processes*, Wiley, New York 1991.

Erbs, D.G., "Methods For Estimating the Diffuse Fraction of Hourly, Daily, and Monthly-Average Global Solar Radiation", Masters Thesis, University of Wisconsin-Madison, 1980.

Erbs, D.G., "Models and Applications for Water Statistics Related to Building Heating and Cooling Loads ", Ph.D. Thesis, University of Wisconsin-Madison, 1984.

Fulop, L., Personal Communication, 1992.

Graham, V.A, "Stochastic Synthesis of Solar Atmospheric Transmittance, Ph.D Thesis, University of Waterloo, 1985.

Hay, J.E. and J.A. Davies, in *Proceedings of the First Canadian Solar Radiation Data Workshop* (J.E. Hay and T.K. Won, editors)

"Calculation of Solar Radiation Incident on an Inclined Surface." Ministry of Supply and Services Canada, 59, 1980.

Herzog, M.E., "Estimation of Hourly and Monthly Average Daily Insolation on Tilted Surfaces", Masters Thesis, Trinity University, 1985.

Klein, S.A., "Calculations of Flat-Plate Collector Utilizability." *Solar Energy*, Volume 21, pp. 393-402, 1978.

Klein, S.A. *et al*, TRNSYS 13.1 User's Manual, Engineering Experiment Station Report 38-13, Solar Energy Laboratory, University of Wisconsin-Madison (1990).

Klein, S.A., EES - Engineering Equation Solver, F-Chart Software, Middleton, Wisconsin (1992).

Klein, St.A. and W.A. Beckman, "Loss of Load Probabilities for Stand-Alone Photovoltaic Systems", Solar'87, Proceedings of the 1987 Annual Meeting, American Solar Energy Society, Solar Energy Society of Canada, pp. 18-25.

Knight, K.M., "Development and Validation of a Weather Generator Model", Masters Thesis, University of Wisconsin-Madison, 1988.

Liu, B.Y.H. and R.C. Jordan, "The Interrelationship and Characteristic Distribution of Direct, Diffuse and Total Solar Radiation." *Solar Energy*, Volume 4(3), pp. 1-19, 1960.

Marion, W. and D. Myers, "A Comparison of Data from SOLMET/ERSATZ and the National Solar Radiation Data Base", NREL Report NREL/TP-463-5118, 1992.

Menicucci, D.F. and J.P. Fernandez, "A Comparison of Typical Meteorological Year Solar Radiation Information With the SOLMET Data Base", Sandia Report SAND87-2379, 1988.

NREL (National Renewable Energy Laboratory), "National Solar Radiation Data Base (1961-1990) User's Manual", 1992.

Perez, R. *et al*, The Development and Verification of the Perez Diffuse Radiation Model, Sandia National Laboratories Contractor Report SAND88-7030 (1988).

Reindl, D.T., "Estimating Diffuse Radiation on Horizontal Surfaces and Total Radiation on Tilted Surfaces.", Masters Thesis, University of Wisconsin-Madison, 1988.

Schaefer, P., "Modeling of Solar Domestic Hot Water Systems", Masters Thesis, University of Wisconsin-Madison, 1991.

Schuler, A., "Solar Radiation Data Analysis", Masters Thesis, University of Wisconsin-Madison, 1986.

SEMRTS (Solar Energy Meteorological Research and Training Sites), 1982.

Skartveit, A. and J.A. Olseth, "The Probability Density and Autocorrelation of Short-Term Global and Beam Irradiance." *Solar Energy*, Volume 49, pp. 477-487, 1992.

SOLMET, Hourly Solar Radiation Surface Meteorological Observations, Volumes 1 and 2, US National Climactic Center, 1978.

Suehrcke, H., "The Performance Prediction of Solar Thermal Systems", Ph.D. Thesis, University of Western Australia, 1988.

Whillier, A., "Solar Energy Collection and Its Utilization for House Heating", Ph.D. Thesis, MIT, 1953.